ISBN 978-82-326-5537-3 (printed ver.)
ISBN 978-82-326-6050-6 (electronic ver.)
ISSN 1503-8181 (printed ver.)
ISSN 2703-8084 (electronic ver.)

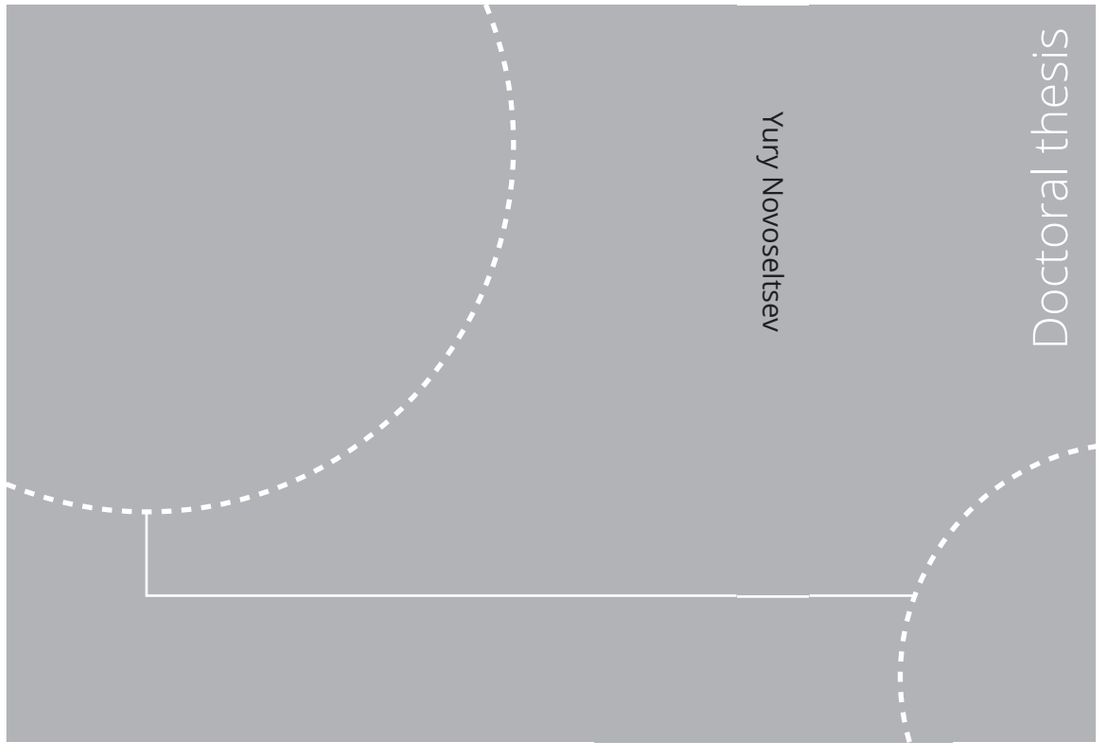

Doctoral theses at NTNU, 2022:294

Yury Novoseltsev

Testing and Modelling of a Wax Control System for Cold Flow Transport of Waxy Oil

NTNU
Norwegian University of
Science and Technology

Doctoral theses at NTNU, 2022:294

NTNU

NTNU
Norwegian University of
Science and Technology
Thesis for the degree of
Philosophiae Doctor
Faculty of Engineering
Department of Energy and Process Engineering

NTNU
Norwegian University of
Science and Technology

Yury Novoseltsev

Testing and Modelling of a Wax Control System for Cold Flow Transport of Waxy Oil

Thesis for the degree of Philosophiae Doctor

Trondheim, October 2022

Norwegian University of Science and Technology
Faculty of Engineering
Department of Energy and Process Engineering

NTNU
Norwegian University of
Science and Technology

NTNU
Norwegian University of Science and Technology

Thesis for the degree of Philosophiae Doctor

Faculty of Engineering
Department of Energy and Process Engineering

ISBN 978-82-326-5537-3 (printed ver.)
ISBN 978-82-326-6050-6 (electronic ver.)
ISSN 1503-8181 (printed ver.)
ISSN 2703-8084 (electronic ver.)

Doctoral theses at NTNU, 2022:294

PRINTED IN NORWAY
NO - 1598

NORDIC SWAN ECOLABEL
Printed matter
2041 0731

Printed by Skipnes Kommunikasjon AS

Abstract

There are no economical ways to tie back subsea waxy oil fields with distances to shore more than 50 km without treating the fluid on a platform or FPSO. For more considerable distances, solutions like heating could be too expensive. In the case of Arctic regions, it may not be possible to install a production facility at sea level at all due to iceberg or icing conditions rendering the development of such fields questionable. Subsea 7 is developing a fully subsea solution for treating well fluid and sending it onshore. The solution enables the development of Arctic fields. Part of this subsea facility is a system for treating wax. The idea is to make a cooling loop that cools the oil to the ambient temperatures and then sends this cold fluid into the export pipeline. This fluid flow at ambient temperatures is called "cold flow." Wax does not deposit at pipeline walls at the same temperature as the fluid. However, wax deposition is expected inside the cooling loop, and pigging the loop is seen as a solution to the wax build-up. A pig circulates inside the loop until it is worn and then is sent for cleaning the export pipeline as its last mission. Initially, this wax control system (WCS) was planned to be working with multiphase flows. However, it was decided to run WCS with single-phase flow as it was found to be impractical to operate WCS in multiphase conditions. This Ph.D. work follows the development of the WCS. It goes from a pilot experiment of checking the feasibility of a constant pigging inside a loop under single-phase conditions without an active control system, continues to experiments with bypass pigging and wax deposition in multiphase conditions, then concludes with a mathematical model for wax deposition tailored for WCS conditions. The main results of the Ph.D. work are:

- Experimental data on bypass pigging in multi-phase flow.
- Decision to construct WCS operating in single-phase flow both due to pigging control and wax deposition predictability.
- Simulator program of wax deposition inside the WCS. The program can be used for the design of a WCS.
- WCS qualification scale rig testing according to Norwegian DNV (Det Norsk Veritas) regulations. The test showed that the system is ready for implementation in an oil field.

Preface

This thesis is submitted to the Norwegian University of Science and Technology (NTNU), Trondheim, Norway, for partial fulfillment of the requirements for the degree of philosophiae doctor.

The doctoral work has been carried out at the Department of Energy and Process Engineering (NTNU), with professor Ole Jørgen Nydal as supervisor (NTNU), professor Even Solbraa(NTNU) and professor Daniel Karunakaran (University of Stavanger) as co-supervisors.

The work has been fully financed by Subsea 7 AS and the Norwegian Research Council and was carried out from August 2015 to July 2021.

Acknowledgements

First of all, I would like to thank my main supervisor, professor Ole Jørgen Nydal, for the constant support, valuable advice, and interesting discussions that helped me with both experimental and modeling work.

I want to express my gratitude to my co-supervisor, Even Solbraa, for helping me understand oil phase behavior and to my co-supervisor Daniel Karunakaran for double-checking the ideas and keeping me focused on the target.

I am grateful to professor Luis Fernando Azevedo and his team from PuC-Rio Brazil for allowing me to visit their laboratory and for sharing their knowledge.

I would like to thank my superiors in Subsea 7: Sigbjørn Daasvatn, Petter Moen, and Thomas Sunde, who made this Ph.D. work possible.

Also, my thanks go to the Norwegian Research Council for partly financing the work.

I want to thank my Subsea 7 colleagues Øivind Stangeland and Torstein Meling, who were making the mechanical design of the WCS for the highest level of collaboration, and Lee Thompson for the help with the design of the WCS qualification stand.

My special thanks to professor Curtis Whitson from the NTNU petroleum department for inspiration and first-hand insights into oil phase behavior.

Furthermore, I want to thank Markus Hays Nielsen from NTNU for his help, challenging questions, and valuable ideas.

Finally, my deepest gratitude goes to my wife Svetlana for her patience and support during all these years of Ph.D. work.

Contents

List of Figures

List of Tables

Chapter 1

Introduction

1.1 Motivation

Currently, there is no practical way to tie back subsea waxy oil fields in Arctic regions with distances to shore more than 50 km, with 50 km being an approximate economical border between gain and spendings on maintaining the oil flow. A major problem is the formation of wax and hydrates in an oil pipeline. Waxes are heavy oil components that usually solidify at temperatures below 60 °C. Hydrates are crystalline structures that form from binding between light hydrocarbons and water molecules. The appearance of hydrates can be prevented by removing water from the multiphase mixture. The formation of wax cannot be prevented in the same way because when waxes are dissolved in the oil phase, it is hard to separate them from other oil components.

Oil has a temperature called WAT (Wax Appearance Temperature), at which wax starts to appear in a pipeline. This WAT could be in the range of 4-60 °C. The oil that comes from a well, in most cases, has a temperature above the wax appearance conditions, so all waxes are in liquid form. While oil is transported in a pipeline on a seabed, the oil temperature drops towards the ambient conditions. The ambient temperature can be below -1 °C for areas close to the Arctic. Eventually, conditions in a pipeline enable the appearance of wax. Wax forms on pipeline walls as the walls have a lower temperature than the bulk. As wax sticks to the walls, it gradually reduces the pipeline diameter and can lead to pipe blockage.

Existing solutions for controlling wax are: maintaining temperature in a pipeline above the appearance conditions, regular pigging, or processing oil at a field on a platform/floating platform. Maintaining the higher temperature is achieved using insulation of a pipeline and active heating. However, at distances above 50 km, the insulation and heating solution requires a non-practical amount of energy and

becomes economically costly. Scraping off the wax from pipeline walls with pigs can be unreliable and impractical for long pipelines and brings other challenges for oils with high wax content. Regarding the floating/stationary process facilities at fields in the Arctic, the main problem comes from the inability to maintain such facilities for the whole year due to ice and icebergs. Production should be shut down in most cases until the danger of damaging the facility by ice or iceberg is removed, for example, by towing an iceberg away from the facility.

"Cold flow" is another possible solution for a tie back that has been considered in research projects for hydrate and wax control, Akpabio [2013]. "Cold flow" is a fluid flow in a pipeline at ambient temperature. Without temperature gradient, there is no wax deposition on the pipe wall and, hence, no risk of blockage Merino-Garcia and Correra [2008]. However, as "cold flow" operates under ambient temperatures, the oil must be cooled down to ambient.

Initially, the plan was to develop a subsea facility unit WCS (Wax Control System). The system will cool dewatered multiphase gas/oil well fluid to ambient in a controlled manner with a suitable wax management method and allow for the "cold flow" solution for a tie back. However, the experiments with pigging showed that pig behavior in multiphase flow is not suitable for the WCS flow loop. So the work focus was shifted towards WCS operation in single-phase flow. The thesis focuses on experimental and modeling work related to the development of WCS as a part of a production facility that can be installed subsea for enabling long-range tiebacks to shore using the "cold flow" concept. Current WCS design assumes operation with single-phase flow. Being placed at the start of a tieback flowline, WCS can feature a pump for boosting pressure to a level when a multi-phase gas/oil flow becomes a single-phase fluid flow.

1.2 State of wax deposition and pigging technology

The wax control system idea is to force wax deposition inside the cooling loop with subsequent pigging of the loop using a pig. The pig should circulate in the loop until it is worn enough to be sent to shore and replaced with a new pig from a pig magazine. Hence, the topics of interest for building the system and system model are wax deposition and pig behavior.

1.2.1 Wax deposition

A petroleum reservoir fluid consists of an enormous amount of different types of molecules. The generic approach is to group molecules based on the similarity of their structure and properties. Some of those groups are heavy paraffinic

groups/compounds that can change their state from liquid to solid. The solid form is called wax. More information can be found in Pedersen et al. [2015] Chapter 11. When oil is warm enough, wax molecules are integral to the total fluid. It is not possible to separate them from the total fluid. Cooling of a pipeline happens from the pipeline wall, meaning the temperature at the wall is always lower than the temperature at the bulk. Hence, wax precipitates from liquid to solid form at the pipeline wall and tends to stick to the wall reducing the pipeline diameter over time. An ideal, but unrealistic, situation would be if wax precipitated in the bulk as small particles that do not block the flow.

The WCS flow loop cools the fluid to the ambient, so wax precipitates and sticks to the wall (deposits) only inside the loop. The amount of the wax deposits, i.e., the wax layer thickness, should be predicted to be able to design the flow loop and assess the required pigging frequency.

The existing research covers single-phase wax deposition in more detail; Aiyejina et al. [2011], Olajire [2021]. The research on multiphase wax deposition phenomena is quite limited so far; Sarica and Panacharoensawad [2012], Rosvold [2008]. Some single-phase wax deposition models are described in Azevedo and Teixeira [2003], Singh et al. [2000], Singh et al. [2001], Venkatesan and Fogler [2004], Zheng et al. [2017], Banki et al. [2008], Hoteit et al. [2008] and they tend to be mechanistic. Multiphase wax deposition models have an empirical background and require empirical coefficients input due to the complexity of the flow; examples are Matzain [1999], Matzain et al. [2002], Rygg et al. [1998].

An attempt will be made to select and adjust the most applicable wax deposition model for the conditions of the WCS. Also evaluated will be: the requirement to include wax mechanical properties variations due to aging Bai and Zhang [2013], effect of operating temperature Lin et al. [2011], and other flow conditions Venkatesan et al. [2005].

1.2.2 Pigging

Pigging is generally an operation of cleaning a pipeline with a device called a pig, Figure 1.1. The cleaning is done by the mechanical scraping off debris from a wall by brushes or cleaning discs mounted on the pig.

Pigs without a bypass

Pigs that close the full bore of the pipe, restricting fluid from passing through the pig, are called conventional pigs or pigs without a bypass. These pigs are simplest

to make and to predict their behavior in a pipeline. However, the downside is that scraped debris piles just in front of the pig. This pile, or in the case of scraping wax "wax candle", in front of the pig can have a length in the range of hundred meters. The candle can be a reason for pipeline blockage, and a pig receiving facility should be able to accommodate it.

Pigs with bypass

Pigs with bypass are solving the issue of the debris pile. These pigs have some bypass allowing a portion of the fluid to pass through, see Figure 1.2. This makes the pig travel slower than average fluid velocity, so flow carries debris away from the pig. The downside is that the bypass pigs are more prone to get stuck than conventional pigs if the bypass hole is sized wrongly.

Special pigs

Pigs that do not have cleaning as the primary purpose can be seen as special pigs. It is possible to install special equipment on a pig to inspect a pipeline from the inside. Then "PIG" can be seen as an abbreviation of Pipeline Inspection Gauge. In comparison, a normal cleaning pig might have been named so due to its sound during cleaning. Another example of a special pig is a dewatering pig to act as a seal between gas/oil and water media when removing water from a pipeline during commissioning. Yet another special pig is a welding pig used for welding pieces of pipe and, if left inside a pipeline according to the procedure, removed from a completed pipeline during commissioning.

1.3 Research objectives

The main goal of the research is to understand the operational behavior of a specifically designed cooling loop related to wax deposition and pigging. The objectives of the research are:

- Perform experimental checks to find an optimal way to operate the WCS loop.
- Develop a suitable mathematical-physical model for predicting wax deposition inside the WCS loop.
- Make software based on the mathematical-physical model. The software should facilitate the design of the WCS loop.

Fig. 1.1—*A six-inch pig. ICberg7,*
CC BY 3.0 US <https://creativecommons.org/licenses/by/3.0/us/deed.en>, via Wikimedia Commons

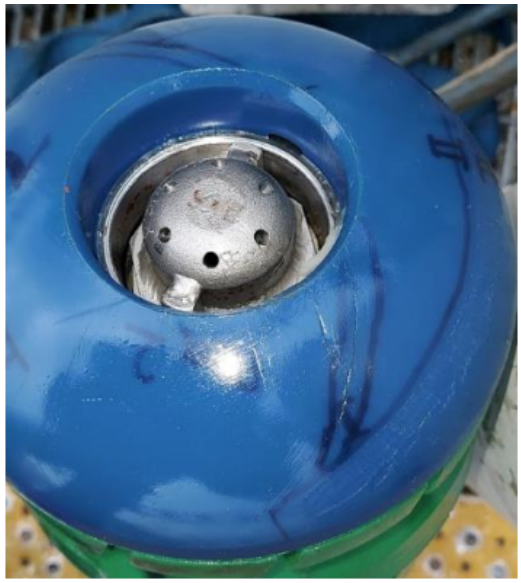

Fig. 1.2—*A pig with bypass holes in the center.*

1.4 Thesis overview and author contribution

The chapters are organized such that they can be read independently. They reflect a timeline of the development of the WCS cooling loop from pilot experimental checks toward the validation of the two-dimensional mathematical model for wax deposition prediction inside the WCS. All work presented in the thesis was carried out solely by the author except for the WCS overall qualification test, where the work was split between Øyvind Stangeland, Sigbjørn Daasvatn and the author, Stangeland et al. [2021]. The author's contribution to the qualification test was the general design of the loop, selection of the test fluid, selection of the test regimes relevant for wax deposition, prediction, post-processing, and presentation of results relevant for wax deposition. Øyvind Stangeland and Sigbjørn Daasvatn were working with other parts of the WCS: automated pig launcher, special directional flow valve, pig, and control system. They were also in charge of the mechanical design and assembly of the test rig. The author helped with the design of the pig and design of the directional flow valve.

- Chapter 2 presents the overview of the experiments performed for this thesis work: pilot experimental check of the idea, lab-scale bypass pigging in multiphase flow, lab-scale wax deposition in multiphase flow, qualification test of WCS. Note that the pilot check is described in more detail in the overview chapter, while other experiments are presented in separate chapters. The pilot check was only to get an initial understanding and demonstrate the feasibility of the setup.
- Chapter 3 focuses on the lab-scale bypass pigging in multiphase flow. The work was done solely by the author.
- Chapter 4 focuses on the lab-scale wax deposition in multiphase flow. The work was done solely by the author.
- Chapter 5 presents the qualification testing of the WCS system. The work split is described above and in the introduction to the chapter.
- Chapter 6 presents the mathematical-physical model. The author developed both the model and the C++ computer code implementation.
- Chapter 7 focuses on the wax deposition prediction in the WCS system. The chapter provides details of the developed mathematical model validation against the results obtained from the qualification test. The work was done solely by the author.
- Appendix A presents the derivation of the equations used in the WCS mathematical-physical model.

1.5 References

[1] Aiyejina, A., Chakrabarti, D. P., Pilgrim, A., and Sastry, M. 2011. Wax formation in oil pipelines: A critical review. *International Journal of Multiphase Flow* **37** (7): 671–694. https://doi.org/10.1016/j.ijmultiphaseflow.2011.02.007

[2] Akpabio, M. G. 2013. Cold flow in long-distance subsea pipelines. Master's thesis, Norwegian University of Science and Technology.

[3] Azevedo, L. F. A. and Teixeira, A. M. 2003. A critical review of the modeling of wax deposition mechanisms. *Petroleum Science and Technology* **21** (3): 393–408. https://doi.org/10.1081/LFT-120018528

[4] Bai, C. and Zhang, J. 2013. Effect of carbon number distribution of wax on the yield stress of waxy oil gels. *Industrial & Engineering Chemistry Research* **52**: 2732–2739.

[5] Banki, R., Hoteit, H., and Firoozabadi, A. 2008. Mathematical formulation and numerical modeling of wax deposition in pipelines from enthalpy-porosity approach and irreversible thermodynamics. *International Journal of heat and mass transfer* **51**.

[6] Hoteit, H., Banki, R., and Firoozabadi, A. 2008. Wax deposition and aging in flowlines from irreversible thermodynamics. *Energy and fuels* **22**.

[7] Lin, M., Li, C., Yang, F., and Ma, Y. 2011. Isothermal structure development of qinghai waxy crude oil after static and dynamic cooling. *Journal of Petroleum Science and Engineering* **77** (3): 351 – 358. https://doi.org/10.1016/j.petrol.2011.04.010

[8] Matzain, A. 1999. *Multiphase flow paraffin deposition modeling.* PhD thesis, University of Tulsa.

[9] Matzain, A., Apte, M., Zhang, H., Volk, M., and Brill, J. 2002. Investigation of paraffin deposition during multiphase flow in pipelines and wellbores part1:experiments. *Journal of energy resources technology* **124** (3): 180–186. https://doi.org/10.1115/1.1484392

[10] Merino-Garcia, D. and Correra, S. 2008. Cold flow: A review of a technology to avoid wax deposition. *Petroleum Science and Technology* **26** (4): 446–459. https://doi.org/10.1080/10916460600809741

[11] Olajire, A. A. 2021. Review of wax deposition in subsea oil pipeline systems and mitigation technologies in the petroleum industry.pdf. *Chemical Engineering Journal Advances* **6**. https://doi.org/10.1016/j.ceja.2021.100104

[12] Pedersen, K. S., Christensen, P. L., and Shaikh, J. A. 2015. *Phase behaviour of petroleum reservoir fluids*. CRC Press, 6000 Broken Sound Parkway NW, Suite 300, 2 edition.

[13] Rosvold, K. 2008. Wax deposition models. Master's thesis, Norwegian University of Science and Technology.

[14] Rygg, O. B., Rydahl, A. K., and Rønningsen, H. P. 1998. Wax deposition in offshore pipeline systems. *Proc.,* North American conference; 1st, Multiphase technology, Banff, Canada, 10-11 Jun. EDB-00:038742.

[15] Sarica, C. and Panacharoensawad, E. 2012. Review of paraffin deposition research under multiphase flow conditions. *Energy&Fuels* **26** (7): 3968–3978. https://doi.org/10.1021/ef300164q

[16] Singh, P., Venkatesan, R., Fogler, H. S., and Nagarajan, N. 2000. Formation and aging of incipient thin film wax-oil gels. *AIChE Journal* **46** (5): 1059–1074.

[17] Singh, P., Venkatesan, R., Fogler, H. S., and Nagarajan, N. 2001. Morphological evolution of thick wax deposits during aging. *AIChE Journal* **47**.

[18] Stangeland, Ø., Sigbjørn, D., and Novoseltsev, Y. 2021. Qualification of wax control system. *Proc.,* Offshore Technology Conference, Houston, Texas, USA, 16-19 August.

[19] Venkatesan, R. and Fogler, H. S. 2004. Formation and aging of incipient thin film wax-oil gels. *AIChE Journal* **50**.

[20] Venkatesan, R., Nagarajan, N., Paso, K., Yi, Y.-B., Sastry, A., and Fogler, H. S. 2005. The strength of paraffin gels formed under static and flow conditions. *Chemical Engineering Science* **60**: 3587–3598. https://doi.org/10.1016/j.ces.2005.02.045

[21] Zheng, S., Saidoun, M., Palermo, T., Mateen, K., and Fogler, H. S. 2017. Wax deposition modeling with considerations of non-newtonian characteristics: Application on field-scale pipeline. *Energy & Fuels* **31** (5): 5011–5023. https://doi.org/10.1021/acs.energyfuels.7b00504

Chapter 2

Description of experimental setups and experiments

The purpose of this chapter is to give an overview of the experiments and the facilities. Summaries of each experimental setup are given in the chapter's sections. The chapter also discusses the reasons for the experiments.

Nomenclature

$CFD -$	Computational fluid dynamics
$IK -$	IK group, provider of services for pipelines
$NTNU -$	Norwegian university of science and technology
$WCS -$	Wax control system

2.1 Introduction

The wax control system (WCS) that Subsea 7 developed is a counter-current pipe-in-pipe heat exchanger in the form of a cooling loop. It features an oil inlet, an oil outlet, a cleaning pig circulating inside the loop until sent to the outlet, and cooling water flowing in the annulus opposite the oil. This setup has an inherent challenge in directing oil to the outlet while returning the pig to the loop. The problem of allowing oil to enter and exit the loop while forcing the pig to say inside the loop have two main solutions:

- An active control system, where the valves are operated depending on the current pig position in the loop.

- A passive mechanical system, where the pig is forced into the loop by pure mechanical construction. The only active valve is the valve directing pig outside the loop

Initially, the decision was to try a passive mechanical system as a potentially more robust solution. The pilot experiment was conducted to check the solution's robustness and feasibility.

Then, as the intention was to operate WCS in multiphase flow, the bypass pigging and lab-scale wax deposition experiments were run.

Combined with a literature study on multiphase flow and wax deposition, those three experiments showed that a single-phase fluid and an active control system is the most robust and predictable choice at the current state. The single-phase flow could be achieved by installing an export pump in front of the system to boost the pressure forcing the single-phase or by separating the gas upstream of the WCS.

The final experiment was a qualification experiment to show that the complete system was working as intended and the prediction of wax deposition was reasonable.

Summary of experiments:

- Continuous pigging of a closed loop in single-phase flow. It was a pilot experiment to assess the feasibility of pigging in a closed loop without an externally driven valve control system. The experiment was performed at IK facilities, Stavanger.
- Lab-scale bypass pigging in multiphase flow. The experiment was performed at NTNU facilities, Trondheim.
- Lab-scale wax deposition in multiphase flow. The experiment was performed at NTNU facilities, Trondheim.
- Qualification test of the wax control system. The qualification was performed at Subsea 7 facilities, Dusavik, Stavanger.

2.2 Continuous pigging of a closed loop in single-phase flow

The first test was dedicated to checking the possibility of directing a pig inside the loop only by mechanical means without an active control system. The idea was to make T connections for an oil outlet and an oil inlet close to each other with a non-return valve between them, so the pig was forced to move straight through the non-return valve propelled by the inertia of the fluid in the loop while the oil was turned to the outlet, 2.1. Based on several CFD simulations, the valve was optimized to facilitate the pig passage, 2.3. However, even in the simulations

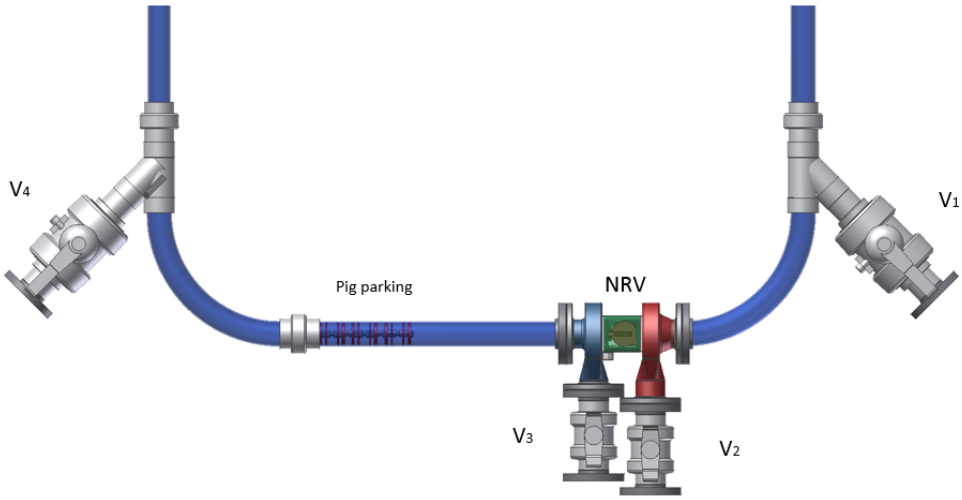

Fig. 2.1—***Pig direction valve.***

representing ideal conditions, the pig tended to be stuck at the non-return valve position. The system was susceptible to parameters like flow velocity, amount of air bubbles in water, and the diameter of the valve bore.

The test showed that even if the pig properly passed for specific settings, Figures 2.4 and 2.5, the pig indeed had a high tendency to get stuck; any pressure fluctuation, a tiny mistake in the machining of the valve, or a change in flow velocity could cause the pig to stop at the non-return valve. Such a condition was not acceptable as a stopped pig at that location would nearly block production and generate high-pressure spikes. The conclusion was that the system was not robust. However, one of the assumptions was that the poor quality of the valve was the main reason. So another attempt was made.

The valve was modified and made from a transparent material. The modifications and better finishing did lead to improvements in the pig's behavior. The pig with a bypass hole could also circulate in the loop. The stuck condition became less frequent than in the first experiment. However, there were occasions when the pig stopped in the valve, 2.6. The conclusion was that the pure passive mechanical system was not robust enough at the pilot scale. It was assumed that the inertia stored in the loop could allow for a higher push force to propel the pig through the valve on a bigger scale. Another issue was related to the wear of the non-return valve, which, for the real scale system, had to open/close due to the pig 1-4 times a day. It could be the limiting factor for a system designed for at least 20 years of design life.

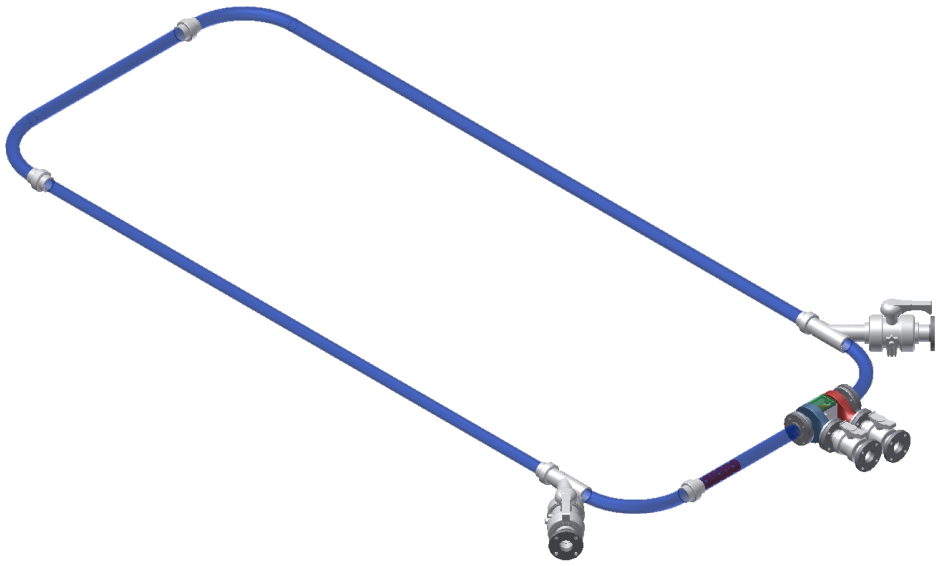

Fig. 2.2—*Flow loop.*

2.3 Lab scale bypass pigging in multiphase flow

The pigging in multiphase experiment flow was performed at the NTNU premises in Trondheim, Figure 3.2. The complete description of the experiment is available in chapter 3. The fluids used were water and air. Flow conditions studied were stratified and slugging; the annular flow was considered outside the applicability range for WCS.

The main observation was that bypass pig forms a slug train or a long continuous bubbly slug depending on the gas velocity. This slug may pose a problem to a valve control system of the WCS that should direct the pig either back into the loop or out to an export pipeline.

2.4 Lab scale wax deposition in a multiphase flow

A lab-scale multiphase experiment on a model waxy oil was performed at the NTNU premises in Trondheim, Figure 4.3. The full description of the experiment is available in chapter 4. The fluids used were Marcol oil 52 with different content of Sasol wax, air for the inner pipe, and water as cooling liquid in the annulus. Flow conditions studied were stratified and slugging.

One interesting observation was that deposition happened at the gas semi-sphere

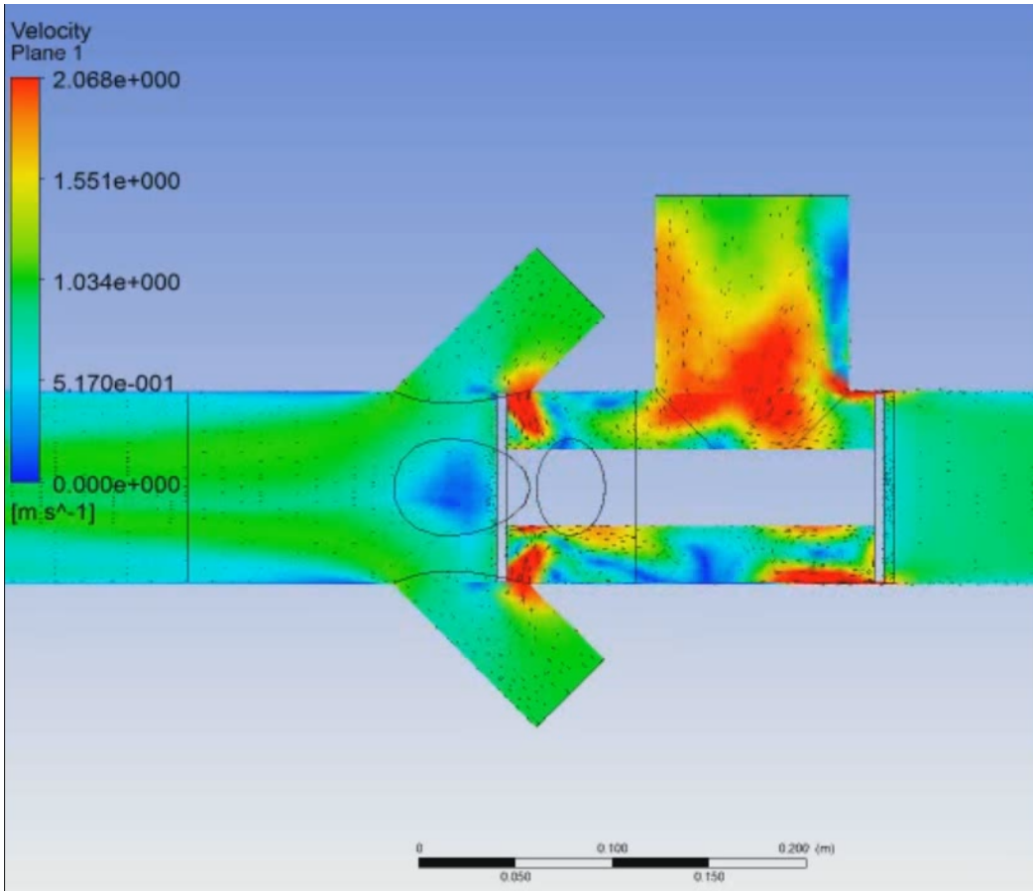

Fig. 2.3—***Pig passage simulation.***

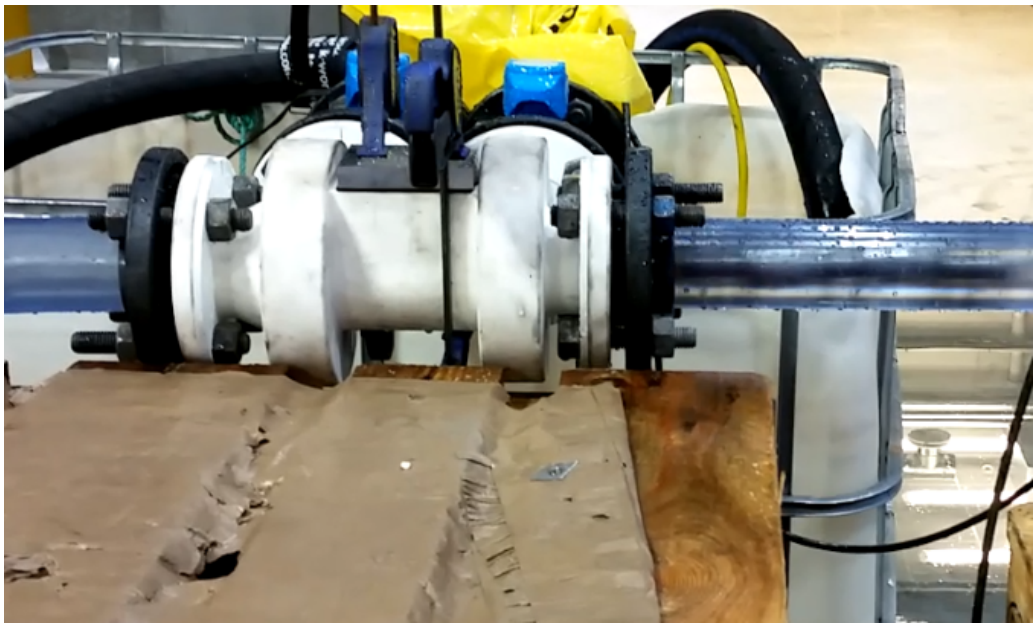

Fig. 2.4—*Pig entrance.*

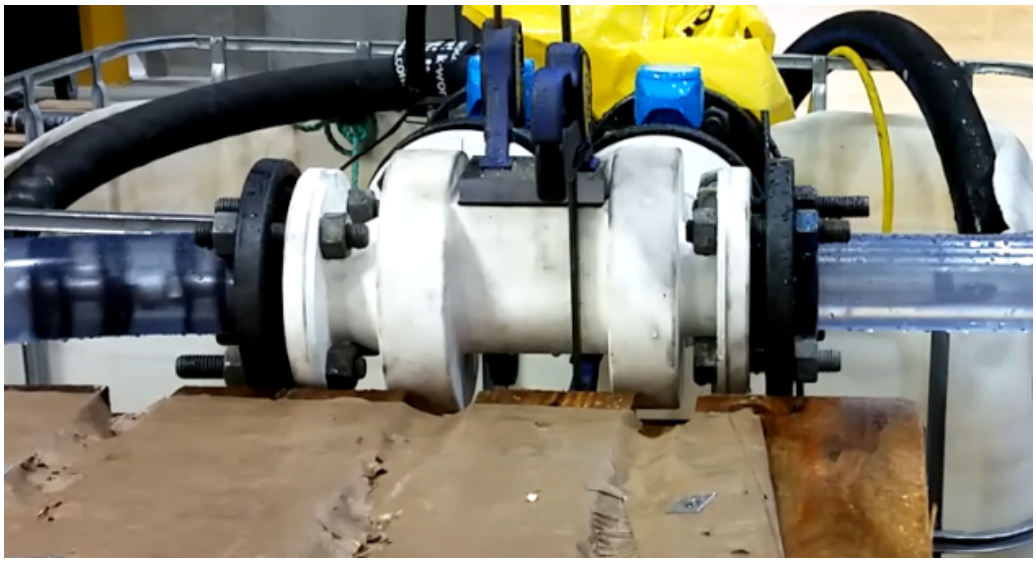

Fig. 2.5—*Pig exit.*

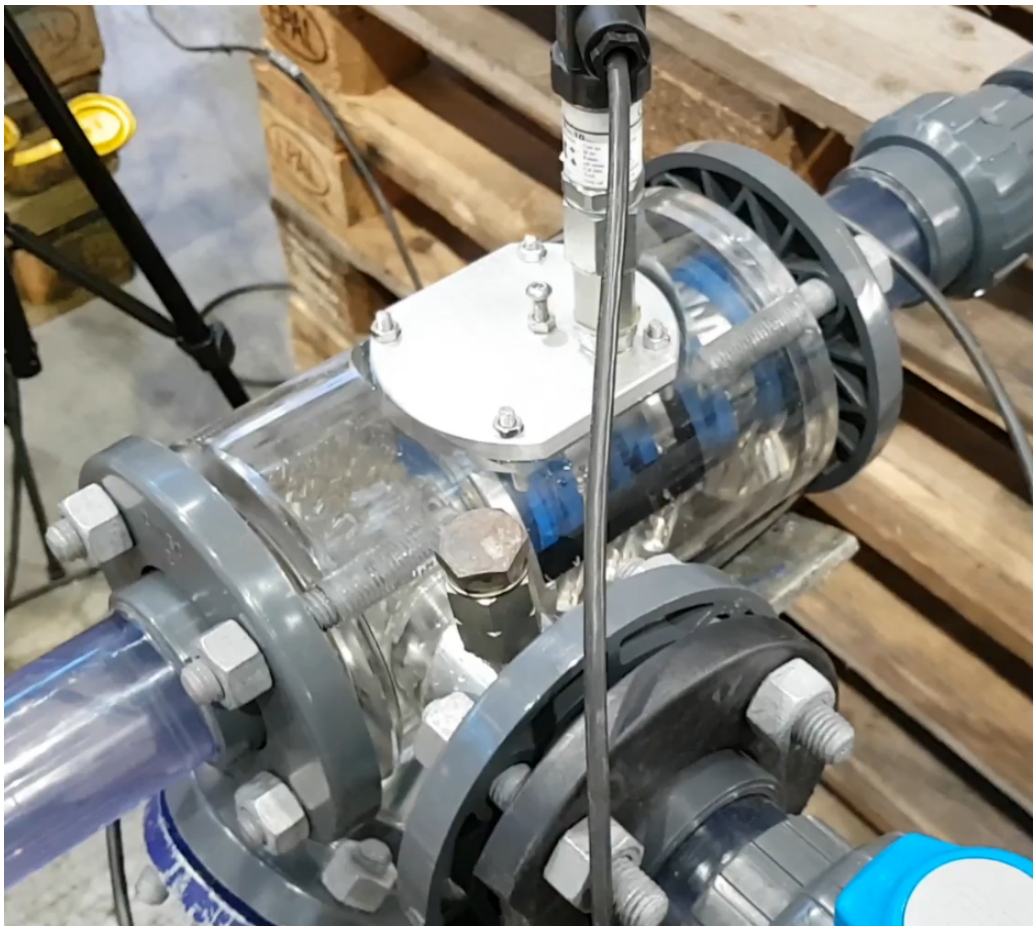

Fig. 2.6—*Pig (blue item) stuck in the modified valve.*

due to droplets in the stratified flow regime. Then the deposit grew. Upon reaching enough mass, it slid into the liquid region and dissolved. This process was continuously happening during the deposition experiment. It may mean that under force cooling conditions at pipeline locations, where the oil bulk temperature is still high enough to stop any deposition inside the liquid region, the deposition can still happen in the gas region.

2.5 Qualification test of wax control system

The qualification test of the complete WCS system, which includes a cooling loop, a pig launcher, a pig magazine, an active valve control system for directing the pig, and the pig itself, was performed at Subsea 7 premises in Dusavik, Stavanger, Figure 2.7. The description of the qualification is available in chapter 5, and the description of the simulation results of the wax deposition is available in chapter 7. The in-depth explanation of the mathematical-physical models used for the simulation is available in chapter 6.

It was found that the system performed as intended. The wax deposition prediction in the simulation was in line with the observed deposition.

Fig. 2.7—*WCS qualification stand.*

Chapter 3

Bypass pigging experiment in gas-liquid flow

Nomenclature

C_{pl}	–	Leakage factor, -
D_{pig}	–	Pig outer diameter, m
D_{pipe}	–	Pipe inner diameter, m
F_{static}	–	Static friction force, N
F_v	–	Viscous friction, N
F_{wf}	–	Wall friction, N
f_1	–	Linear friction factor, N·s/m
f_2	–	Quadratic friction factor, N·s^2/m^2
f_{wf}	–	Wall friction factor, N·s/m
Q_{fl}	–	Film leakage volumetric flow rate, m^3/s
U_{pig}	–	Pig velocity, m/s
U_{pl}	–	Pig leakage velocity, m/s
ΔP_{pig}	–	Pressure drop over a pig, Pa
ρ	–	Density, kg/m^3
v_f	–	Average film velocity, m/s

3.1 Introduction

From time to time, oil and gas pipelines require cleaning from wall deposits. Cleaning can be performed with various methods. The simplest and most used one is a

mechanical scraping off wall deposits from pipeline walls with a cleaning PIG device. Pig could be an abbreviation of Pipeline Inspection Gauge or just a name due to the sound they produce during cleaning. Pigs can have other purposes: pipeline inspection, measuring, and inhibitor distribution. Cleaning pigs are usually the most unsophisticated ones. Three different types can be distinguished: conventional without bypass, conventional with bypass, and pigs with a bypass with a specially designed nose to form a jet to clean the deposits using the energy of the bypassed liquid. A pig design overview is well presented in Quarini and Shire [2007].

A conventional pig acts as a moving sealing barrier and is propelled by the fluid pressure upstream. A pig without a bypass moves at the fluid velocity if the leak between the sealing disks and the pipe wall is negligible. Removed material accumulates in front of the pig and increases the required pressure difference to move the pig. One possible way to resolve this issue is by implementing a bypass. The bypass is usually a hole located in the middle of the pig to allow some fluid to pass through. A part of the fluid escapes through this hole, causing the average velocity of the pig to be smaller than the average velocity of the fluid. Hence, fluid carries scraped material away from the pig, preventing the material accumulation in front of the pig and subsequent increase in friction. Another important use of bypass pigging is to avoid slug catcher liquid overloading. One major downside of introducing a bypass is that the pig can become stalled more easily in some situations compared to a pig design without the bypass. Careful selection of the bypass hole size is required to match operating conditions. Changes in the conditions along a pipeline or during a lifetime must be considered. One of the design requirements for the bypass hole could be formulated in the following way: the rate of bypass should be more or equal to the rate of removed wax/debris, O'Donoghue [2004]. Another solution to changing conditions is making the bypass hole size dependent on the pig velocity, so the hole closes when the pig stops, and such closing removes the pressure leak through the hole, see Groote et al. [2015]. Special design pigs, like jetting pigs, have a bypass with a jetting arrangement. In this way, debris is removed with high fluid velocity streams rather than with mechanical scraping. Jets also facilitate pushing the material away from the pig. Several designs of jetting pigs are discussed in Southgate [2004]

Correct prediction of a pig behavior in a pipeline helps to estimate pig arrival times, assess pig efficiency, and reveal possible issues. Models could also predict the liquid slug size that a slug catcher should manage. A literature review shows some lack of knowledge on bypass pigging in multiphase flows. This chapter partially fills this gap by presenting experimental results for bypass pigging in an air-water small-scale flow loop. Experiments were performed as part of the Subsea 7 project of building a wax control system for long-distance tie-backs, where continuous

bypass pigging in a loop is used as a wax build-up prevention method.

3.2 Literature review of pigging in multiphase flow

The majority of publications have focused on the prediction of the behavior of pigs without bypass in single-phase flows and two-phase flows:

- Minami and Shoham [1995] Conducted experiments on passage of spheres in horizontal two-phase flow. They proposed a mathematical model and showed that their model prediction was close to the experimental results. The model uses a correlation for the liquid holdup in the slug region and features mass and momentum equations.
- Tolmasquim and Nieckele [2008] Looked into the modeling of pigging in single-phase gas flow with conventional pigs. They investigated the possibility of obtaining the desired pig motion by using a PID pressure controller for the driving pressure.
- Solghar and Davoudian [2012] modeled conventional pig motion in single-phase flow. They added the energy equation to the momentum and mass equations to describe the fluid and coupled the fluid to the pig motion equation.
- Nieckele et al. [2001] Estimated friction between pig and wall with structural buckling formulation and a structural solver, then coupled pig motion equation with one-dimensional single-phase flow equation.
- Lima [1999] Made a model for a pig in multiphase flow and conducted experiments on a conventional pig in a two-phase flow for a riser. The experimental stand had a 69 m length and featured a 9 m high riser section. The focus of their study was gas lift with the pig. During the experiments, it was found that gas leaked through the pig. Therefore, the model was adjusted to accommodate the gas leakage as a bypass in the pig.
- As part of his Ph.D. thesis, O'Donoghue [1996] described pigging research history and discussed the effect of wear on the pig. He presented a way to find the pig/wall friction based on several contact theories. The final implementation of the proposed friction model and pig motion model was made in the form of a computer program.
- Boghi et al. [2017] and Boghi et al. [2018] discuss a model in OpenFOAM of wax particle transport in a single-phase oil with a scraping pig. Their model is a 3D model, requiring a long computational time.

An important part of a pig model is a pig/wall friction model. Several authors studied the resistance force.

- Souza Mendes et al. [1999] propose a model that tries to predict the resistance caused by a wax layer.

- den Heijer [2016] presents a way of estimating frictional interaction between pig and wall and gives an overview of other models available in the literature.
- Southgate [2004] uses metal cutting models for estimation of resistances from removed material.

IJsseldijk [2016] researched bypass pig behavior in single-phase gas lines. Galta [2014] considers bypass pigging of wax in a single-phase oil pipeline. Research on bypass pigging in multiphase is limited. Liang [2015] investigated a flow around a bypass pig in stratified flow conditions. They used a 3D simulation of the domain that included a pig and a relatively small pipe section, so they did not couple the pig motion to the pipeline flow but focused on forces affecting the pig. Singh and Henkes [2012] looked into a flow through a pig bypass hole by performing a 3D simulation for single-phase and a 2D channel simulation for multiphase. The pig motion was not coupled to the flow. Olaniyan and Larrey [2014] compare results obtained from commercial software simulators OLGA and LEDAFLOW with actual field data for pigging in multiphase pipelines. The simulators are 1D, and pig motion is coupled to the flow.

3.3 Experimental stand

The flow loop consisted of three 15 m straight sections connected with flexible hose bends, see Figures 3.1 and 3.2. Hence, the total travel length for the pig was around 55 m, where 45 m of the path was along the straight sections. As shown in Figure 3.3, the pig was of bi-directional type composed of three bodies connected with flexible joints. The middle body had four guiding disks, whereas the left and right bodies had two sealing and two guiding disks. All sealing disks were perforated with four equal diameter holes yielding 4 % bypass area together. A transparent acrylic pipe with an ID of 60 mm was used for the straight sections. The flexible hose bends also had an ID of 60 mm. Ball valves operated from LabView software controlled the flow. The flow rates were measured with flow meters installed upstream of the control valves. Measuring equipment for pressure and liquid holdup was installed on the last straight section. All pressure sensors were Aplisence PCE-28 calibrated for 0-2 bara pressure. The pig was launched manually using a 3.5 bar air kick line from the pig launcher and received at a pig catcher at the end of the last straight section line. The design of the catcher and the launcher were the same, Figure 3.4. Video recording was done with a GoPro HERO4 and with four Basler cameras. The GoPro was used to record the complete stand overview, while the Basler cameras were used to record the last straight section with a high frame rate resolving the flow around the pig.

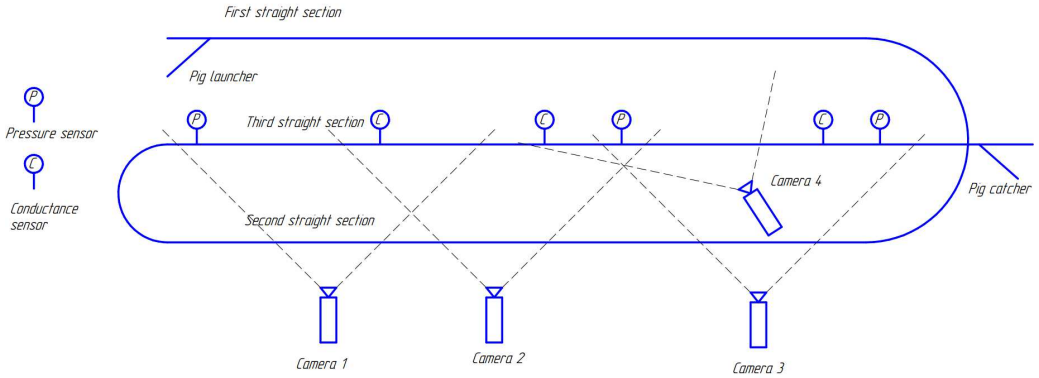

Fig. 3.1—*Stand overview.*

Fig. 3.2—*NTNU multiphase flow loop.*

Fig. 3.3—*Pig in transparent section.*

Fig. 3.4—***Pig launcher and catcher.***

Table 3.1—*Instrumentation.*

Instrument	**ID**	**Range**	**Position**
Absolute Pressure sensor	P3	0-2 bar	0.1 m
Conductance ring	C1	0-1	2.1 m
Conductance ring	C3	0-1	7.0 m
Absolute Pressure sensor	P8	0-2 bar	8.2 m
Conductance ring	C6	0-1	11.1 m
Absolute Pressure sensor	P12	0-2 bar	13.0 m

Table 3.2—*TestMatrix.*

Water Flow, l/s	AirFlow, kg/h				
	7	29.9	66	109	170
0.3	O	L	W	W	T
0.51	L	L	W	W	O
0.62	O	L	O	O	O
0.8	O	L	O	O	O
1.12	L	L	O	L	O

T-stratified, L-slug, W-stratified wavy

O-not performed

3.4 Experimental procedure

Experiments were performed for a pig with a bypass area of 4 % of the internal pipe area. The friction was found by stopping the pig in the straight section between pressure sensors and then increasing airflow until the pig moved. The friction force was estimated from the measured pressure difference. Several flow conditions were studied, Table 3.2. The table gives information about the observed flow pattern before the insertion of the pig. Each test was done 3-5 times. The following procedure was adopted:

- Run flow condition until it showed a stabilized pattern. (Usually, this took around 5 minutes).
- Launch the pig by quickly opening and closing the air kick valve on the pig launcher. (Usually, this took less than a second).
- Stop the flow as soon as the pig enters the pig receiver.

The pig receiver had a somewhat smaller pipe than the main test acrylic pipe, and the pig had to turn to enter the pig receiver fully. There were events in which the pig got stuck in the receiver. This event enabled pressure spike measurement caused by a subsequent liquid slug hitting a pig, effectively measuring a liquid slug's kicking force (water hammer effect) on a stuck bypass pig. The following procedure was adopted for measuring the effect:

- Fill the pipe with approximately 0.2 liquid holdup.
- Increase air flow until slugs are generated in the flow loop.
- Accelerate a liquid slug that will hit the pig by increasing the flow further. The slug was accelerated in the final straight section, see Figure 3.1.

3.5 Results and discussion

The pig showed qualitatively different behavior depending on the flow conditions. The behavior could be split into four cases. The videos of the cases, represented in

Figures 3.5 to 3.12 are available in the folder "CH3" of the appendix to the thesis. Starting from low gas and liquid flow rates, the cases are:

- **Case 1**: Gas flow rate 7 kg/h, liquid flow rate 0.51 l/s. Gas velocity was insufficient to accumulate pressure behind the pig; gas escaped through the bypass. The pig moved when a liquid slug pushed it. Slugs also leaked through the bypass, so slugs moved faster than the pig. After the slug passage, the pig stopped and waited for the next slug. Figures 3.5 and 3.6 show a slug passing through the pig.
- **Case 2**: Gas flow rate 30 kg/h, liquid flow rate 0.3 l/s. At this gas flow rate, the gas partly accumulated behind the stationary pig, increasing the pushing pressure; at some point, the pressure was high enough to overcome pig-wall friction, and the pig started to move. While moving, the pig picked up the liquid film in front of it and generated a liquid slug that moved away from the pig. After traveling some distance, the pig stopped because the gas pressure behind the pig dropped below a level required to overcome friction. The generated liquid slug continued to travel downstream. The flow resembled slug flow for some distance in front of the pig. However, as the initial flow could not support slugs, the slugs generated by the pig eventually died out. See Figures 3.7 and 3.8.
- **Case 3**: Gas flow rate 66 kg/h, liquid flow rate 0.3 l/s. Gas velocity was high enough to maintain constant pig movement. Slugs in front of the pig had higher velocity than the pig because gas velocity in front of the pig was higher than the pig velocity. Each slug moved away from the pig. The flow along a certain length in front of the pig could be characterized as a series of slugs moving away from the pig. The larger the gas velocity, the smaller the distance between individual slugs in the series, see Figures 3.9 and 3.10. It is worth mentioning that for longer pipe lengths than those available in the experimental stand, the slug series length might take a constant value because the rate of new slugs generation at the pig could equal the rate of old slugs dying out.
- **Case 4**: Gas flow rate 109 kg/h, liquid flow rate 0.3 l/s. Gas velocity was high enough to maintain constant pig movement. It was not possible to distinguish individual slugs in front of the pig. The series of slugs converged into one single bubbly slug. The gas that leaked through the pig bypass made the whole slug look like a bubbly flow. The flow downstream of this pig-generated bubbly slug was the same as the flow with no pig present. See Figures 3.11 and 3.12.

Pig motion videos were post-processed with VirtualDub and Python with the OpenCV library to track the pig and produce position values over time. First, a video file was stripped from all static items in a frame. In this way only pig, slugs,

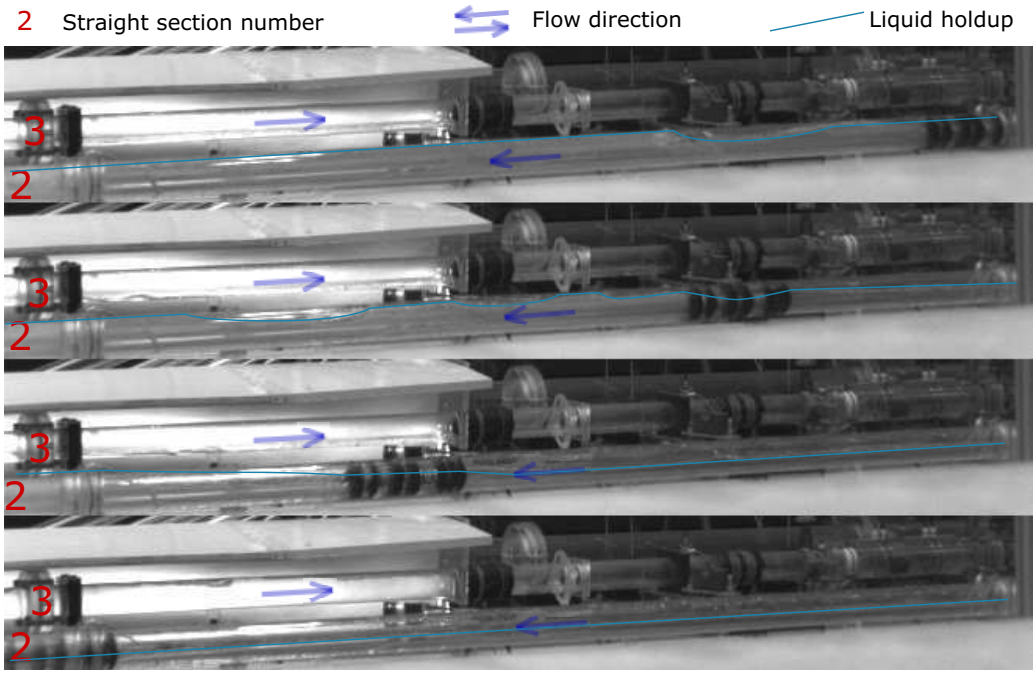

Fig. 3.5—*Case 1: slug leaking through pig at the second straight section.*

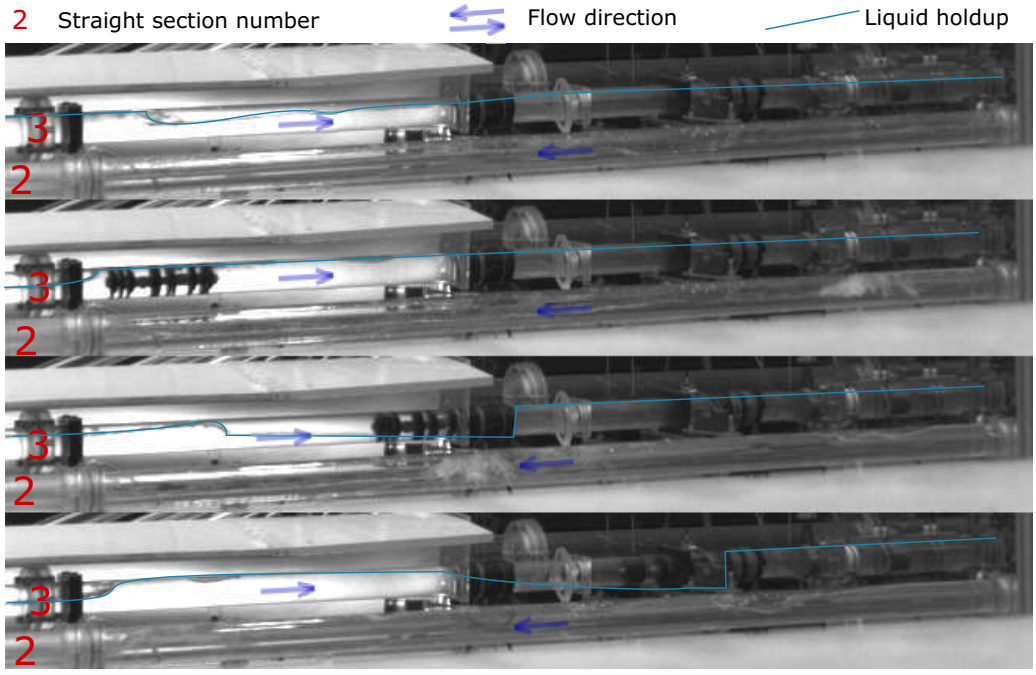

Fig. 3.6—*Case 1: slug leaking through pig at the third straight section.*

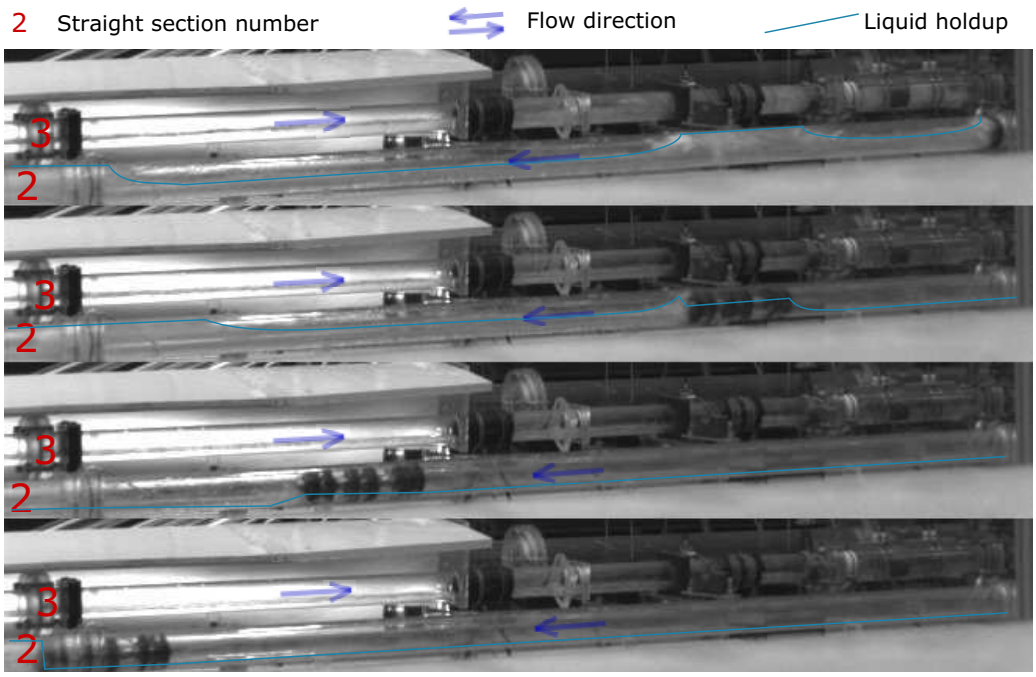

Fig. 3.7—*Case 2: pig pushed by gas accumulated behind at the second straight section.*

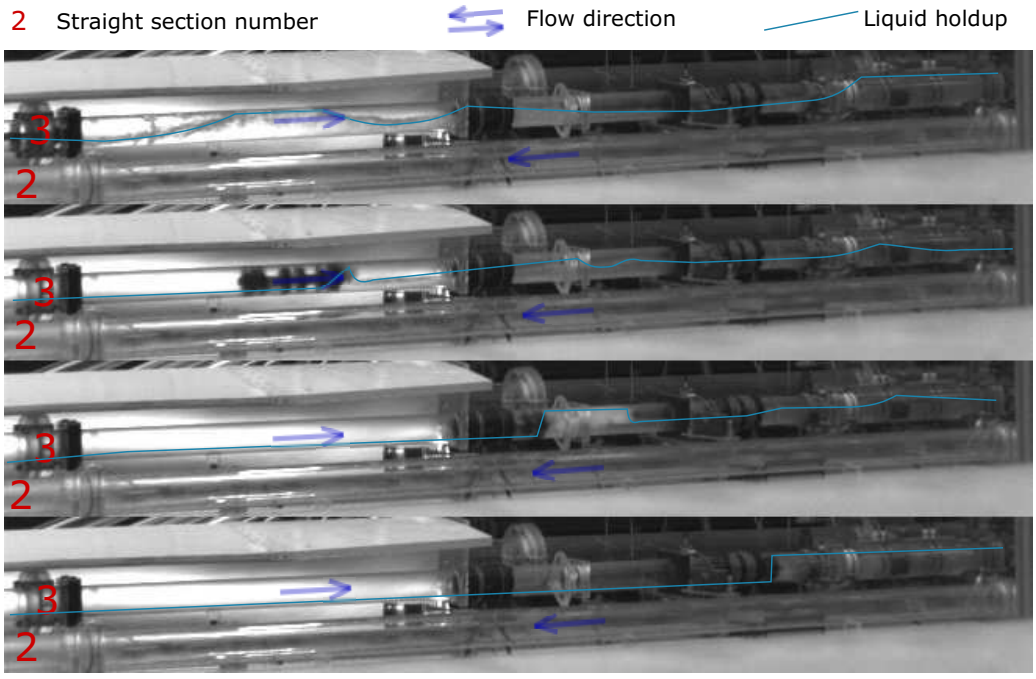

Fig. 3.8—*Case 2: pig pushed by gas accumulated behind at the third straight section.*

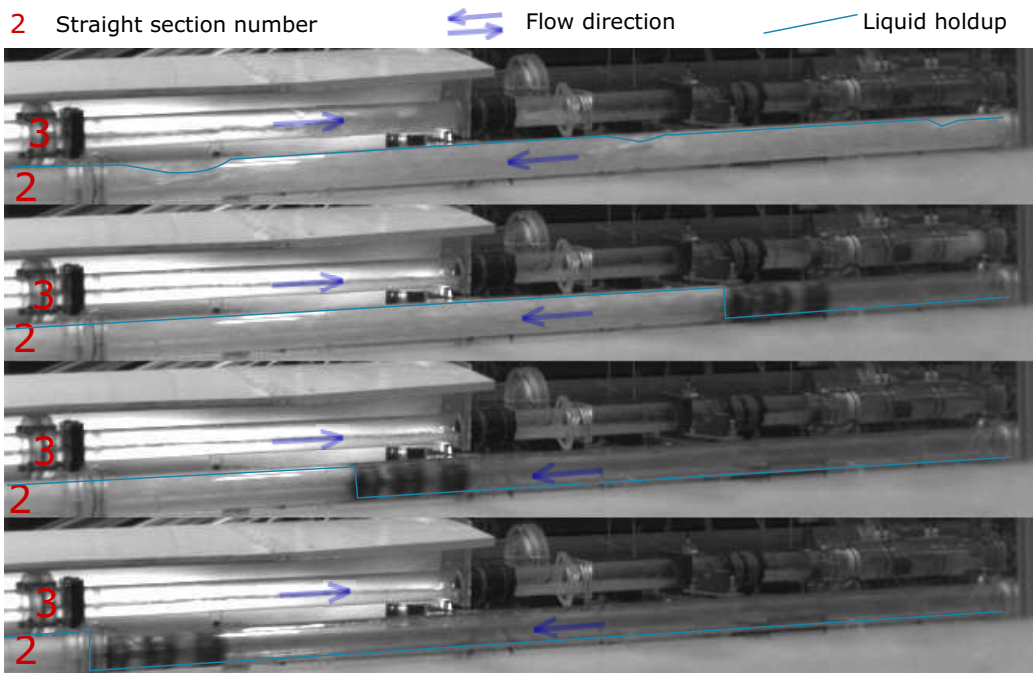

Fig. 3.9—*Case 3: pig constantly pushed by gas at the second straight section.*

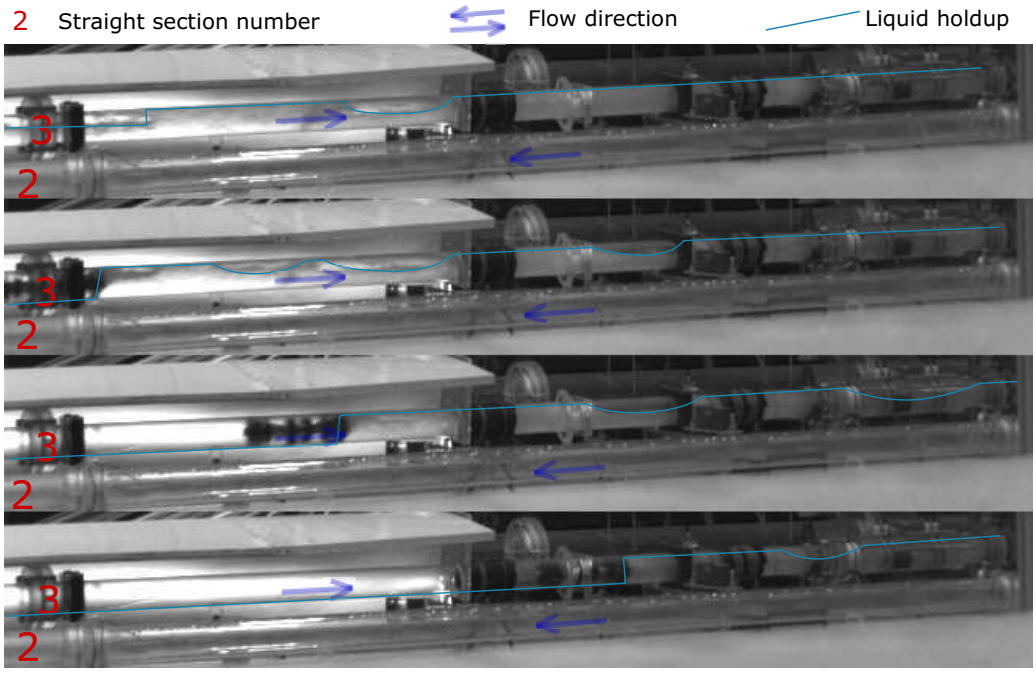

Fig. 3.10—*Case 3: pig constantly pushed by gas at the third straight section.*

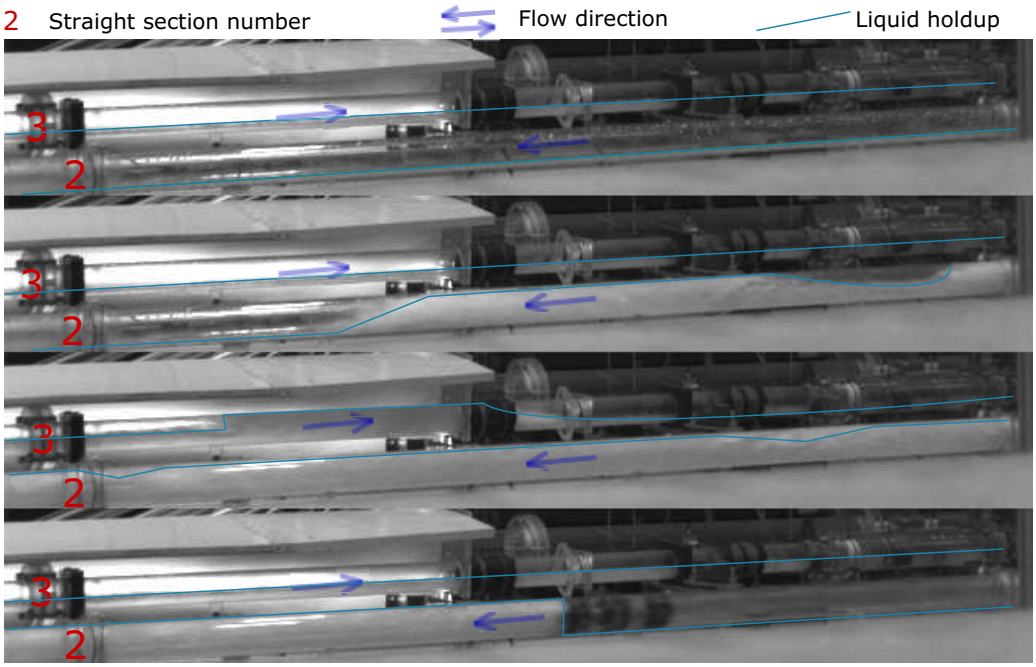

Fig. 3.11—*Case 4: bubbly slug in front of the pig at the second straight section.*

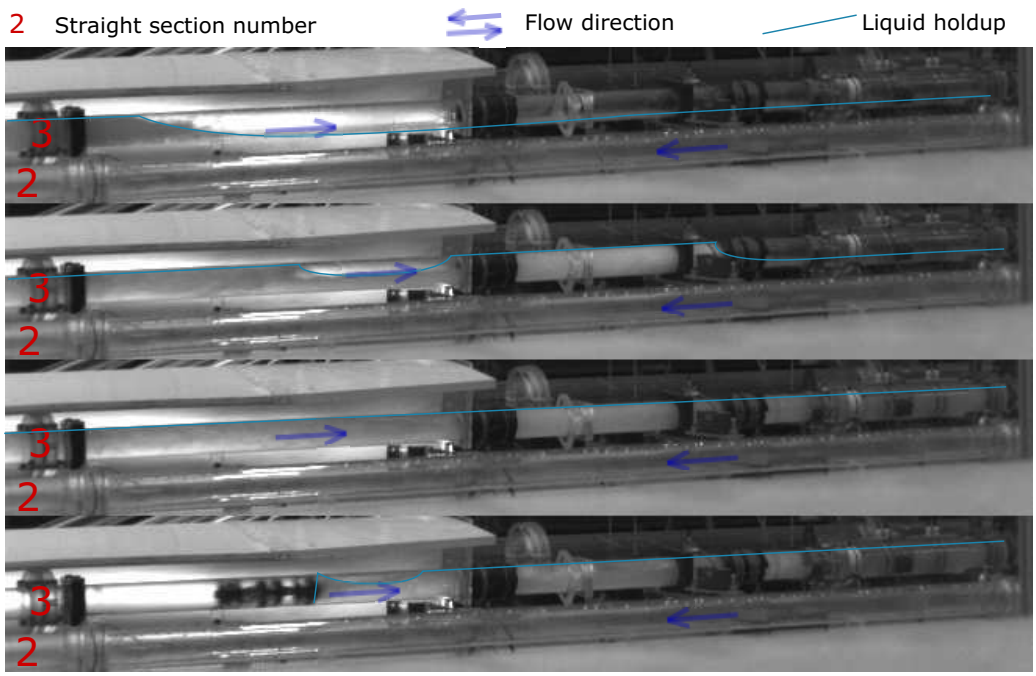

Fig. 3.12—*Case 4: bubbly slug in front of the pig at the third straight section.*

and the liquid-gas interface remained. Then the pig was tracked, and its position versus time was saved. Time history data from measuring sensors were matched with the pig position time history based on one of the two conditions: liquid holdup dropped to zero just after the pig had passed the conductance rings sensor, or liquid holdup rose to 1.0 when a clean liquid slug had entered conductance rings sensor. The first condition was relevant for the cases where the pig propelled by gas was removing liquid from the pipe. The second was relevant for a low gas flow rate when passing-through liquid slugs accelerated the pig. Results are presented in the Figures 3.13 to 3.16 that combine sensors time history and pig position time history. The graphs describe the pig passage through the third straight section. The sensors graph has six lines. Each line represents a reading from a corresponding sensor. The sensors locations are specified in Table 3.1 and shown in Figure 3.1. "C" are conductance sensors showing a liquid holdup. "PT" are pressure sensors showing absolute pressure in bara. The horizontal axis is the time axis, with the time set to 0 s when the pig passes the first pressure sensor, "PT3". The negative values on the time axis represent what happens before the pig arrives at the first pressure sensor. Vertical lines on the graph represent the moments when the pig is passing the corresponding sensor. The last conductance sensor, "C6", and the last pressure sensor, "P12", vertical lines deviate from the actual positions because of a position error coming from distortion in a recorded video image. The error is +/-3 %.

The **case 1** measurements are shown in Figure 3.13. It can be seen from the pig position graph that the pig movement was a start-stop process. The sensors' graph shows that liquid holdup readings spiked to 1.0, first on "C1", then "C3", and finally "C6" at negative values on the time axis. It tells that a liquid slug passed through the straight section before the pig arrived at the first pressure sensor. A close look at the period around the 20 s mark when the pig was stationary reveals that after passing the "C3" sensor, the pig stopped. During the period, there was a liquid slug passing "C1" ("C1" spike), then passing "C3" ("C3" spike). The pig started to move when the "C3" spiked, indicating that the slug propelled the pig. The pressure graph from "PT3" (the pressure sensor upstream of the stopped pig) shows a gradual pressure increase from the moment the pig stopped at "C3" until the slug fully passed the pig. For **case 1** the slugs were present before and after the pig, and the pig was propelled by the slugs.

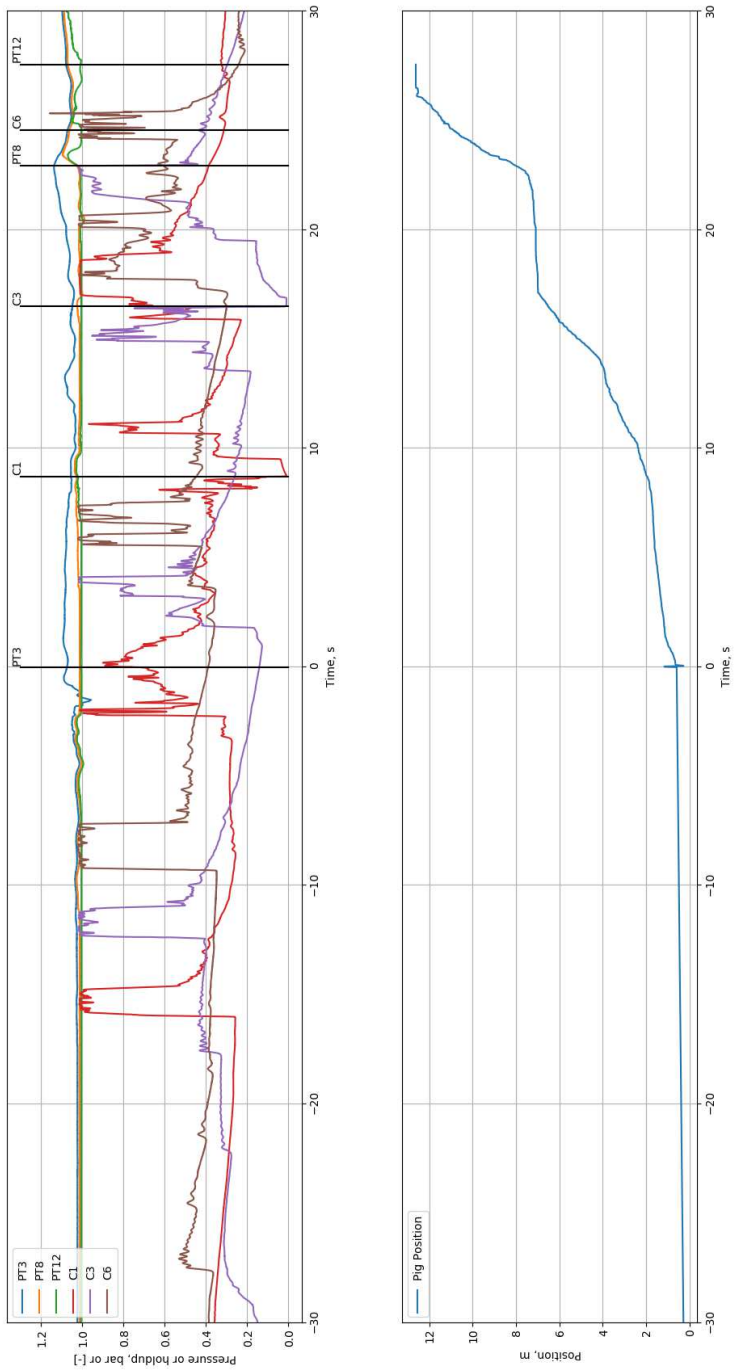

Fig. 3.13—*Case 1: gas 7 kg/h, liquid 0.51 l/s.*

The **case 2** measurements are shown in Figure 3.14. The pig propelled by gas moved faster than the non-disturbed liquid slugs. The sensor reading dropped to zero when the pig passed a conductance ring, indicating no liquid content. The pig velocity had relatively large fluctuations compared with its average velocity, as the gas had to accumulate behind the pig to drive it. Due to these fluctuations, slugs in front of the pig were separated by bubble sections. Based on liquid holdup readings, it could be seen that there was a sequence of slugs before the pig. Before the pig passage through a conductance ring, the holdup fluctuated between 0.2 and 1.0. After the pig passage, the pipe was filled with gas, dropping holdup readings to 0. The pig generated slugs in front and left the pipe free of liquid behind.

The measurements for higher gas flow rate condition, **case 3**, are shown in Figure 3.15. In this case, the pig was propelled by gas. After the pig had passed a conductance ring, the ring showed zero liquid content. The pig velocity had relatively small fluctuations compared with its average velocity. Hence, the bubble sections separating the slugs in the slug train were not as profound as in the lower gas flow rate case. The bubble sections in the train had liquid holdup >0.5 and a length of $\sim$5 times shorter than the liquid section. The pig generated a slug train in front of it. The pipe behind the pig was free of liquid.

The results with an even higher gas flow rate condition, **case 4**, are shown in Figure 3.16. The pig was propelled by the gas at a constant velocity. Conductance ring readings fluctuated between 0.6 and 1.0 during the bubbly slug passage and zeroed after the slug and pig had passed. The slug in front of the pig had a high gas content, and the gas content appeared to be relatively constant along its length. The pig generated a long bubbly slug in front of it and left the pipe free of liquid.

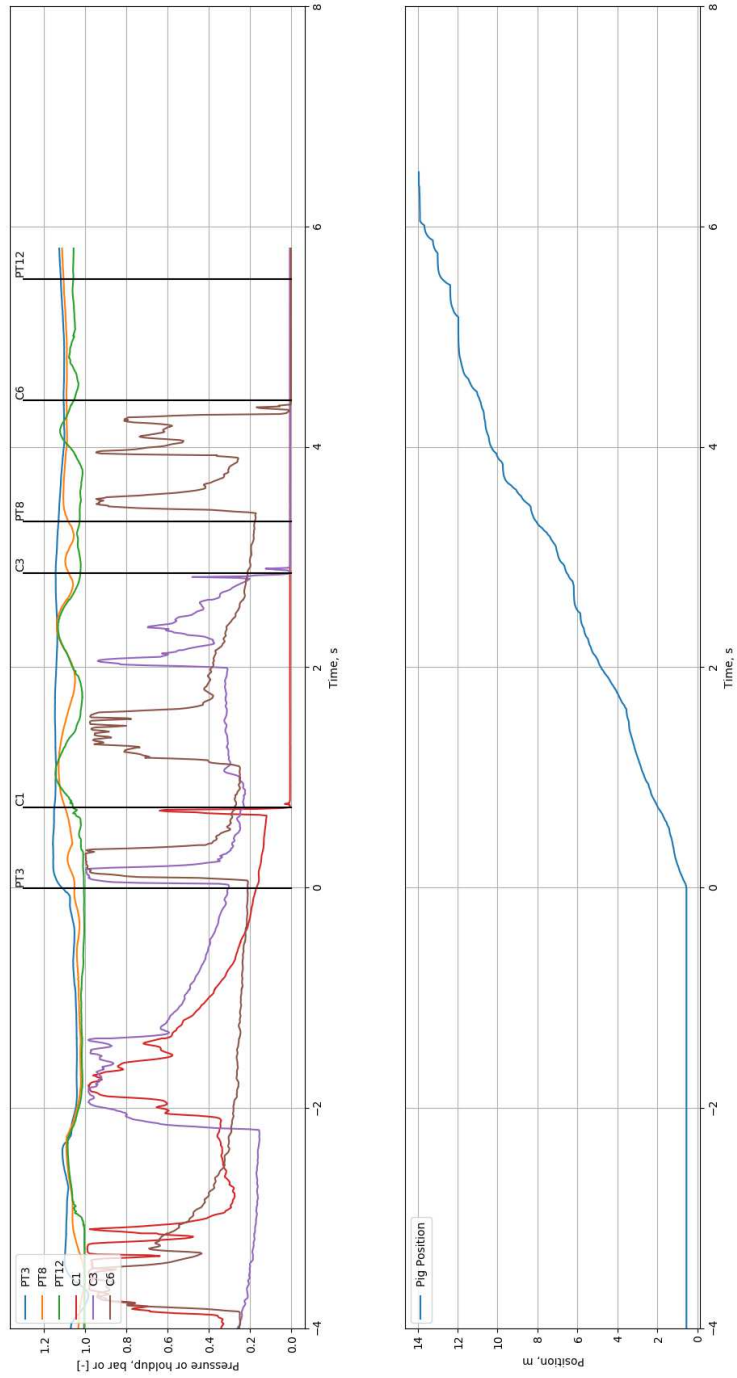

Fig. 3.14—*Case 2: gas 30 kg/h, liquid 0.3 l/s.*

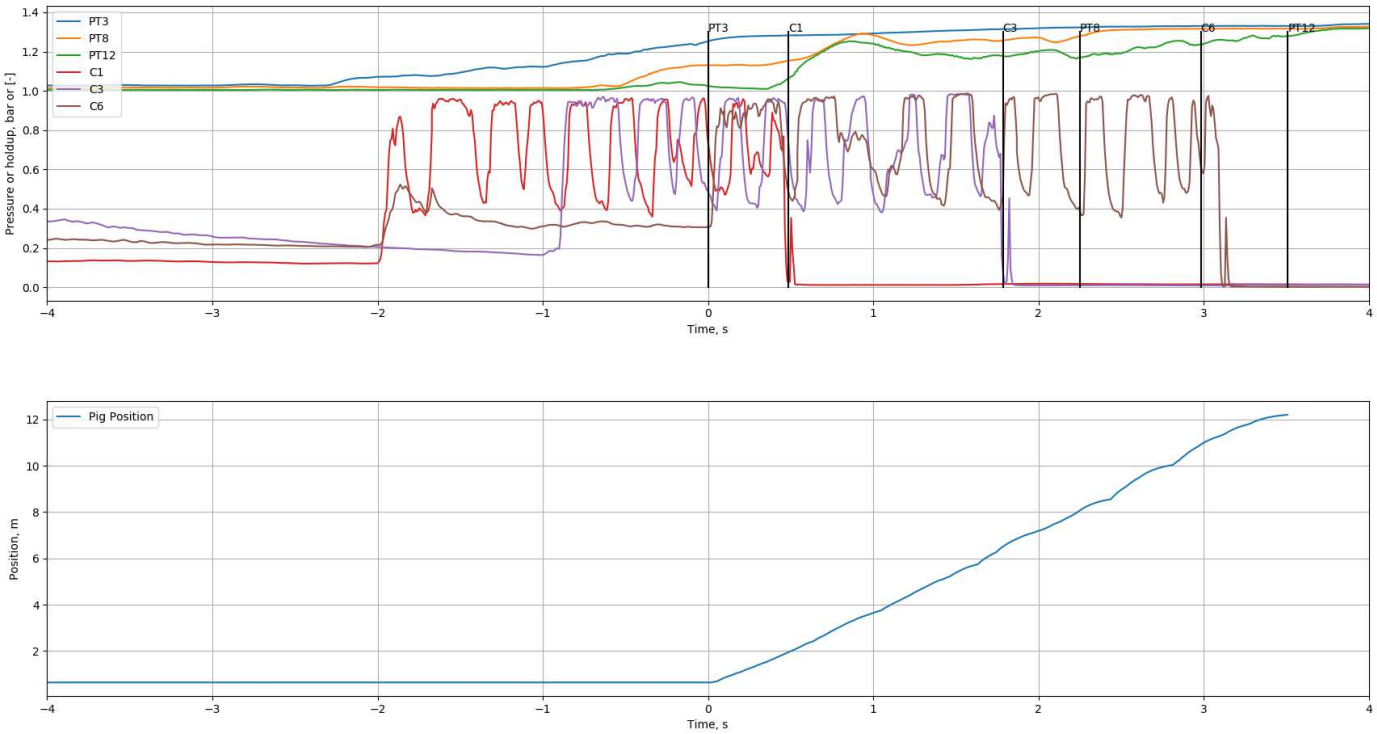

Fig. 3.15—*Case 3: gas 66 kg/h, liquid 0.3 l/s.*

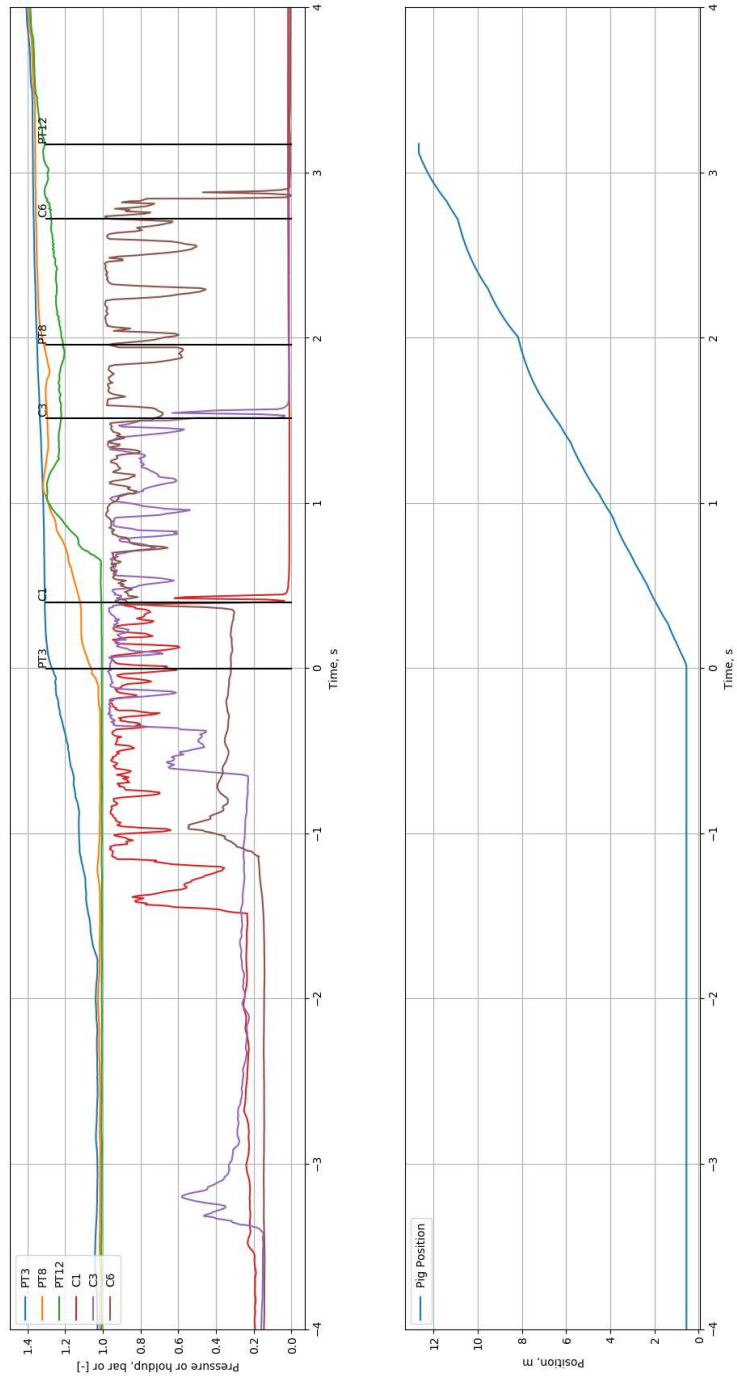

Fig. 3.16—*Case 4: gas 109 kg/h, liquid 0.3 l/s.*

Table 3.3—*OLGA model parameters.*

Geometry	
Pipe ID, m	0.06
Entrance pipe length, m	42
Test pipe length, m	16
After test pipe length, m	20
Grid segment length, m	1.0
Pig model	
Mass, kg	1
Leakage factor, %	2.5
Lin friction coef, N*s/m	0
Quad friction coef, N*(s/m)^2	2.5
Static friction force, N	5
Wall friction, N*s/m	1
Boundary conditions	
Outlet pressure, bar	1
Air flow rates, kg/h	30, 66, 109
Water flow rates, l/s	0.3, 0.3, 0.3
Mass flow total, kg/h	1111, 1146, 1189
Water fraction	0.973, 0.942, 0.908

3.6 Tuning a commercial simulator pig model

It was interesting to know how close OLGA software would simulate the experiment with built-in functionality. OLGA version 7.3.5.122428 was used for this purpose. Air with water PVT table generation was done in NeqSim, see Solbraa [2002]. The modeling parameters are shown in Table 3.3. The leakage through the pig due to pressure drop across a pig is formulated in OLGA in the following way:

$$U_{pl} = C_{pl}\sqrt{\frac{\Delta P_{pig}}{\rho}}, \tag{3.1}$$

where U_{pl} is leakage velocity [m/s], C_{pl} is leakage factor, ΔP_{pig} is pressure drop over the pig [Pa], ρ is density [kg/m^3]. The second type of leakage calculated is a back leakage due to slip. This is a leakage between pig and pipe walls.

$$\begin{aligned} Q_{fl} &= \frac{\pi(D_{pipe}^2 - D_{pig})}{4}\upsilon_f \\ \upsilon_f &= \frac{1}{2}U_{pig}, \end{aligned} \tag{3.2}$$

where υ_f is average film velocity [m/s], U_{pig} is pig velocity [m/s], Q_{fl} is volumetric flow rate [m^3/s], D_{pipe} and D_{pig} are respectively inner pipe diameters [m] and outer pig diameter [m]. The two equations that link the pig velocity to the pig/wall and

film friction have the following form:

$$F_{wf} = max(0, F_{static} - f_{wf}|U_{pig}|)\frac{U_{pig}}{|U_{pig}|}$$
$$F_v = f_1 U_{pig} + f_2 U_{pig}|U_{pig}|, \tag{3.3}$$

where F_{wf} is wall friction due to pig wall contact [N], F_{static} is static friction force [N], f_wf is wall friction factor [N·s/m], F_v viscous friction force [N], f_1 and f_2 are linear [N·s/m] and quadratic [N·s^2/m^2] friction factors. After tuning the leakage factor, the wall friction factor, and the static friction force for a stationary pig against experimental results, **case 2**, **case 3**, and **case 4** were simulated in OLGA with the slug tracking in front of the pig option. **Case 1** could not be simulated as slugs pushed the pig, and a general slug tracking option was not available together with the activation of the pig model option in that version of OLGA. Then the leakage factor and the wall friction factor were further tuned to get the OLGA results for the pig velocity to match the experimental results. Table 3.3 presents values that were used after tuning. The leakage factor is 2.5 % compared with 4.0 % bypass of the actual pig. This stems from the desire to have the same pig velocities in OLGA as in the experiment. The 4.0 % leakage factor would give a better correlation if the goal was to get the same pressure difference over the pig. For each case pressure, liquid holdup, and pig position were plotted against time, see Figures 3.17 to 3.25. OLGA results were taken at positions that correspond to the physical sensor locations. The time is set to zero when the pig enters the test section.

All graphs show the same trends. The pressure reported by OLGA at a location starts to increase when a liquid slug passes the location. The difference in pressures between locations disappears when the pig passes the location, leaving only gas behind. Experimental pressure shows the same trend. There are two differences between simulated and experimental pressure results: magnitude and time offset. Magnitude is different because of leakage factor tuning. Analysis of the liquid holdup graphs can explain the difference in time offset. The reason is similar for all cases. The liquid holdup graph for **case 3** can be used as an example. In Figure 3.21 the fluctuations of the holdup from experiment, "C1, Exp", start at the -2 s mark indicating a pig-generated slug arrival at the first conductance ring sensor. The -2 s mark corresponds to pressure increase, "P3, Exp" Figure 3.20. The small time difference between "P3" and "C1" comes from their different positions along the studied pipe section, "P3" is in front of "C1". The liquid holdup fluctuations are caused by a bubbly slug train. Then, there is an abrupt change of the holdup to zero, indicating pig passage with only gas left behind. OLGA results show that liquid slug reaches "C1" location at -8 s mark, then the holdup is gradually reduced before the abrupt drop to zero. Average

amounts of liquid from OLGA and the experiment are very close when taking the integral from the -8 s mark to the +1 s mark. The slug in OLGA arrives earlier. There is a separation between a slug and the pig in OLGA; this separation is not present in the experiment. While not resolving the slug train, the software predicts the average holdup values to a reasonable precision. Considering real pipelines and pigging, it is not necessary to resolve such slug trains or be sharp at slug separation from the pig. Predicting the total liquid in the slug coming in front of the pig is enough in most cases.

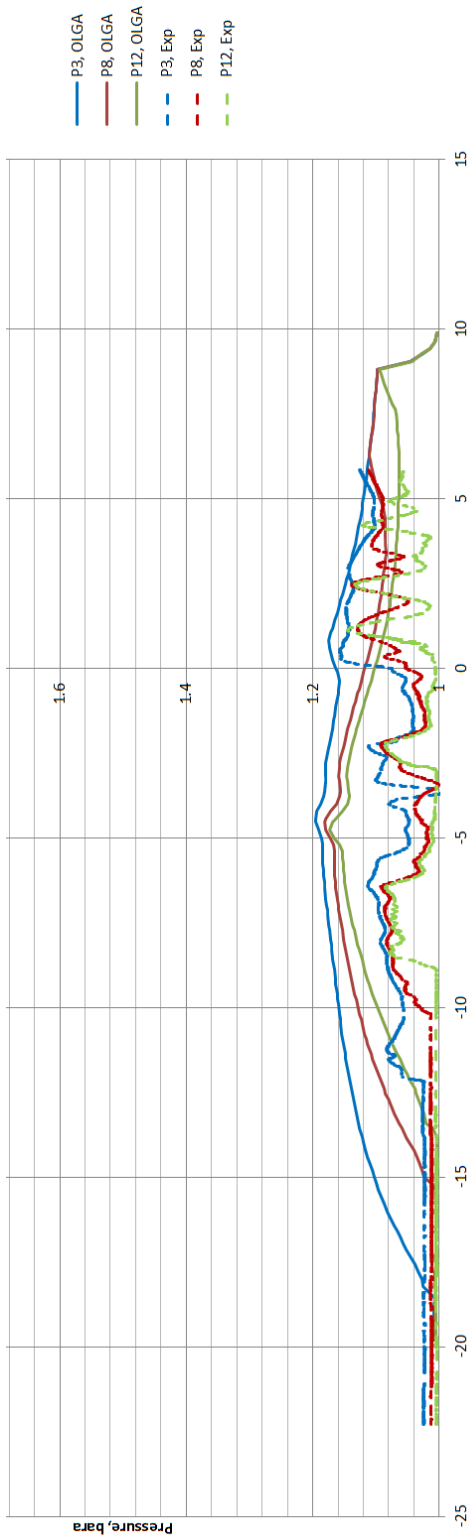

Fig. 3.17—*Pressures in a test pipe: case 2.*

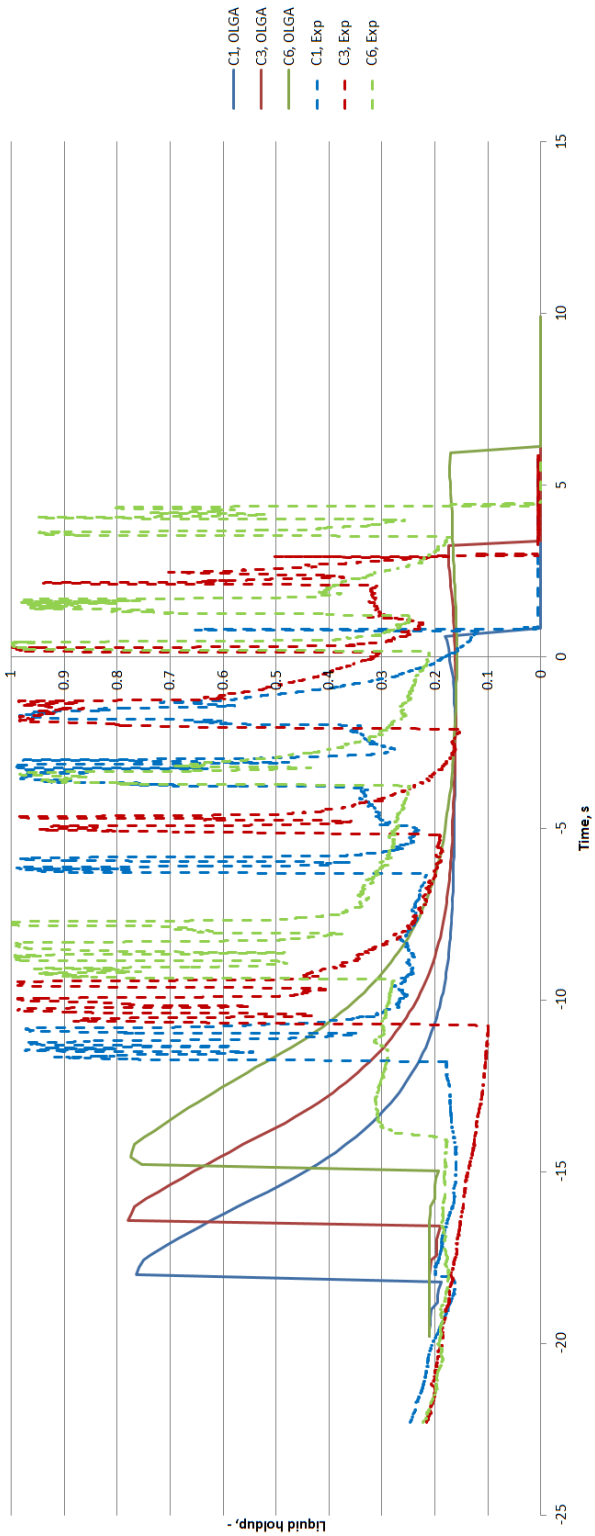

Fig. 3.18—*Liquid holdup in a test pipe: case 2.*

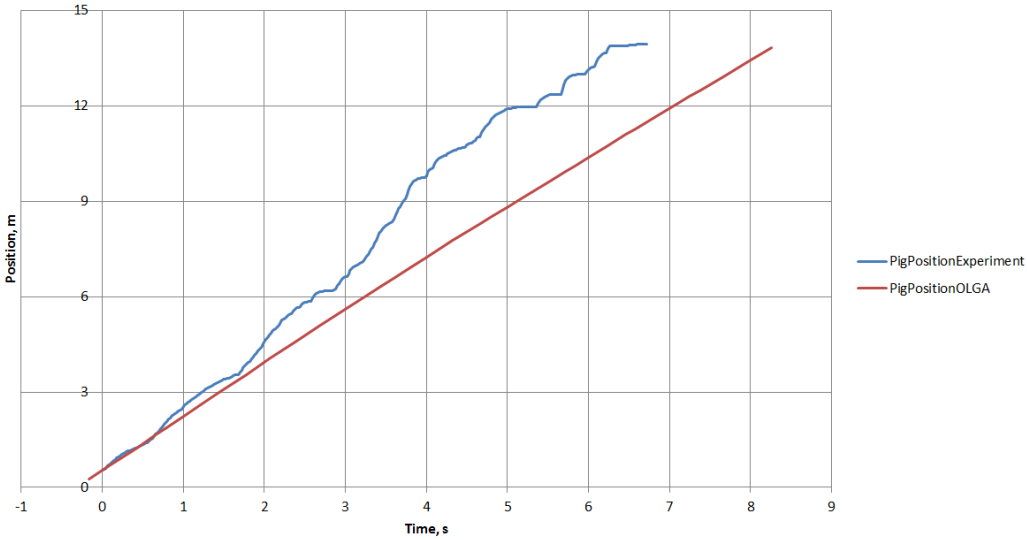

Fig. 3.19—***pig traveled distance in a test pipe: case 2.***

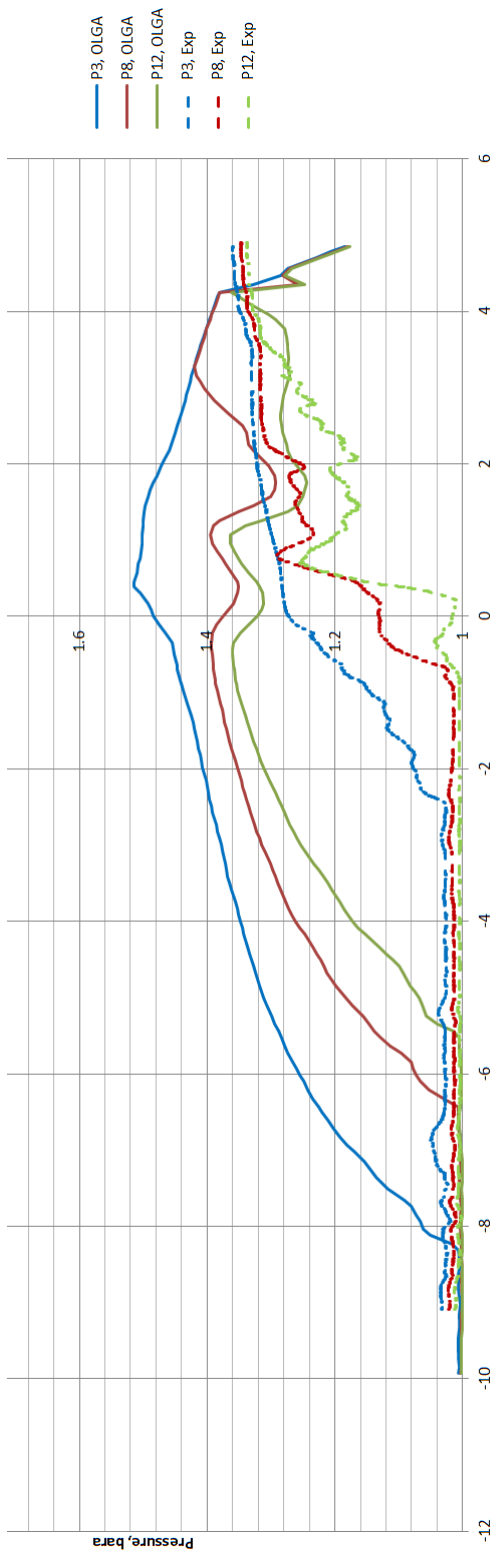

Fig. 3.20—*Pressures in a test pipe: case 3.*

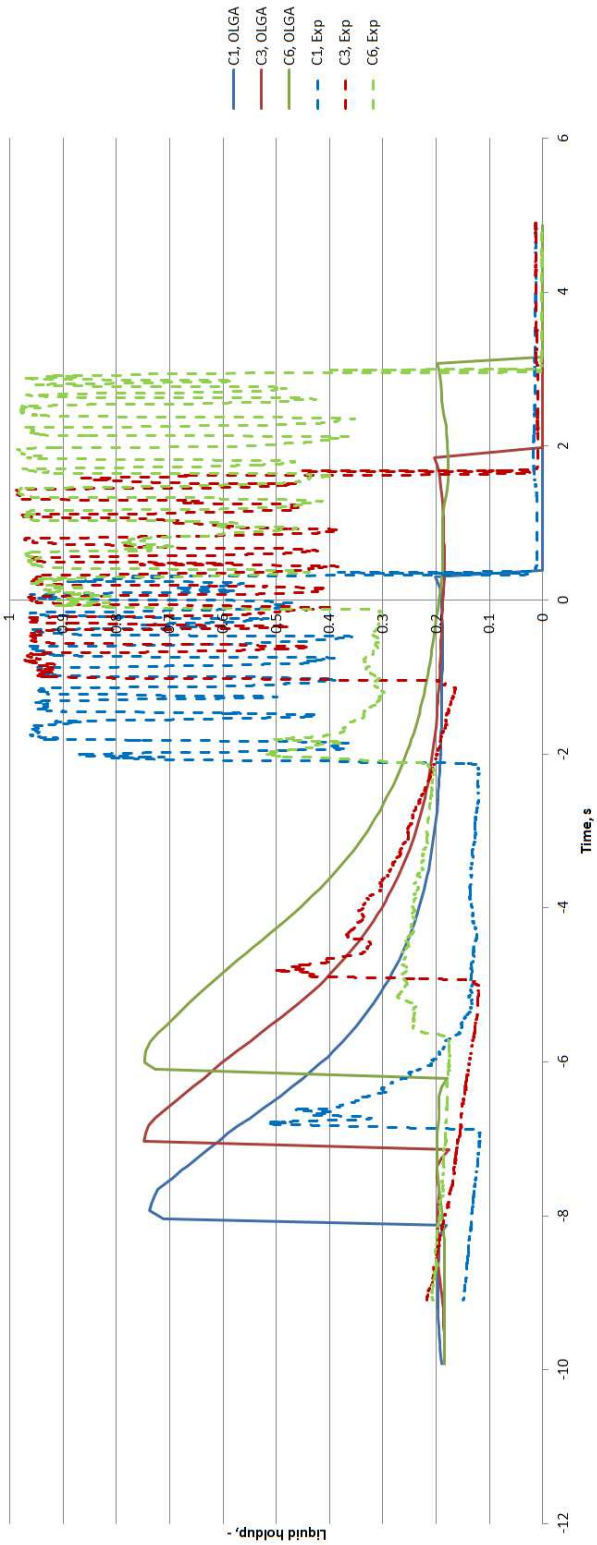

Fig. 3.21—*Liquid holdup in a test pipe: case 3.*

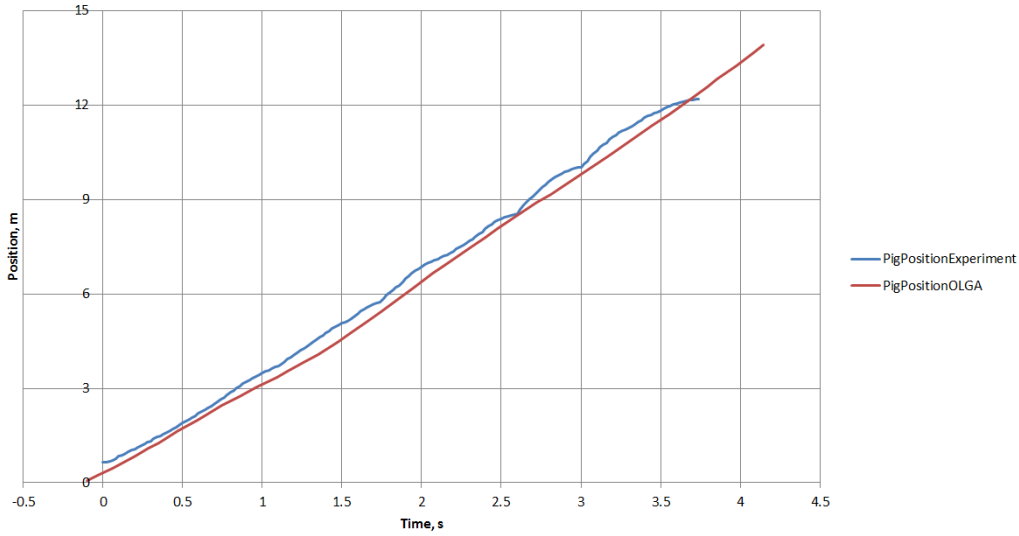

Fig. 3.22—***pig traveled distance in a test pipe: case 3.***

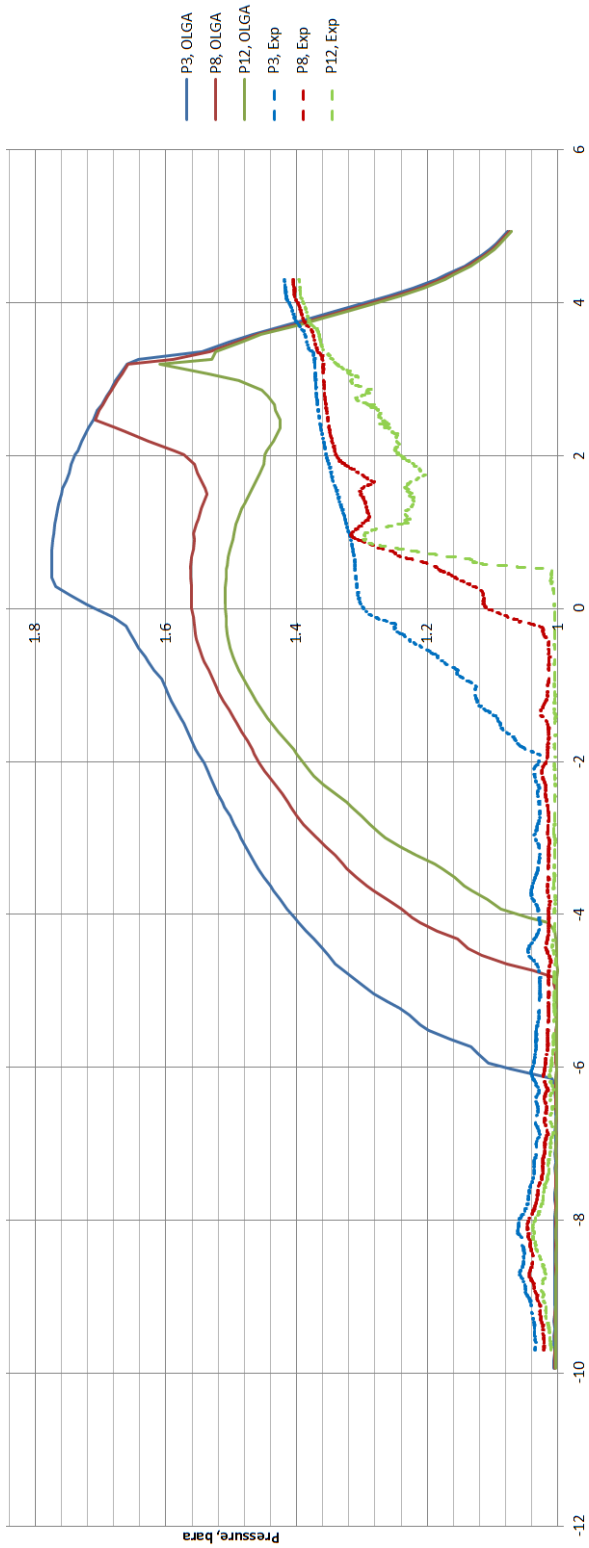

Fig. 3.23—*Pressures in a test pipe: case 4.*

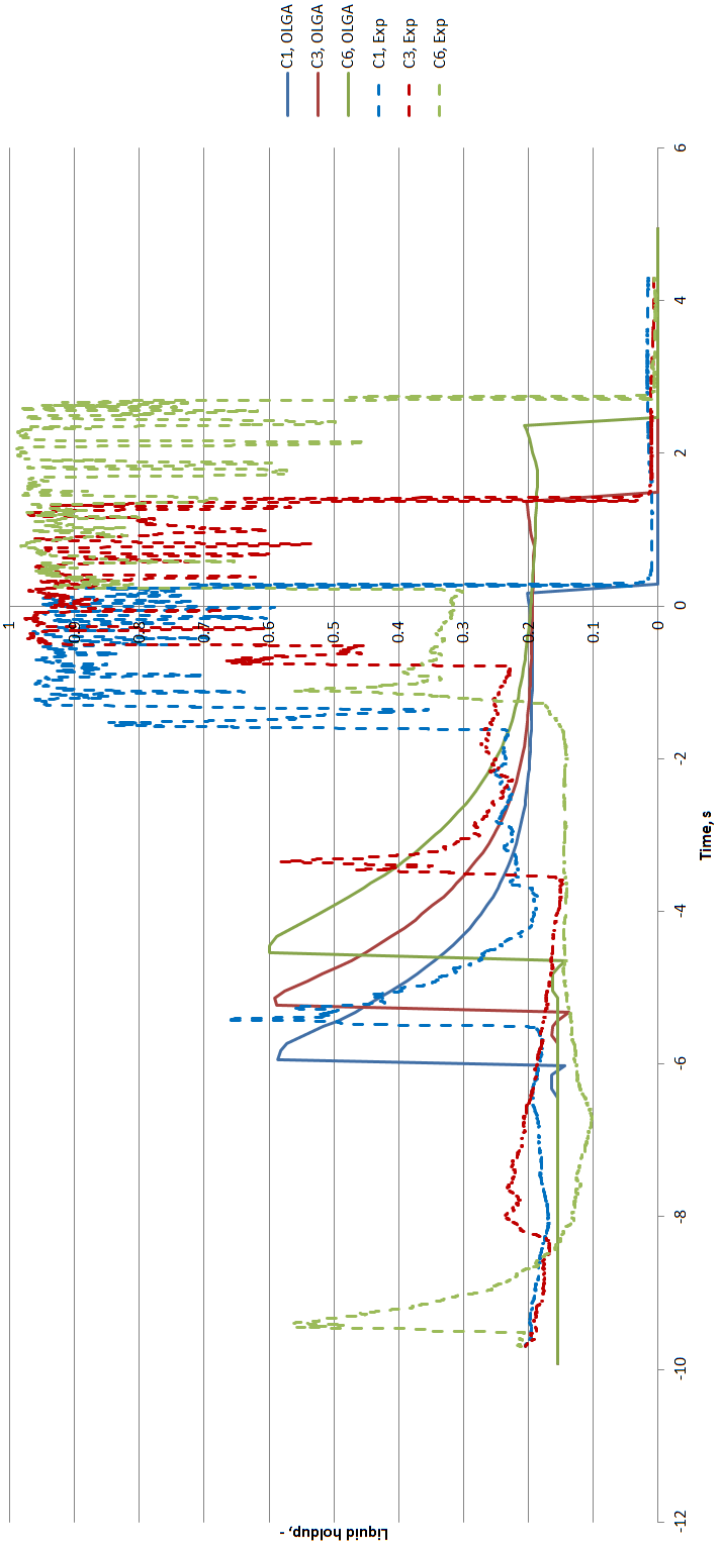

Fig. 3.24—*Liquid holdup in a test pipe: case 4.*

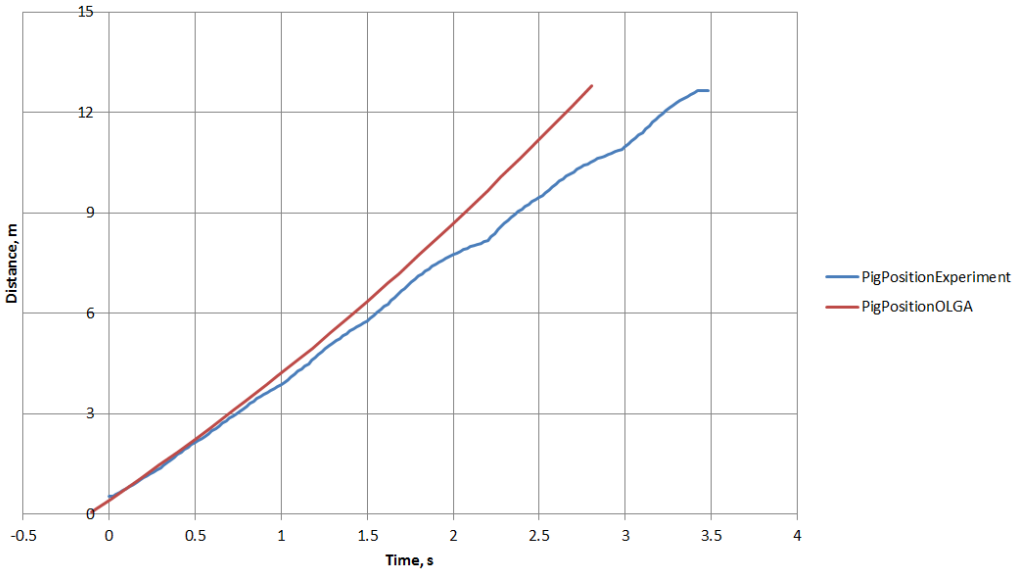

Fig. 3.25—*pig traveled distance in a test pipe: case 4.*

In summary, OLGA results differ from experimental readings in the following way:

- The software uses an averaged slug flow model and thus cannot resolve individual slugs, so the software presents averaged holdups. These averages are close to the averages from the experiment.
- It appears that the pig-generated slug or slug train is detached from the pig.
- Pressures from OLGA are higher than pressures from the experiment. The difference increases with increasing gas flow rates.
- Pressures in OLGA rise earlier and then fall earlier than pressures in the experiments. It could be because slugs generated in OLGA are separated from the pig, enter the test section earlier than a real slug/slug train, and exit the pipe earlier.

Overall, with the selected parameters, OLGA seems to overpredict pressures while predicting average liquid holdups close to corresponding values from the experiment. The selection of the parameters could be different when matching the pressure drop against the stationary pig: a somewhat larger leakage factor with a smaller wall friction. Such a choice would better match peak pressures between OLGA results and the experiment, but the pig travel times would be longer in OLGA. For low gas flow rate conditions, the travel time is up to 3 times longer.

3.7 Uncertainty in measured data

Pressure sensors were calibrated and had an accuracy of 0.2 %. Conductance rings were calibrated for a stratified flow condition, and it is uncertain how accurate they perform in a slug/bubble flow. Therefore liquid holdup values could not be considered accurate enough for resolving the flow but could be used to describe the flow qualitatively. The pig travel distance was measured using a GoPro camera picture and reference points on the experimental stand. As the camera had a "fish-eye" lens, the distortion could not be compensated entirely, which resulted in a distance measurement error of 3 %. The difference in pig travel distances/velocities between runs of the same case was estimated to be within 5.5 %.

3.8 Conclusion

There is a lack of experimental data for bypass pigs in two-phase flows in the literature. Pigging experiments were performed with a bypass pig in multiphase air/water flow in a 2-inch flow loop. Several gas and liquid flow rates were studied, resulting in four cases that were identified as representing typical patterns for the flow with bypass pig. Pig travel distance, pressure, and liquid holdup time series were compared with results from OLGA software. After parameter tuning, OLGA produced sensible results. However, models which resolve the individual slug dynamics with pigging are lacking.

3.9 References

[1] Boghi, A., Brown, L., Sawko, R., and Thompson, C. P. 2017. An inertial two-phase model of wax transport in a pipeline during pigging operations. *International Journal of Multiphase Flow* **94**: 17–30. https://doi.org/10.1016/j.ijmultiphaseflow.2017.04.007

[2] Boghi, A., Brown, L., Sawko, R., and Thompson, C. P. 2018. A non-inertial two-phase model of wax transport in a pipeline during pigging operations. *International Journal of Multiphase Flow* **165**: 664–672. https://doi.org/10.1016/j.petrol.2018.02.071

[3] den Heijer, A. 2016. Frictional behaviour of pigs in motion. Master's thesis, Delft University of Technology.

[4] Galta, T. 2014. Bypass pigging of subsea pipelines suffering wax deposition. Master's thesis, Norwegian University of Science and Technology.

[5] Groote, G. A., van de Camp, P. B. J., Veenstra, P., Broze, G., and Henkes, R. A. W. M. 2015. By-pass pigging without or with speed control for gas-condensate pipelines. *Proc.,* International Petroleum Exhibition and Conference, Abu Dhabi, UAE, 9-12 November. SPE-177819-MS. https://doi.org/10.2118/177819-MS

[6] IJsseldijk, H. P. 2016. By-pass pigging, experiments and simulations. Master's thesis, Delft University of Technology.

[7] Liang, X. 2015. Numerical study of flow around bypass pigs. Master's thesis, Delft University of Technology.

[8] Lima, P. C. R. 1999. *Modelling of Transient Gas-Liquid Flow and Pigging in Pipes.* PhD thesis, Cranfield University.

[9] Minami, K. and Shoham, O. 1995. Pigging dynamics in two-phase flow pipelines: Experiment and modeling. *SPE Production and Facilities* **10** (04). SPE-26568-PA. https://doi.org/10.2118/26568-PA

[10] Nieckele, A. O., Braga, A. M. B., and A., A. L. F. 2001. Transient pig motion through gas and liquid pipelines. *Journal of Energy Resources Technology* **123** (4). https://doi.org/10.1115/1.1413466

[11] O'Donoghue, A. 2004. Pigging as a flow assurance solution estimating pigging frequency for dewaxing. *Proc.,* Pipeline World, volume 49.

[12] O'Donoghue, A. F. 1996. *On the steady state motion of conventional pipeline pigs using incompressible drive.* PhD thesis, Durham University.

[13] Olaniyan, Y. and Larrey, D. 2014. Bypass pig modeling - a three phase gas condensate pipeline field case. *Proc.,* 9th North American Conference on Multiphase Technology, Banff, Canada, 11-13 June. BHR-2014-J1.

[14] Quarini, J. and Shire, S. 2007. A review of fluid-driven pipeline pigs and their applications. *Proc.,* Institution of Mechanical Engineers, Part E: Journal of Process Mechanical Engineering, volume 221, pages 477–491. https://doi.org/10.1243/0954408JPME108

[15] Singh, A. and Henkes, R. A. W. M. 2012. Cfd modeling of the flow around a by-pass pig. *Proc.,* 8th North American Conference on Multiphase Technology, Banff, Alberta, Canada, 20-22 June. BHR-2012-A016.

[16] Solbraa, E. 2002. Neqsim documentation. [Online; accessed 6-July-2017]. http://folk.ntnu.no/solbraa/neqsim/NeqSim.htm

[17] Solghar, A. A. and Davoudian, M. 2012. Analysis of transient pig motion in natural gas pipeline. *Mechanics & Industry* **13** (5): 293–300. https://doi.org/10.1051/meca/2012039

[18] Southgate, J. 2004. *Wax removal using pipeline pigs*. PhD thesis, Durham University.

[19] Souza Mendes, P. R., Braga, A. M. B., A., A. L. F., and S., C. K. 1999. Resistive force of wax deposits during pigging operations. *Journal of Energy Resources Technology* **121** (3): 167–171. https://doi.org/10.1115/1.2795977

[20] Tolmasquim, S. T. and Nieckele, A. 2008. Design and control of pig operations through pipelines. *Journal of Petroleum Science and Engineering* **62** (3-4): 102–110. https://doi.org/10.1016/j.petrol.2008.07.002

Chapter 4

Two phase small scale wax deposition experiment

Nomenclature

A –	Area, m^2
Cp –	Heat capacity, J/kg/K
D –	Hydraulic diameter, m
f –	Friction factor
Fr –	Friction force per unit volume, N/m^3
h –	Thermal convective transfer coefficient, $W/m^2/K$
k –	Thermal conductivity, W/m/K
$\dot{M}$ –	Mass flow rate, kg/s
PID –	Proportional integral derivative (controller)
Pr –	Prandlt number, -
R –	Radius, m
Re –	Reynolds number, -
Re_ϵ –	Roughness Reynolds number, -
$\frac{\partial p}{\partial x}$ –	Pressure drop, Pa/m
T –	Temperature, K
WAT –	Wax appearance temperature, °C

Latin

α – Fluid fraction
ϵ – Roughness, m
ρ – Density, kg/m^3
υ – Velocity, m/s

Subscripts

G – Gas
GL – Gas liquid interface
GW – Gas wall interface
i – Inner pipe wall, pipe wall-oil|wax interface
L – Liquid
LW – Liquid wall interface
oil – Oil domain
o – Outer pipe wall, pipe wall-water interface
$pipe$ – Pipe wall properties
w – Wax-liquid interface
$water$ – Water domain
wax – Wax layer|Wax particle

4.1 Introduction

The wax deposition is one of the main issues in the flow assurance of oil and gas pipelines. A growing wax deposit decreases the available pipeline diameter and will reduce production, and it can even lead to pipeline blockage. Pigs may also get stuck during attempts to clean the pipeline. It is imperative to quantitatively predict the amount of wax deposit to assess the risks and mitigate them if required. Therefore, experimental data and accurate models are needed to predict the amount, location, and evolution in time of wax deposits in a pipeline. Waxes, wax formation, and deposition have been studied since the beginning of the previous century; maybe one of the first publications on the topic is Reistle [1928]. However, the first paper that provides an in-depth study of wax deposition mechanisms appeared in 1981, Burger et al. [1981], which became a reference work on the topic. Since then, significant experimental and modeling research has been devoted to wax in a single-phase oil flow. The research improved our understanding of the physics

behind the deposition phenomena. Azevedo and Teixeira [2003] discussed the pros and cons of the available models. Aiyejina et al. [2011] provided a comprehensive overall review of wax deposition, wax detection, and wax mitigation technologies. Soedarmo et al. [2017] compared available single-phase wax deposition models to recent laboratory-scale experimental data. Zheng et al. [2017] looked into a wax deposition in a non-Newtonian flow. Some researchers studied deposition in multiphase flows. Sarica and Panacharoensawad [2012] made a review of such models. Experimental work for the multiphase condition is limited Gong et al., Matzain et al., Matzain, Duan et al. [2011, 2002, 1999, 2018]. This work adds to multiphase gas/oil wax deposition experiments. The flow patterns studied were stratified flow and slug flow under fast cooling rates. The fluids used were Marcol 52 white oil with SasolWax 5603, food-grade wax, and air. Because the model oil was transparent, it was possible to visualize wax deposition using a transparent Plexiglas pipe in the test section. In addition to the experimental runs with the transparent pipe, several runs with copper pipe were performed where it was possible to measure temperature along the test section.

4.2 Experimental stand

Experiments were performed in a small-scale loop with an internal pipe diameter of 30 mm. Stand scheme is shown in Figure 4.1. The separator also acted as a heater. The temperature in the separator was measured with a K-type thermocouple installed inside the separator at the outlet hole. Flexible hoses and piping between the separator outlet and inlet of the test section were insulated and taped with heating tape. A PID controller was used to control the heating tapes to maintain the desired temperature at the test section entrance. The waxy oil flow rate was measured with a displacement flowmeter. The test section was a pipe-in-pipe heat exchanger with coolant flowing in the annulus opposite to the flow in the inner pipe. Water was used as the coolant. Eight thermocouples were installed along the test section on the inner pipe for the copper test section: four on top and four at the bottom. Because the test section length was only 2 m, the applied cooling was enough to see a temperature decrease along the test section. A pressure drop was measured with APLISENS pressure transmitters. Information about instrumentation is summarized in Table 4.1. The manufacturer provided the wax carbon number distribution, see Figure 4.4. WAT (Wax Appearance Temperature) was estimated to be 41 °C using Ares G2 rheometer, see Figure 4.5.

The locations of the thermocouples along the inner pipe of the test section are shown in Figure 4.2.

Table 4.1—*Material data.*

Flowmeters	
Oil Flowmeter	Covol oscillating piston 2.5-25 l/min
Water Flowmeter	HMP 09-180 turbine 3-30 l/min
Gas Flowmeter	Tecfluid glasstube 35-350 l/min
Pumps	
Water pump	17 l/min
Oil pump	13 l/min
Pressure and Temperature	
Pressure trasmitters	APLISENS PCE-28
Temperature	K-type thermocouples
Other equipment	
PID	Program on Arduino Mega receiving thermocouple readings as input and producing on/off signal as output to power up the heating tape
Heating tape	70 W/m
Rheometer	Ares G2
Chiller	Applied thermal control K9
Fluids	
Air	
Oil	Marcol 52
Wax	SasolWax 5603

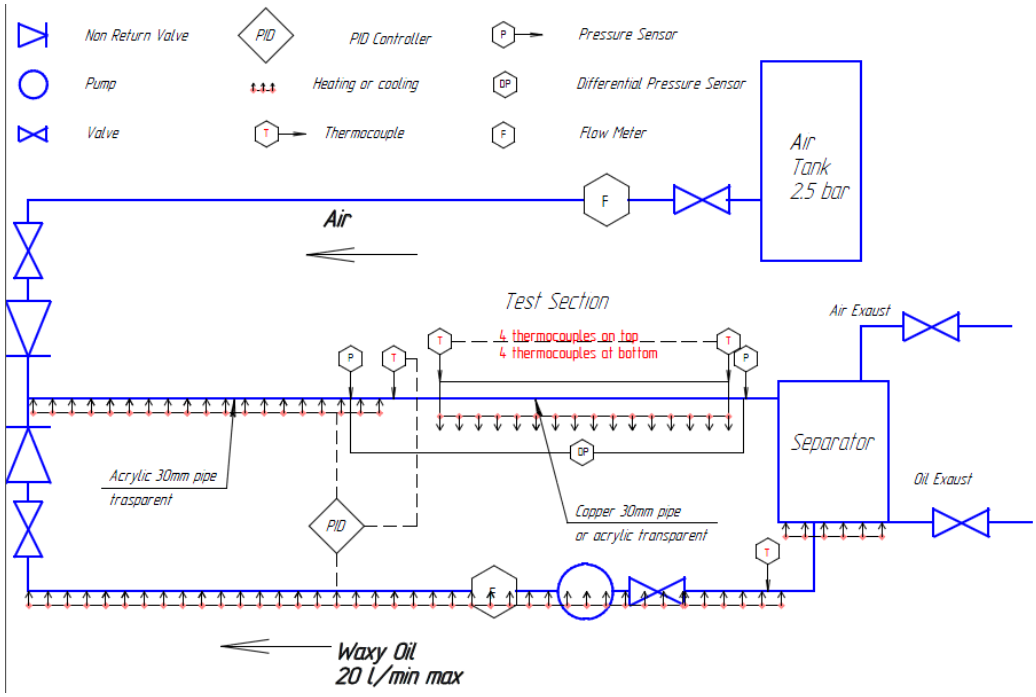

Fig. 4.1—***Stand scheme.***

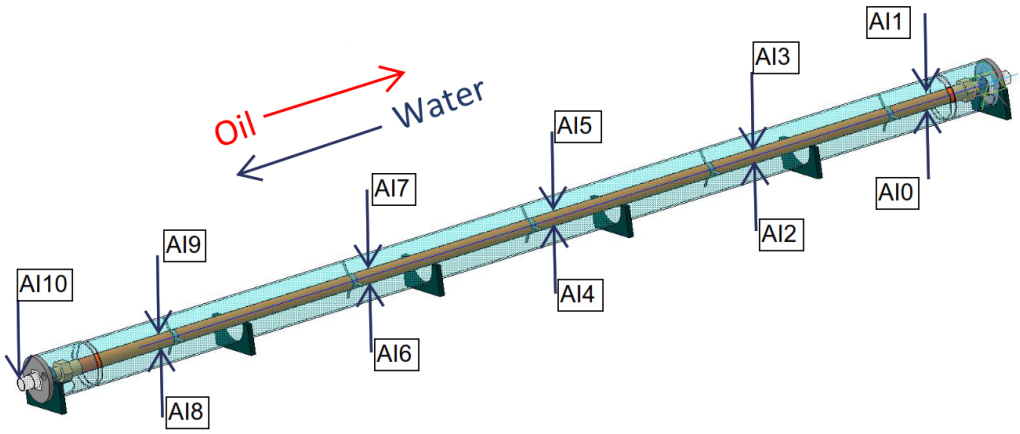

Fig. 4.2—***Thermocouples locations along the test section.***

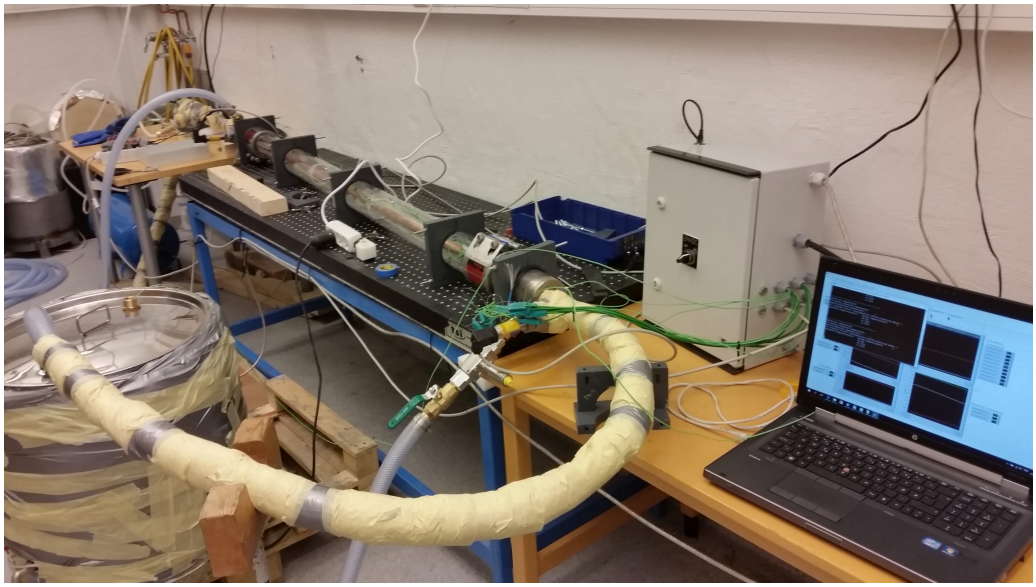

Fig. 4.3—***Stand overview.***

Table 4.2—*Test matrix.*

ID	Oil Flow	Air flow	Water Temp.	Duration	Regime
	l/min	l/min	°C	mins	
1	5	237	20	30	Stratified
2	5	237	5	30	Stratified
3	5	145	5	45	Slug
4	10	145	5	45	Slug

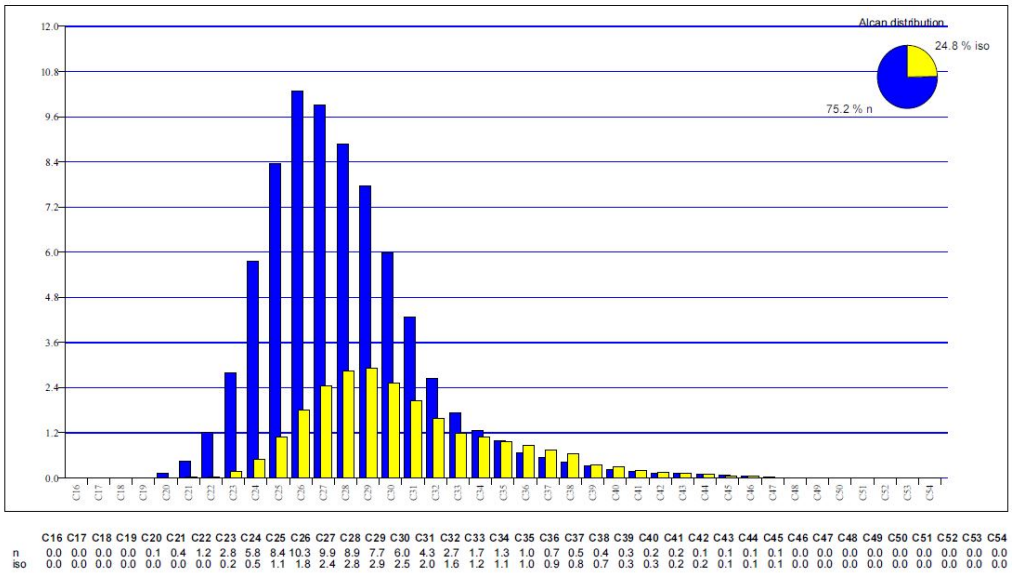

	C16	C17	C18	C19	C20	C21	C22	C23	C24	C25	C26	C27	C28	C29	C30	C31	C32	C33	C34	C35	C36	C37	C38	C39	C40	C41	C42	C43	C44	C45	C46	C47	C48	C49	C50	C51	C52	C53	C54
n	0.0	0.0	0.0	0.0	0.1	0.4	1.2	2.8	5.8	8.4	10.3	9.9	8.9	7.7	6.0	4.3	2.7	1.7	1.3	1.0	0.7	0.5	0.4	0.3	0.2	0.2	0.1	0.1	0.1	0.1	0.0	0.0	0.0	0.0	0.0	0.0	0.0	0.0	0.0
iso	0.0	0.0	0.0	0.0	0.0	0.0	0.0	0.2	0.5	1.1	1.8	2.4	2.8	2.9	2.5	2.0	1.6	1.2	1.1	1.0	0.9	0.8	0.7	0.3	0.3	0.2	0.2	0.1	0.1	0.1	0.0	0.0	0.0	0.0	0.0	0.0	0.0	0.0	0.0

Fig. 4.4—*SasolWax 5603 Composition.*

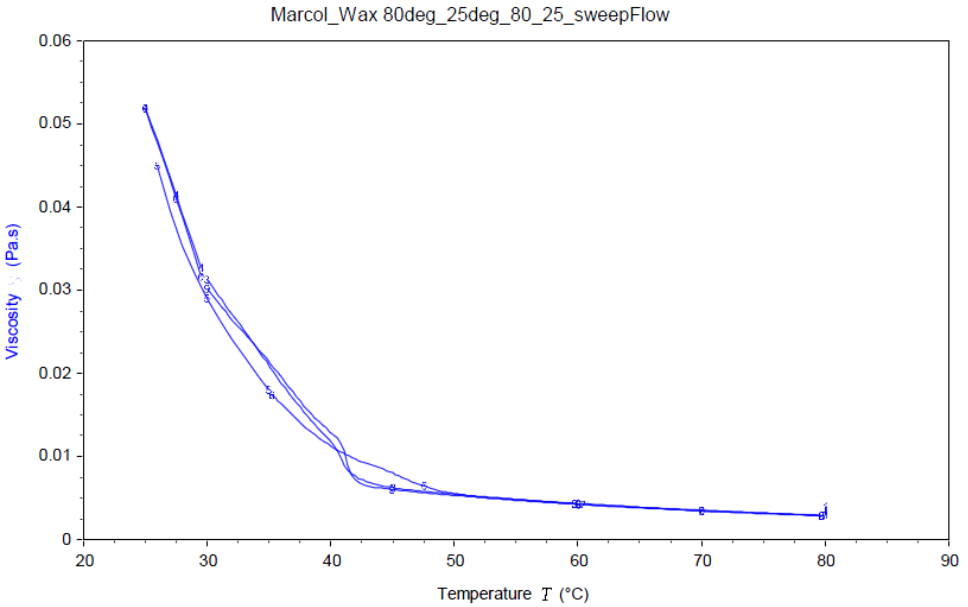

Fig. 4.5—*WAT estimation using viscosimetry.*

Table 4.3—*Test matrix transparent.*

ID	Oil Flow	Air flow	Water Temp.	Duration	Regime
	l/min	l/min	°C	hours	
1	5	117	5	4	Slug
2	5	117	5	4	Slug
3	5	237	5	4	Stratified

4.3 Experimental procedure

The experiments were performed to look into the effect of flow conditions on wax deposition. To get more information, the inner pipe in the test section had two options: a copper pipe for measurement and a transparent plexiglass pipe for visualization. Wax and oil were mixed to get 10 % wax content by weight. The following procedure was adopted:

- Heat the tank to 55 °C, circulate the oil under 55 °C for 1 hour, and visually confirm that no wax is present in the oil.
- Flush with air, record pressure drop for a clean pipe.
- Start the cooling water loop, run the water until it reaches the desired temperature.
- Start the air flow, start the oil flow, run the experiment.
- Increase the air flow while decreasing the oil flow to stop the experiment. This mitigates the amount of wax deposition in stationary oil.
- Drain water.
- Flush the remaining oil with air and record the pressure drop.
- Remove the test section and weigh it to measure the mass of the wax gel.

Test cases are listed in Table 4.2. Runs with the transparent test section were done for cases listed in Table 4.3. The second run of the slug flow regime was done with the gradually lowered tank temperature. The idea was to see what happens when the entering oil temperature is close to WAT temperature.

4.4 Results and discussion

Visualization provided valuable qualitative information about wax deposition and wax gel layer movement. Plexiglas pipe has small thermal conductivity. So Plexiglass pipe simulates either an insulated steel pipe or a steel pipe with a plastic liner. Experiments with the transparent pipe showed that for the slug flow regime, when the entry oil temperature is higher than WAT, the deposition on the walls is negligible, and there is a small amount of wax gel moving along the bottom of the pipe. When the same slug flow regime was combined with a gradual cooling of the

tank at a rate of 2 °C per 10 minutes, the same pattern of wax deposition was observed until oil bulk entry temperature became close to WAT. When close to WAT, the amount of wax gel traveling along the bottom of the pipeline thickened and started to stick. At the WAT, wax appeared circumferentially and, during only 5 minutes, deposited in such amounts that it was not possible to look through the transparent pipe. In the slug flow regime, slugs provided enough shear force to clean the transparent pipe from depositions while bulk oil temperature was above WAT. Considering real pipelines, it looks like pipeline insulation and slug flow regime will move wax deposition to the point where oil bulk temperature reaches WAT.

In stratified flow, there is continuous deposition on the transparent pipe in the gas-wetted section and nearly no deposition in the liquid-wetted section when oil bulk temperature is at least 10 °C above WAT. The deposition on the gas-wetted pipe wall section can be due to oil droplets reaching the pipe wall, sticking to the wall, and crystallizing as wax deposits. As the gel layer at the gas/wall interface grows, it becomes heavier and eventually slips into oil, where it dissolves, see Figure 4.18. The pipe sees this cycle of growing-sliding down wax deposits until oil bulk temperature goes as close as WAT+10 °C for the studied case. Considering a real insulated pipeline, it may indicate that for a stratified flow regime, the deposition at the gas/wall interface will be seen upstream of any deposit at the liquid/wall interface, provided droplets are present. After the pipe location, where oil bulk temperature is closer to WAT, the deposition will happen circumferentially, assuming that droplets reach the gas wetter section.

Experiments with copper pipe showed good repeatability in measuring pressure drop for stratified flow conditions. After filtering noise from pressure difference measurements, the pressure readings showed the same gradual increase in pressure drop for the same flow conditions over time. However, because wax can form at the pressure sensors' locations and the temperatures of the pressure sensors were not measured during the tests, there might be an error in the pressure measurement. During preparation for a test when oil was circulated at temperatures above WAT to clean the loop, the readings on the pressure sensors showed a gradual increase and then a decrease in values during the first 5 minutes of the process with an amplitude less than 0.1 kPa. The solution could be the installation of temperature controlling tools at the pressure sensors locations to keep their temperatures above the wax appearance temperature.

Figure 4.6 shows an increase of pressure drop during the deposition in stratified flow for cases 1 and 2. Figure 4.7 presents the same for slug flow cases 3 and 4. As pressure sensors readings were noisy, the high-frequency noise was filtered out

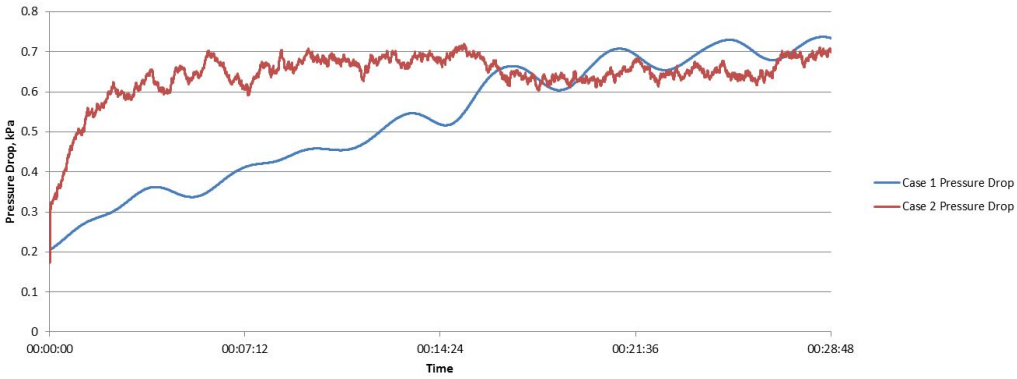

Fig. 4.6—*Pressure drop during the deposition in stratified flow.*

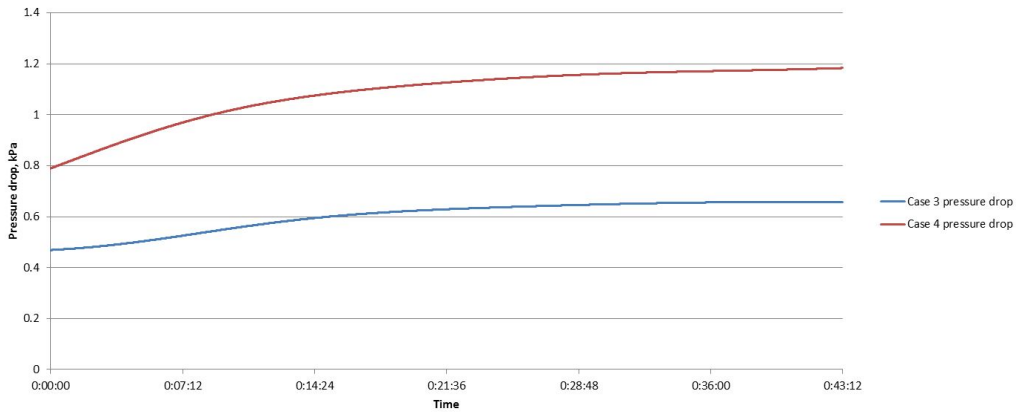

Fig. 4.7—*Pressure drop during the deposition in slug flow.*

using a low pass filter to see the pressure drop change caused by wax deposition. Such filtering also removed pressure spikes from passing slugs for cases 3 and 4.

Temperature readings of thermocouples for stratified flow in case 1 are shown in Figure 4.8. The setup of the thermocouples graphs is the same for all studied cases. The axis to the left gives values for thermocouples installed on the inner pipe inside the test section. The thermocouples locations are shown in Figure 4.2. The axis to the right shows values for the thermocouple at the entrance to the test section and for the thermocouple inside the tank. The evolution of the water cooling loop inlet and outlet temperatures are shown in Figure 4.9 with values on the left vertical axis. Temperatures for case 1 are wobbly in the beginning because of water temperature fluctuation during the water cooling loop stabilization. Then the oil test section temperatures show steady readings. The oil inlet temperature grows because the inlet stream PID was overheating the flow. Steady temperatures along the test section with oil inlet temperature increase indicate the growing wax

layer insulating oil from cooling water.

Case 2 had water inlet temperature set to 5 °C, see Figure 4.9. The temperature readings along the test section are presented in Figure 4.10 with values on the right vertical axis. The oil loop for this case was started after the stabilization of the water cooling loop at 5 °C. The temperature readings from the water and test section thermocouples reflect the start-up process. Water is heated to 6 °C, then the temperature is reduced to 5 °C by the water PID. The test section thermocouples also start from 5 °C, then spike on first contact with oil. A consequent temperature increase for the first 7 minutes comes from oil slowly reaching the requested temperature.

The slug flow cases 3 and 4 with 5 °C cooling water demonstrate same behavior as case 2, see Figures 4.11 and 4.12. Case 3 test section temperatures stopped changing after 20 min, while for case 4 the changing continued to around 40 min mark. It can be assumed that deposition speed reached or was close to zero. The temperatures for case 4 were higher than for case 3, because of the larger oil flow in case 4.

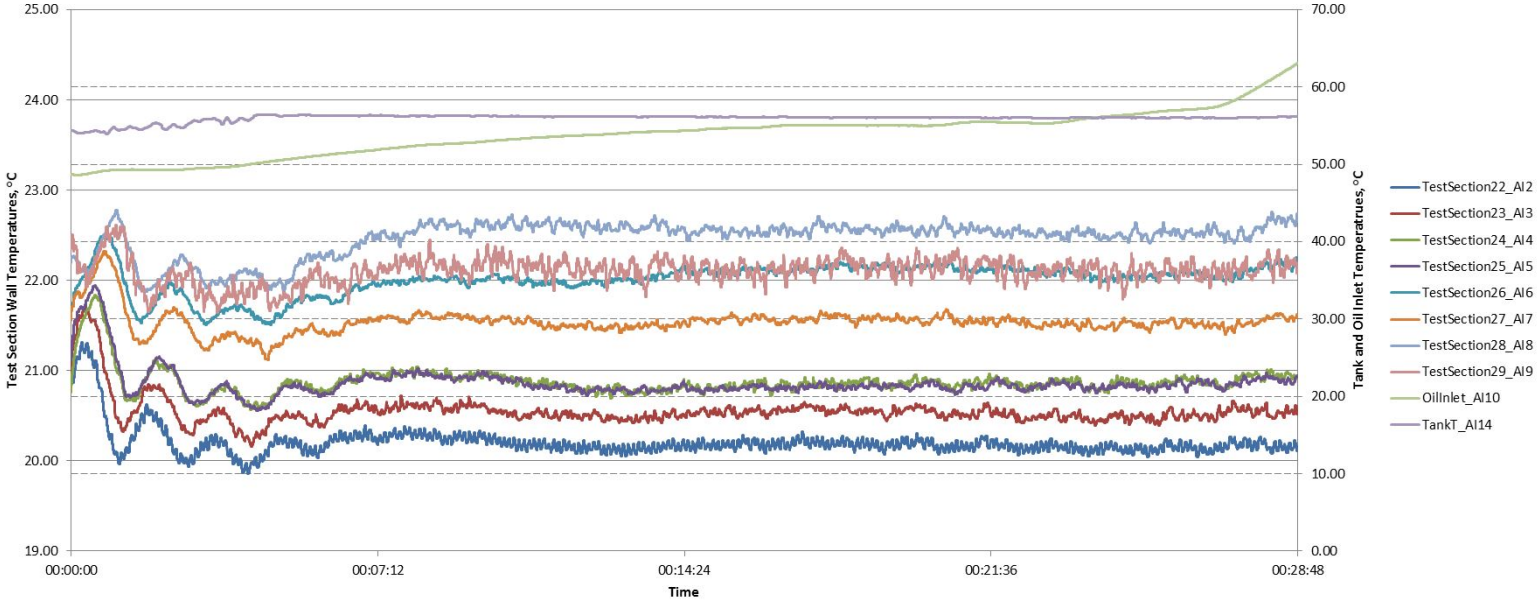

Fig. 4.8—*Case 1 thermocouples readings.*

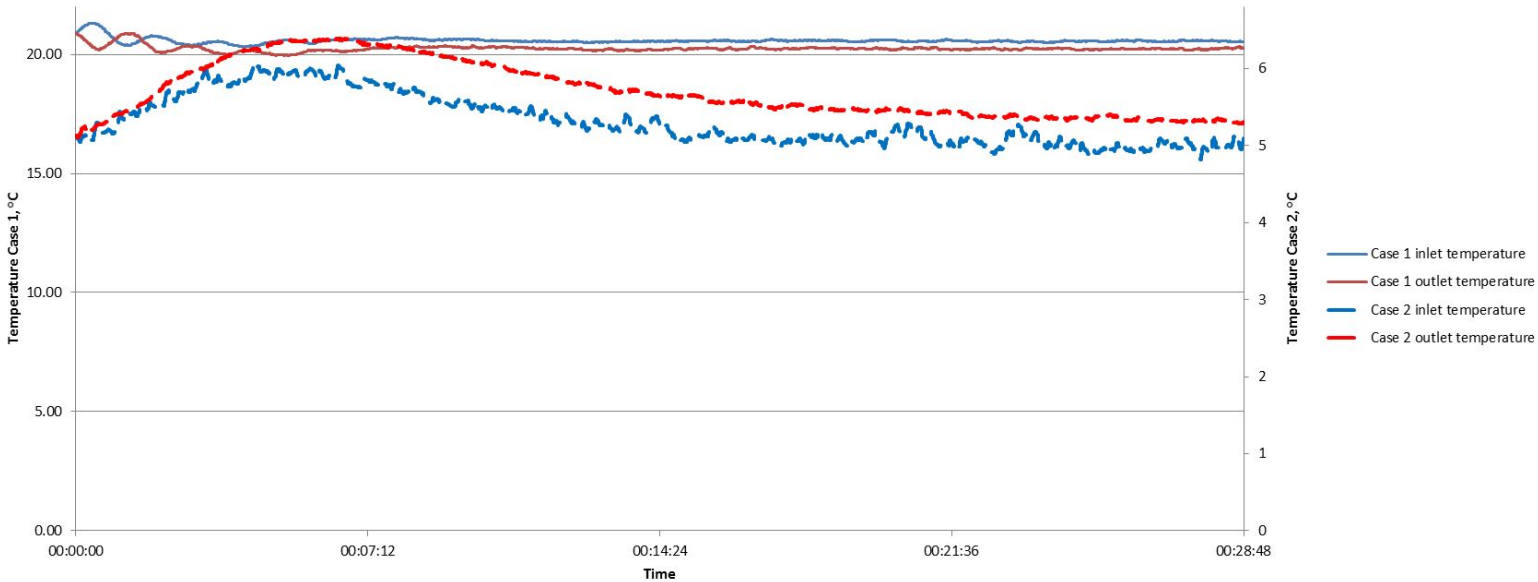

Fig. 4.9—*Case 1 and case 2 cooling water temperatures.*

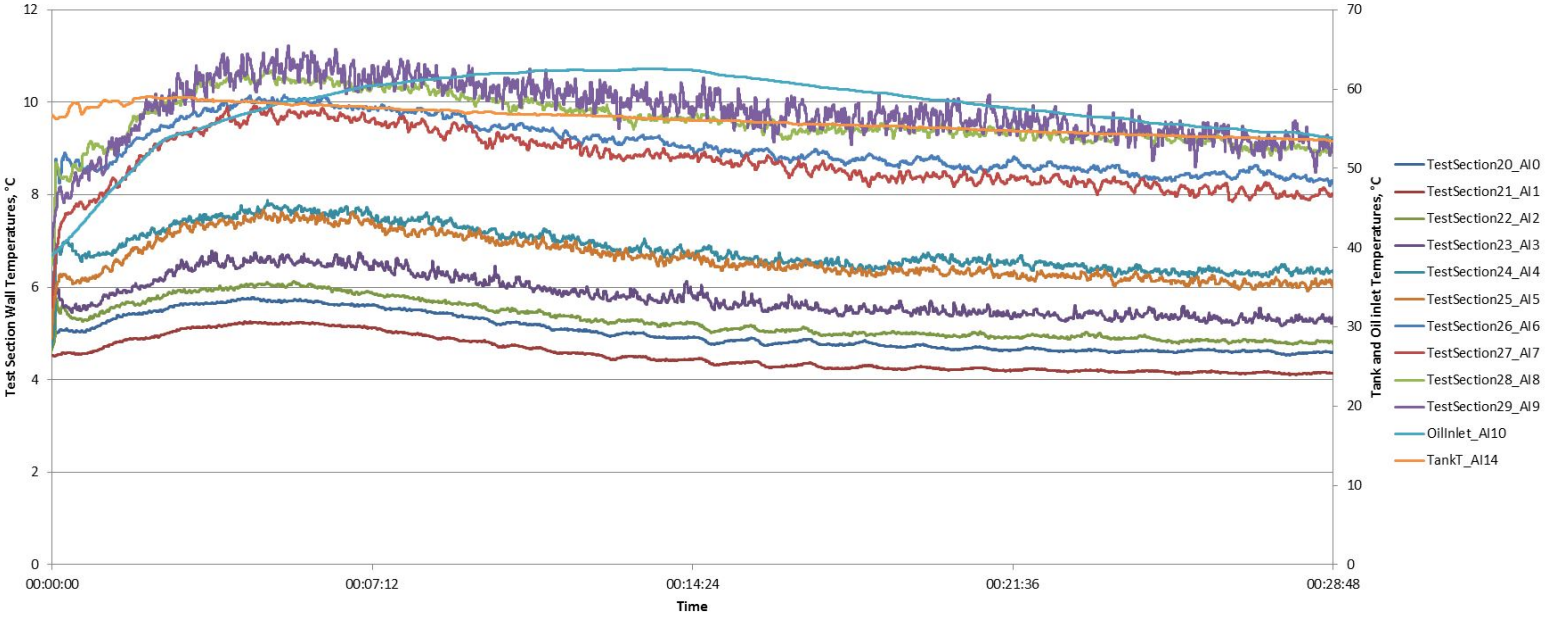

Fig. 4.10—*Case 2 thermocouples readings.*

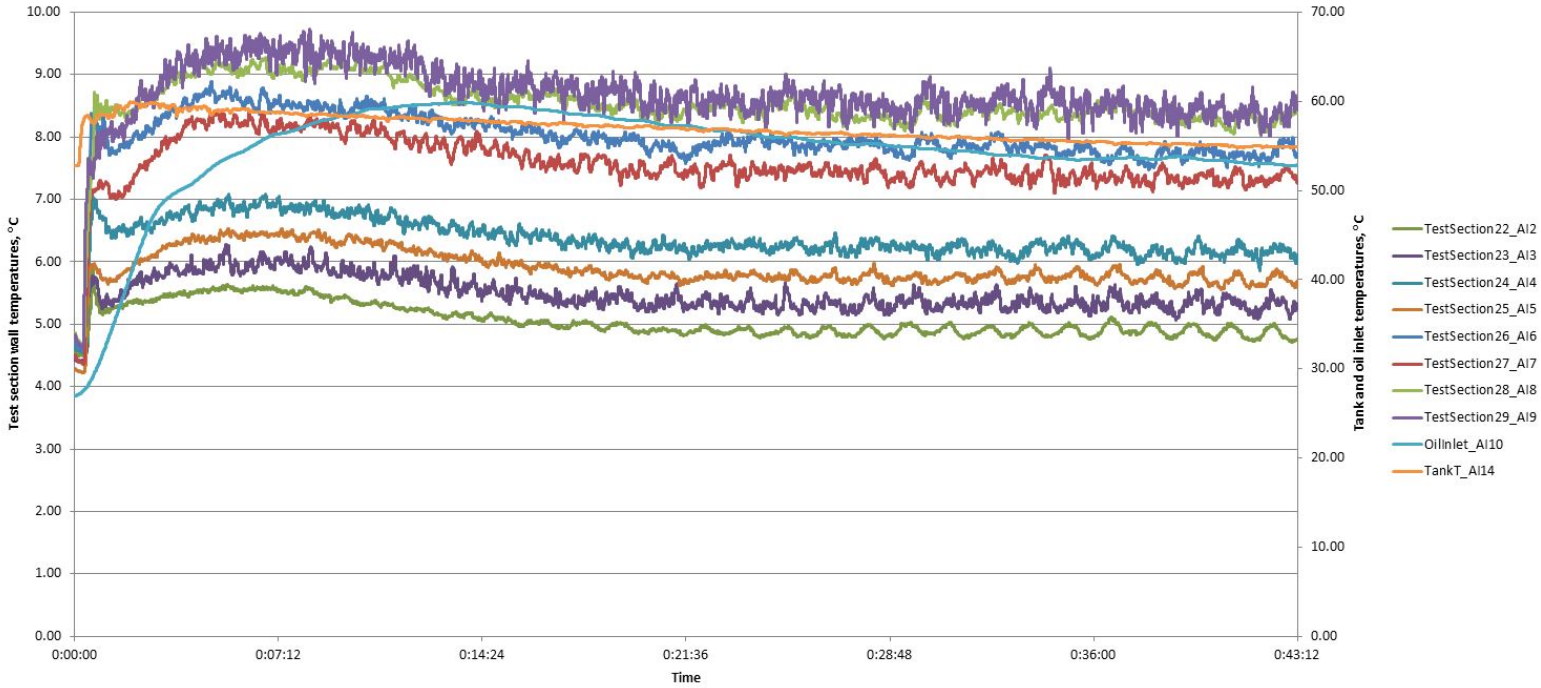

Fig. 4.11—*Case 3 thermocouples readings.*

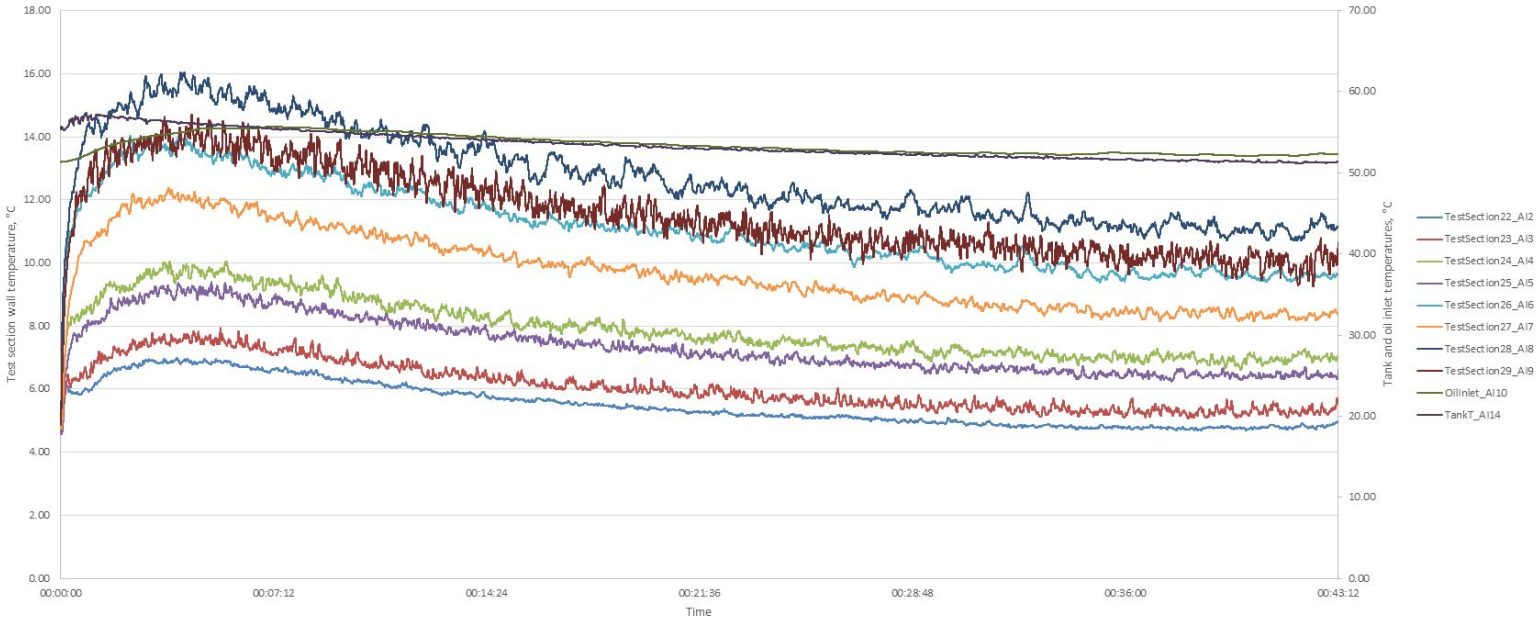

Fig. 4.12—*Case 4 thermocouples readings.*

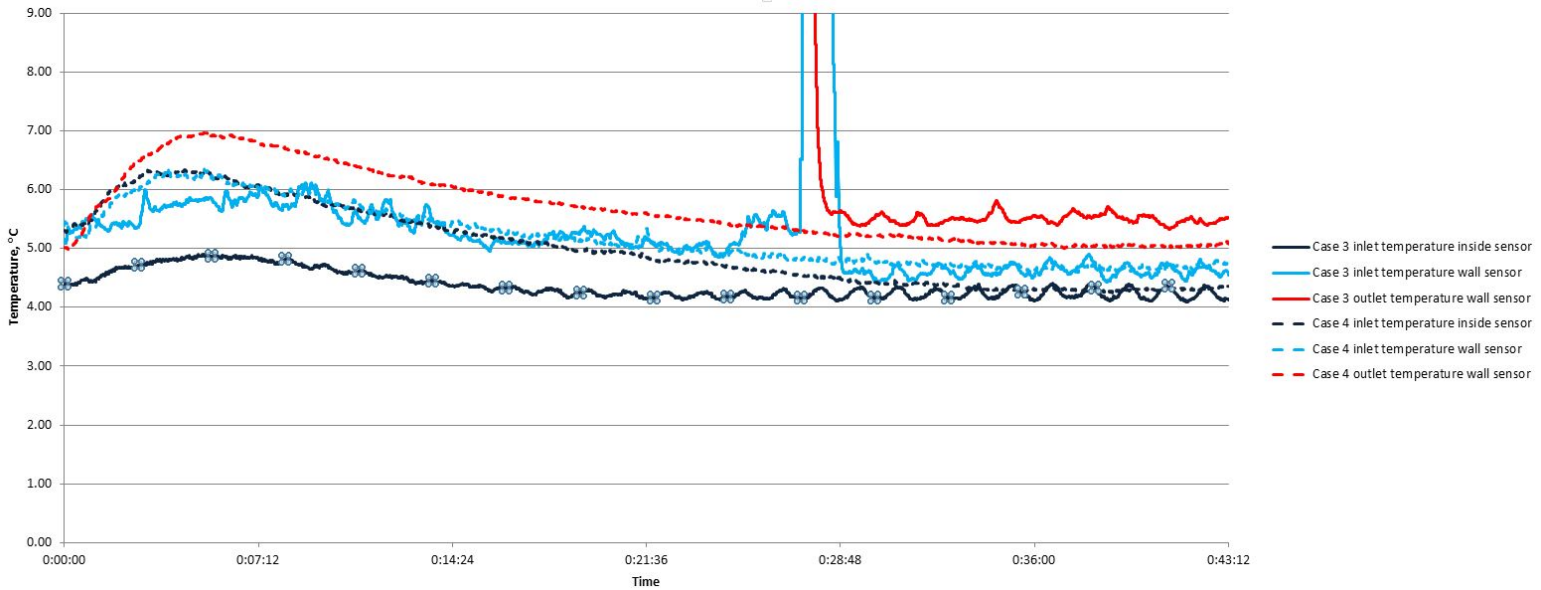

Fig. 4.13—*Case 3 and case 4 cooling water temperatures.*

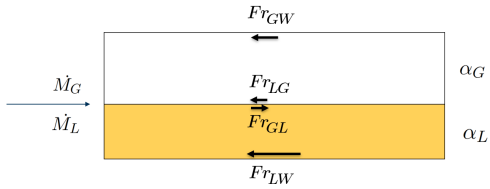

Fig. 4.14—*Illustration of Eq. 4.1 terms.*

Considering that slug frequency was low, the flow in the test section could be seen as stratified most of the time. Hence, after filtering the pressure spikes, a pressure drop estimation for both slug and stratified flows could be made using a stratified flow formulation. The formulation used describes an incompressible steady-state flow; a derivation is available in Bratland [2013] section 3.6. The involved terms are shown in Figure 4.14.

$$\begin{aligned} \alpha_G \rho_G \upsilon_G - \frac{\dot{M}_G}{A} &= 0 \\ \alpha_L \rho_L \upsilon_L - \frac{\dot{M}_L}{A} &= 0 \\ \frac{Fr_{GL}}{\alpha_G} - \frac{Fr_{GW}}{\alpha_G} + \frac{Fr_{GL}}{\alpha_L} + \frac{Fr_{LW}}{\alpha_L} &= 0 \\ \alpha_G + \alpha_L &= 1 \end{aligned} \tag{4.1}$$

In the derivation, the pressure drop term was eliminated. After solution of 4.1, the pressure drop can be found from Eq. 4.2.

$$\alpha_G \frac{\partial p}{\partial x} = -Fr_{GL} + Fr_{GW} \tag{4.2}$$

A simple countercurrent heat exchanger model was used to calculate a wax layer thickness from the thermocouples reading. The model is a steady-state because it assumes that the flow and the temperature conditions are always stable for a certain wax thickness. The model computes the insulating wax layer thickness required to obtain a temperature distribution from thermocouples readings.

- Inner pipe air and oil flow velocities and volume fractions are found the same way as in pressure drop calculations, Eq. 4.1.
- The spatial system of differential equations for heat transfer between cooling water and oil is solved with the Runge-Kutta method:

$$Cp_{oil} \rho_{oil} R_w^2 \upsilon_{oil} \frac{\partial T_{oil}}{\partial x} = \frac{-2R_w (T_{oil} - T_{water})}{R_{thermal}} \tag{4.3}$$

$$Cp_{water}\rho_{water}A_{water}v_{water}\frac{\partial T_{water}}{\partial x} = \frac{2R_w(T_{oil}-T_{water})}{R_{thermal}}, \tag{4.4}$$

where $R_{thermal}$ is the total thermal resistance between the oil bulk and the water bulk:

$$R_{thermal} = \frac{1}{2\pi h_{oil}R_w} + \frac{ln\frac{R_i}{R_w}}{2\pi k_{wax}} + \frac{ln\frac{R_o}{R_i}}{2\pi k_{pipe}} + \frac{1}{2\pi h_{water}R_o} \tag{4.5}$$

The following assumptions were made:

- Wax layer thermal conductivity is 0.25 W/m/K.
- The area of heat transfer from pipe to water is based on the full circumference. The heat transfer area from oil to wax is based on the wetted perimeter.
- The water-copper pipe Nusselt number is calculated according to the correlation presented in Bhatti and Shah [1987].
- The oil-wax layer Nusselt number is calculated using correlation for a thermally developing flow with the assumption of constant heat flux. It was done based on oil flow in a laminar regime with a thermal boundary layer development length greater than the test section length. The hydraulic diameter of a channel flow was used.
- The oil-wax layer Nusselt number is adjusted to have the calculated wall temperature equal to the measured wall temperature at the start of the test when there are no wax deposits. The adjustment takes care of heat transferred with droplets and additional heat transferred because of slugs mixing and wetting in a slug flow regime. The maximum adjustment was a factor of 2.0 in the slug flow regime case 4.

$$Nu = \frac{(f/8)Re_D Pr}{1+\sqrt{f/8}(4.5Re_\epsilon^{0.2}Pr^{0.5}-8.48)}F_{adj} \tag{4.6}$$

$$Re_\epsilon = Re_D\frac{\epsilon}{D}\sqrt{f/8} \tag{4.7}$$

$$f = \frac{1}{\left[1.8log_{10}\left(\frac{6.9}{Re_D}+\left(\frac{\epsilon/D}{3.7}\right)^{1.11}\right)\right]^2} \tag{4.8}$$

Masses of wax from measurement, pressure drop calculations, and temperature calculations are presented in Table 4.4. The mass calculation from the pressure drop measurements could predict the mass with accuracy within 70 % for the stratified cases; the primary source of error seems to be the assumption of uniform shrinkage of diameter around the circumference. For the stratified cases shown in Figures 4.15 and 4.16 wax does not deposit uniformly but forms a river at the bottom of the pipe. However, for the slug cases, the wax river at the bottom is

Table 4.4—*Wax mass.*

Case	Wax mass, g		
	Measured	From pressure drop	From Thermocouples
1	352	500	340
2	229	390	160
3	172	160	210
4	188	210	120

Fig. 4.15—***Deposition in stratified flow case 2a.***

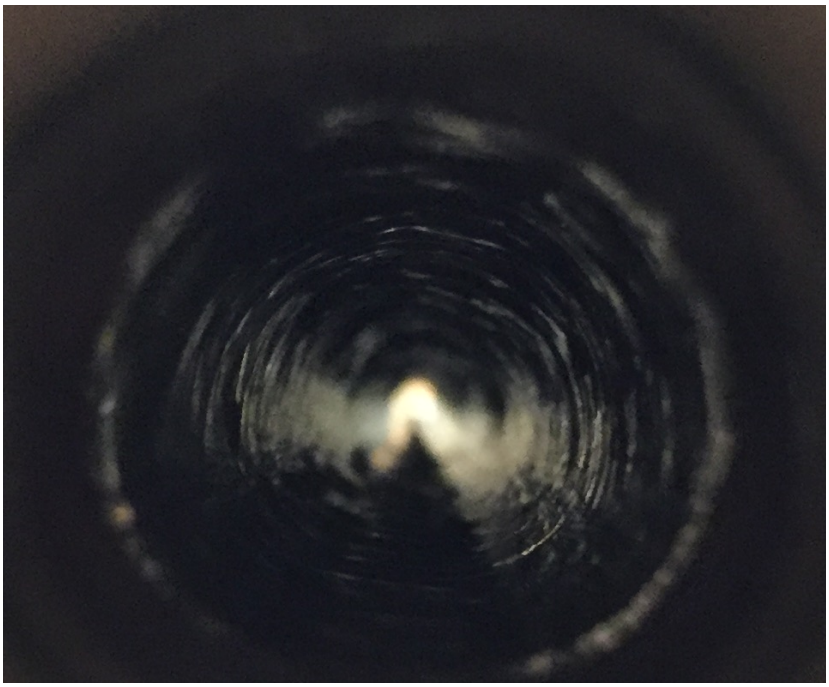

Fig. 4.16—*Deposition in stratified flow case 2b.*

less, see Figure 4.17, and the accuracy is within 30 %. Other sources of error are selections of viscosity, wax roughness, and interface friction. The measurement of wax using thermocouples readings showed a better agreement with the subsequent wax weighing.

4.5 Conclusion

Small scale wax deposition experiments in multiphase flow were performed for stratified and slug flow conditions. The development of the wax layer was visualized using a transparent test section. In the stratified flow cases, the wax deposits at the gas/wall interface, which appeared mainly with the help of droplets, after gaining enough mass, tended to slide down into the oil section with subsequent re-dissolution, see Figure 4.18. The video of the sliding deposit is available in the "CH4" folder of the attachment to the thesis. In the slug flow cases, slugs provided enough shear forces to prevent any significant accumulation of deposits in the gas section. For the studied case of a countercurrent heat exchanger, the temperature measurements method provided better wax thickness estimation than the pressure drop method. However, the error was still as high as 30 %.

Fig. 4.17—*Deposition in slug flow case 4.*

Fig. 4.18—***Deposit evolution in stratified flow conditions.***

4.6 References

[1] Aiyejina, A., Chakrabarti, D. P., Pilgrim, A., and Sastry, M. 2011. Wax formation in oil pipelines: A critical review. *International Journal of Multiphase Flow* **37** (7): 671–694. https://doi.org/10.1016/j.ijmultiphaseflow.2011.02.007

[2] Azevedo, L. F. A. and Teixeira, A. M. 2003. A critical review of the modeling of wax deposition mechanisms. *Petroleum Science and Technology* **21** (3): 393–408. https://doi.org/10.1081/LFT-120018528

[3] Bhatti, M. S. and Shah, R. K. 1987. Turbulent and transition flow convective heat transfer in ducts. In Kakac, S., Shah, R. K., and Aung, W., editors, *Handbook of Single-Phase Convective Heat Transfer*. Wiley-Interscience.

[4] Bratland, O. 2013. *Pipe flow 2: Multiphase flow assurance*. drbratland.com.

[5] Burger, E. D., Perkins, T. K., and Striegler, H. 1981. Studies of wax deposition in the trans alaska pipeline. *Journal of Petroleum Technology* **33** (6): 1075–1086. SPE-8788-PA. https://doi.org/10.2118/8788-PA

[6] Duan, J., Deng, S., Xu, S., Liu, H., Chen, M., and Gong, J. 2018. The effect of gas flow rate on the wax deposition in oil-gas stratified pipe flow. *Journal of Petroleum Science and Engineering* **162**: 539–547. https://doi.org/10.1016/j.petrol.2017.10.058

[7] Gong, J., Zhang, Y., Liao, L., Duan, J., Wang, P., and Zhou, J. 2011. Wax deposition in the oil/gas two-phase flow for a horizontal pipe. *Energy&Fuels* **25** (4): 1624–1632. https://doi.org/10.1021/ef101682u

[8] Matzain, A. 1999. *Multiphase flow paraffin deposition modeling*. PhD thesis, University of Tulsa.

[9] Matzain, A., Apte, M., Zhang, H., Volk, M., and Brill, J. 2002. Investigation of paraffin deposition during multiphase flow in pipelines and wellbores part1:experiments. *Journal of energy resources technology* **124** (3): 180–186. https://doi.org/10.1115/1.1484392

[10] Reistle, C. 1928. Methods of dealing with paraffin troubles encountered in producing crude oils. Technical report, Bureau of Mines, Washington, D.C. (USA). BM-TP-414.

[11] Sarica, C. and Panacharoensawad, E. 2012. Review of paraffin deposition research under multiphase flow conditions. *Energy&Fuels* **26** (7): 3968–3978. https://doi.org/10.1021/ef300164q

[12] Soedarmo, A. A., Daraboina, N., and Sarica, C. 2017. Validation of wax deposition models with recent laboratory scale flow loop experimental data. *Journal of Petroleum Science and Engineering* **149**: 351–366. https://doi.org/10.1016/j.petrol.2016.10.017

[13] Zheng, S., Saidoun, M., Palermo, T., Mateen, K., and Fogler, H. S. 2017. Wax deposition modeling with considerations of non-newtonian characteristics: Application on field-scale pipeline. *Energy & Fuels* **31** (5): 5011–5023. https://doi.org/10.1021/acs.energyfuels.7b00504

Chapter 5

Qualification of wax control system

This chapter is a copy of the published OTC paper describing the whole WCS qualification test. This was a test of the whole system, including an automated pig launcher, cooling loop, pig/flow diverter valves, and control system. The work was split between the authors of the OTC paper. The paper's main author was responsible for the automated pig launcher, the special flow valve, the control system, pig design, and the system's mechanical design. He was also writing the main body of the paper. The contribution of the thesis author (the third author of the paper) was the design of the cooling loop, preparation of the testing procedure related to wax deposition, selection of the fluid, prediction of wax layer thickness, processing of the results related to wax deposition, and writing sections of the paper related to wax deposition. The thesis author also participated in the design of the special flow valve and the pig.

Please fill in the name of the event you are preparing this manuscript for.	Offshore Technology Conference 2021
Please fill in your 5-digit OTC manuscript number.	OTC-31303-MS
Please fill in your manuscript title.	Qualification Of Wax Control System

Please fill in your author name(s) and company affiliation.

Given Name	Middle name	Surname	Company
Øivind		Stangeland	Subsea 7
Sigbjørn		Daasvatn	Subsea 7
Yuri		Novoseltsev	Subsea 7

Abstract

A cold flow plant consists of a Water Management System (WMS) for separation and treatment of produced water, and a Wax Control System (WCS) for making solid wax particles that can travel through the long tieback line without further deposition on the pipe wall. Pre-conditioning to a level of 1-2% remaining water implies that avoidance of hydrate formation can be handled by reasonable volumes and traditional chemical methods.

The Wax Control System enable a temperature independent transport of oil dominated flows by continuous removal of deposited wax from the pipe wall, allowing the solid wax particles to travel with the flow in the export line without any risk of further deposition of wax along the export pipeline. The technical qualification work included design and operation of a Pigging Loop that allowed continuously removal/ handling of wax within a bundled pipeline.

Introduction

As the offshore activities moves into more remote, deeper and colder environments, it becomes more challenging to design well working tie-back solutions that handles *hydrate formation* and *wax precipitation and deposition* in flowlines.

Hydrates are crystalline structures that form from a binding between light hydrocarbons and water molecules. Appearance of hydrates can be prevented by removing water from the multiphase mixture by separation. Waxes are heavy oil components that usually solidify at *Wax Appearance Temperatures* (WAT) below 60°C. Appearance of wax cannot be prevented in the same way as hydrates, because when waxes are in liquid form, it is hard to separate them from other oil components.

The WAT varies in a typical range of 4-60°C. Well streams will normally have temperatures above the appearance conditions, so waxes are mostly in liquid form as the well stream hit the seabed. As the oil temperature is gradually reduced during the transport inside a pipeline at the seabed, the oil temperature drops towards ambient of around -1 to 10°C, depending on the specific region for the subsea plant and its export pipeline. Wax starts to deposit at pipeline walls as the walls have temperature lower than bulk temperature. The *temperature difference* is thus the driving force of the wax deposition mechanism.

Flow assurance strategies for controlling wax are typically one or several of the following:

- maintaining temperature in a tieback flowline above the appearance conditions
- regular pigging
- processing oil at field on a platform/floating platform

Maintaining the raised temperature above WAT is achieved using insulation of a pipeline to avoid heat losses and potentially with active heating inside the insulation layers to raise the temperature to an acceptable level above WAT.

Traditional heating of the flowlines over longer distances beyond 50km becomes economical inefficient and environmentally challenging when seen from a future low CO_2 footprint perspective. FPSO would typically represent an even more expensive and higher CO_2 footprint solution. Alternative flow assurance strategies are therefore needed for longer tiebacks. One such alternative is to transport *pre-conditioned fluid* with solid wax particles in a slurry at ambient seawater temperature, therefore introducing the term *Cold Flow*.

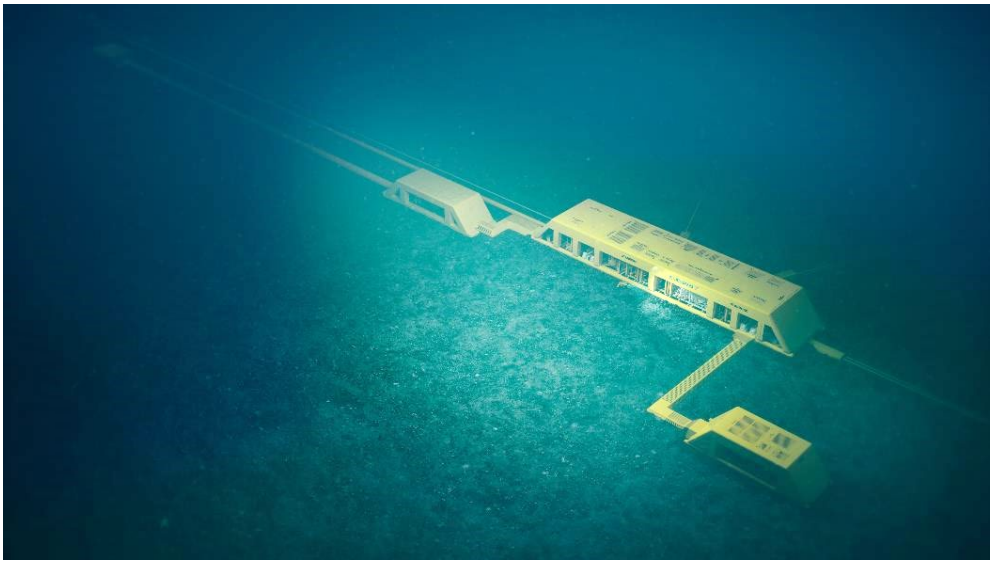

Figure 1 Cold Flow plant with WCS at left side, the pre-conditioning system in the middle, and a water injection system closest to the reader, lower right corner.

Background

Evolvement of a Cold Flow Strategy

Cold flow transport of oil dominated flows has been proposed as a solution to long distance tiebacks for more than 25 years [1], although it has never been in operation yet. Instead, the industry has developed heated flowlines to handle the issues. This is getting increasingly difficult with the increasing tie-back distance as the power consumption increases dramatically with the increased distance. When exceeding around 50km tie-back distance, the cost of heated solutions will exceed the CFS solution, and the CO_2 footprint will make the heated solution even less favourable. As an industry, we need to initiate the use of lower energy focused methods as "Cold Flow Technology" if we want to reduce the energy consumption, and hence produce less CO_2.

Several Cold Flow concepts have been developed by different teams within the industry during the past decades. [3] describes some of the previous work performed within this area by Brown and Root/Halliburton Subsea around year 2000. At that stage, the subsea separation part was not yet sufficiently developed, so the concept stranded. However, the "Wax Eater" described in [1] forms an initial stage of the current development described in this document.

The mechanisms of hydrate formation and precipitation of wax have been in focus during the gradual development work for various systems proposed to handle these issues. This have included a two-stage development consisting of a *Water Management System* (WMS) for separating out most of the water, and a *Wax Control System* (WCS) for making solid wax particles that can travel through the long tieback line without further deposition on the pipe wall. The key principle of the WCS has been to apply simple components that individually has been in use for a long time, such as pigging, cleaning pigs, pig diverters, single phase pumps and pig launchers. The WCS has been designed by a new configuration of the mainly well proven individual technologies, with some additional development to make the assembly work as a system.

Pre-conditioning of well streams for handling hydrates

The main goal of the well stream fluid processing is all about producing oil and gas to a quality that support transportation of valued product.

The pre-conditioning of the well stream ensures that the hydrate formation issue is handled in a controllable manner by regular subsea separation and produced water treatment. Having added the suitable chemicals for treatment of the remaining water, the hydrate issue has been handled before the pre-conditioned well stream is entering the WCS for cooling and wax removal.

At the same time there is a challenge to manage the co-production of produced water. The separation of liquid from gas, and water from oil while managing sand represents an advantage for subsea field developments following in higher production and enhanced recovery.

In the WMS, the fluid is pre-conditioned for long, cold transport by separating out most of the water and sand, and by treating the remaining approximately 1% of water by anti-agglomerates to avoid hydrate formation as the fluid cools down below the hydrate formation temperature of the specific composition. This treatment will ensure that no hydrates will form even if the multi-phase fluid is cooled to ambient seawater temperature.

Boosting for long distance tie-back

A multi-phase boosting station is required to increase the pressure sufficiently for long distance seabed transportation. The booster station will normally require the largest request to the power budget for the cold flow plants.

The boosting system is positioned upstream the WCS to ensure any present gas is compressed to liquid state before entering the cooling and pigging loop inside the pipeline bundle.

Cooling and Wax Removal by pigging

Wax will precipitate and deposit inside pipelines when the temperature is lowered below its Wax Appearance Temperature (WAT). A growing wax deposit decreases a pipeline inner diameter and can lead to a reduction in production and eventually to the pipeline blockage. Cleaning pigs are run to open the pipes again, but such pigs may also get stuck during attempts to clean the pipeline. In general, wax has been one of the dominating flow assurance issues and challenges during the entire history of oil production.

Since the aim is to make sure that wax will not represent any challenge in the long-distance tie-back line, wax needs to be precipitated in the bulk flow and controlled in a defined part of the system prior to the long-distance export. Therefore, a *Wax Control System* (WCS) has been designed and tested.

The WCS cool down the fluid to ambient temperature and remove wax continuously from the heat exchanger by a continuous pigging operation. After cooling, no more wax formation and deposition will occur downstream the WCS, and fluid is transported at ambient seawater temperature.

Towed Production Systems

The increased focus on subsea processing leads to larger subsea structures for such particular solutions. The installation of these structures typically required use of expensive heavy lift vessels. Similar installation assets can be expected if traditional template and processing function technologies are extrapolated into future larger subsea processing plants. This implies a high manufacturing and installation cost for large structures. In remote regions, the negative cost effect will raise significantly. An alternative to larger lifted structures is towed structures and pipeline bundle systems. [2, 3]

A consequence of gradually more functions located at the seabed is larger footprint of the plants. Two main features are leading towards towed solutions for large plants, namely the cost of the installation spread, and secondly, the available weather windows for this type of installations. Towing large plants is more cost effective than installing them by lifting, and the solution can be applied under typical wave height conditions up to 4m significant wave height. This allows for cost effective installation all year around. [4]

Advantages by the Cold Flow development approach

The main advantages of cold flow technology are:

- Cold flow enables a full subsea production plant with a simple, long tie-back export line to a host platform for offloading to shuttle tankers at power budgets and a cost level far below a comparable FPSO or heated pipeline solution.
- Risk exposure to personnel is significantly reduced compared to FPSO solutions since there are no people present during daily operation.
- The entire pipeline system could be simplified since insulation is not required at any location after the SPU. This will reduce the pipeline cost.
- Since water and gas is separated out, the fluid can be handled by simpler single-phase pumps and pipeline diameters can be reduced.
- Location of separator at seabed increased the production from the reservoir due to the reduced back pressure.

- The removal of water from the production stream reduces the system static head and allows use of smaller pipes.
- Separation processes are more effective at wellhead temperature than at topsides fluid arrival temperatures.
- Removal of the water will lead to a reduction in chemical injection requirements.
- Short installation campaigns using a non-specialized vessel spread.
- Installation of a cold flow plant is not very schedule dependent on other construction vessels to finalize work.
- The new system is basically a *smart collection* of *matured technologies*, assembled and joined together on a useful transport platform which turns it into a low budget installation, with a future simple retrieval and eventually removal.

This paper will focus on the design and qualification of the Wax Control System.

Design of Wax Control System

At the inlet of a WCS, the wellstream will be in a pre-conditioned state, with a de-watered wellstream, at temperature approximately at wellhead temperature. The pressure may be boosted to match the requirements of the specific long-distance transport. This will ensure that any gas is liquified before the fluid enters the long heat exchanger.

The goal is to design a system that lead to an outlet temperature without any significant temperature gradient to ambient seawater. This means that we need to analyse the flow through the heat exchanger and pigging loop and tune the design to match the specific chemical composition of the fluid. The flow rate and temperature of the cooling water is important input to the calculations. Similarly, the production fluid composition, its flow rate and associated temperature are other important parameters. Heat will be transferred between the two counter current media as long as there is a temperature gradient. As the temperature difference is reduced, the heat exchange rate becomes lower, and the efficiency is reduced. At some temperature difference, one need to do a cut-off of the process and accept a minor temperature difference of, say 2-5 degrees. This cut-off point will then determine the cooling length, as well as the pipeline bundle design length.

An efficient *wax deposition zone* is created inside the pig loop of the pipeline bundle as a consequence of the large temperature gradient that is set up by the cooling water. This temperature gradient is the driving force that moves precipitated wax particles in the flow radially outwards, so the particles stick to the outer wall.

The counter current annulus-cooling case is validated to reduce the temperature to adequately knock out potential wax from the oil in the wax deposition zone.

The annulus cooling approach is considered to provide an efficient and economic wax control strategy for the mechanical removal of wax in a wax control zone when pigging of wax is to be employed in a flowline eliminating excessively long pigging routes and high cost of pigging operation in typical subsea

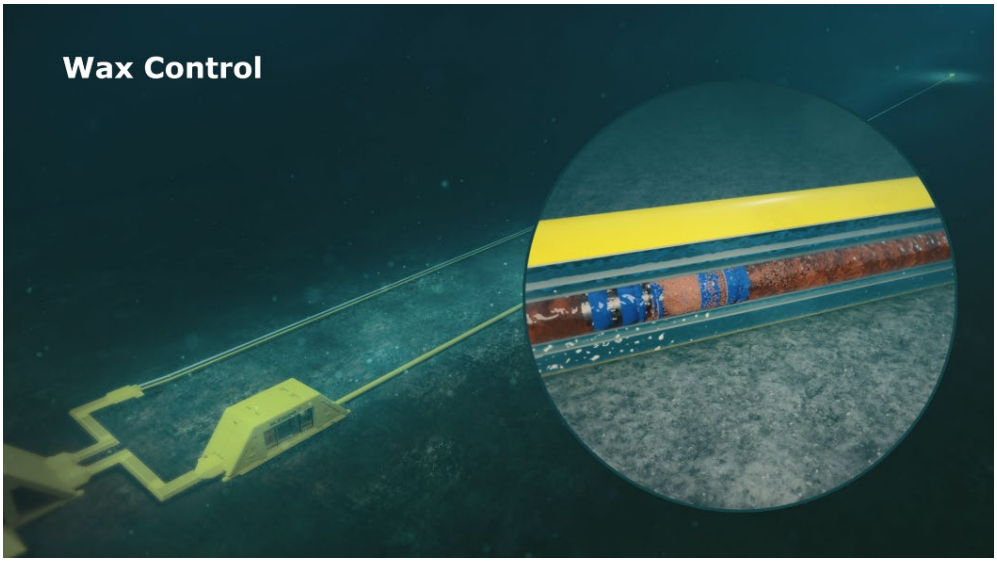

Figure 2 The Wax Control System components are installed mainly in the leading towhead connected to the subsea pre-conditioning plant. The cooling and pigging loop is designed to fit into a pipeline bundle system of, typically 3-4km long. Cooling length will be twice this length since the flowline turn at the end and flows back up the line.

Theoretical basis for wax control

Waxes, wax formation, and deposition have been studied since the beginning of the previous century (Reistle, 1928). The first paper that provides an in-depth study of wax deposition mechanisms was published many years later [5]. This paper became a reference work on the topic. Since then, there has been a significant amount of experimental and modelling work related to wax prediction in single phase oil flows. This resulted in improvements in understanding the physics behind the deposition phenomena.

In relation to a wax control system, it is imperative to be able to calculate the wax growth rate and predict the amount of wax deposit quantitatively with time. Therefore, as part of the development work, there was a need for developing experimental data and accurate models for the prediction of amount, location, and evolution in time of wax deposits in a pipeline.

A Ph.D. program to further study this theme have been initiated in order to reveal a suitable formulation of equations necessary to describe the theory of wax precipitation and deposition inside a counter current heat exchanger used to force cool the fluid. The study incorporated selection from available wax deposition models [6, 7, 8, 14, 15, 16] and associated optimisation to output reasonably accurate predictions for the conditions of the WCS. Additionally, feasibility assessment of having multi phase fluid in the WCS was done. The requirement to include wax mechanical properties variations due to aging [17], effect of operating temperature [18], flow conditions [19], was evaluated as well. The mathematical model should provide prediction of wax deposition in the laminar or turbulent waxy oil flow under relatively fast cooling conditions and allow design of such system. The PhD work is expected to be completed and issued by second quarter of 2021.

Software for design of WCS

A software simulation module has been developed to control the governing equations of the WCS. The simulation module replicates a pipe-in-pipe system with oil flow in the inner pipe and water flow in the anulus between inner and outer pipes. The software can work with two formulations: one dimensional or two dimensional. One dimensional formulation is fast but has only longitudinal axis, meaning that all values are averaged radially. The two dimensional one has longitudinal and radial axes, so it is possible to get radial profile of the variables, i.e. temperature change from the pipe wall towards the pipe center.

For one dimensional formulation concentration gradient at the wall is based on temperature gradient from a correlation and solubility curve, while for two dimensional it comes "naturally" as part of the equation's solution.

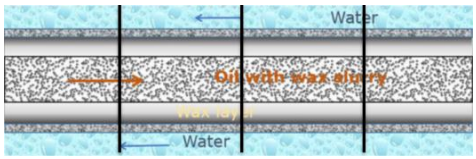

Figure 3 Principles of one-directional heat flow inside WCS.

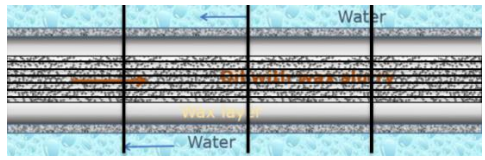

Figure 4 Principle of two-dimensional heat flow inside WCS.

The above figures show the one dimensional and two-dimensional computational grids for the WCS cooling and pigging loop.

The wax deposition in one dimensional follows the idea described in [7] and [8]. The set of coupled equations comprises equations for oil energy, water energy, solid particle wax transport, dissolved wax transport, wax layer thickness growth and wax layer solid are found from well-known correlations, for example Nusselt number is found from Gnielinski and Petukhov equations.

The benefit of the one-dimensional formulation flow is that it is simpler, and it is faster to solve due to smaller grid. However, the calculation of the wax concentration transport in radial direction can only be done empirically and is tied to temperature gradient and solubility curve only.

The formulation model is changed in the two-dimensional model. Now, the equations comprise a common formulation of Oil and Water energy, an equation for solid particle wax transport, and a formulation for dissolved wax transport. The two-dimensional solution requires more calculation time but improves the full description of the problem through the modified couplings in the calculations. The wax concentration gradient and temperature gradient are part of a coupled solution rather than locked empirically versus each other.

The main caveat of the two-dimensional formulation is that it requires radial velocity profile and estimation of the radial turbulent transport coefficients. Instead of solving for velocity and turbulence the formulation follows the idea in [9]. Closure relations includes, but are not limited to [10, 11, 12], friction factors for Herschel Bulkley fluid [13], velocity profile, waxy oil viscosity correlation, etc.

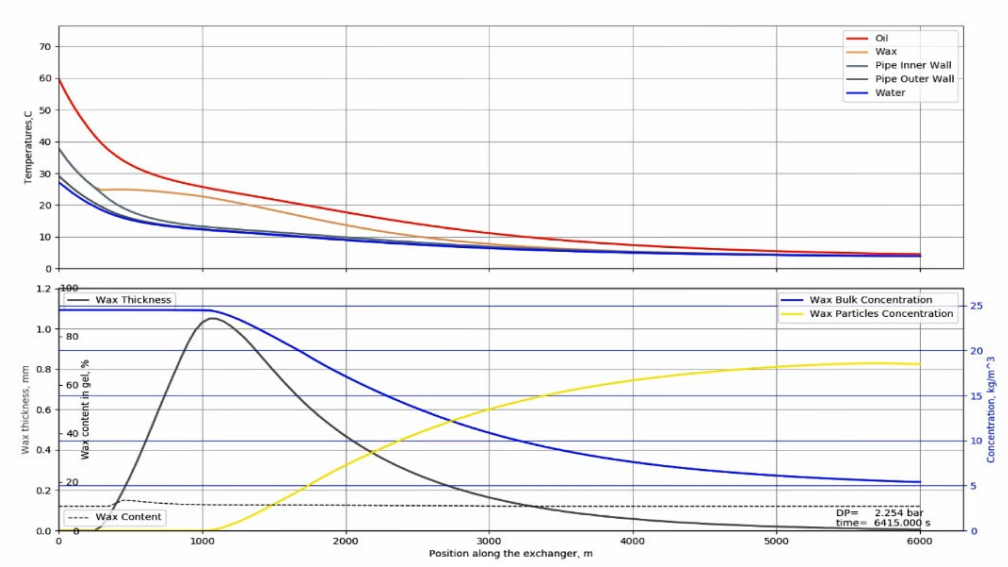

Figure 5 Simulation of wax precipitation and pipe wall deposit along a 6000m Pig Loop.

Towed Production Systems

The WCS has been integrated into a Towed Production System (TPS), see [2] and [3].

A classic example of this alternative is Towed Pipeline Bundle Solution where multiple flowlines packaged inside a carrier pipe terminated with towhead structures (manifolds), fabricated onshore in a single length. This solution serves for the production, water injection, gas lift, service, controls and insulation.

The TBS technologies for larger subsea solutions is no being further developed. This is based on even more extensive pre-fabrication and assembly onshore, and fast installation offshore requiring significantly less marine operations to perform the work.

A practical WCS has been developed, based on existing technologies like the towed pipeline bundle in combination with single phase cooling water pumps and traditional pigging technology with remotely controlled pig launching. The latter has been developed through the project and is now qualified together with two different flow diverters which aids in the process of running the pigs.

Qualification of Wax Control System

Focus for the technical qualification (TQ) work has been to verify functionality of the pigging principle and long lifetime for the system. This has been achieved through novel design of multiple automated pig launcher, cleaning pig and other related equipment.

The premise for the work has been taken from DNV-GL RP A203 which gives guidelines and recommendations for this type of technical qualifications. DNV-GL RP A203 describes some key documents and activities that have formed the basis for the qualification work:

1. Technology Qualification Basis
2. Risk Assessment Workshops
3. Technology Qualification Plan
4. Test procedures and test reports

The Technology Qualification Basis (TQ-basis) is the document describing the technology to be qualified. Critical parameters that defines the envelope for the qualification work is listed. Typical parameters are:

- Oil temperature: Inlet temperature > Wax Appearance Temperature
- Oli flow velocity: Up to 2 m/sec
- Oil field water cut (H_2O content, volume %): Up to 1%
- Oil field wax content: Up to 7.5% (weight)
- Nominal oil pipe size: from OD 8" to OD 14"
- Design Life: 25 years

New Components for Wax Control System

The main function for the WCS is to condition the wax in oil so it can be transported as solid particles in main flow without depositing on export pipeline. This is done by continuously pigging and removal of deposited wax from a bundled part of the pipeline, while flow is actively cooled down to ambient temperatures. The wax scraping pig is "looped" in the bundled pipeline, which is done with novel designed pig diverter, pig station and flow directional valve.

The following novel equipment have been developed and built as a part of the qualification:

1. *Automated Multiple Pig Launcher* (AMPL) - The AMPL is a subsea pig launcher with a 5-pig magazine in vertical configuration. It will launch Cleaning Pigs at required interval (typ. 3-6 months) depending on wear and lifetime for the looped pig.
2. *Heat exchanger and Pig Loop* - The bundled Pig Loop is stretched out to exchange heat between flowline and seawater. The flushing of cooling water using cooling water pumps lead to wax precipitation and depositioning at the inside pipe wall. The production pipe comprises a pipe in pipe seawater cooling system that lowers the oil temperature to ambient before entering the export line.
3. *Flow and pig controlling equipment* - The Cleaning Pig is looped within the bundled Pig Loop. This is done by control of inlet and outlet flow through Flow Directional Valve (FDV), Pig Diverter, and Pig Station.

4. *Cleaning Pig* - The Cleaning Pig is a flow driven wax scraping unit that circulates within the Pig Loop. It will be in service for 3-6 months before replacement, with up to 12 rounds in Pig Loop each day.
5. *Control System* - The WCS is operated through a dedicated control system. The control system comprises of already qualified equipment, like pressure sensors, temperature sensors, pig detectors, etc.

Pictures below illustrates a real life WCS, with main components. Note that bundle length is shortened for illustration purposes. Typical length could be 3-4 km.

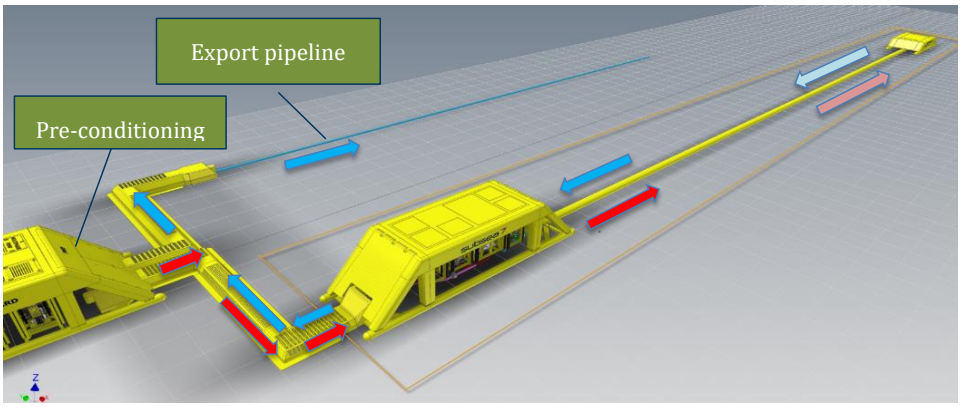

Figure 6 Wax Control System downstream SPU - Upstream export line. RED=Hot oil with melted wax BLUE=Cold oil-wax slurry

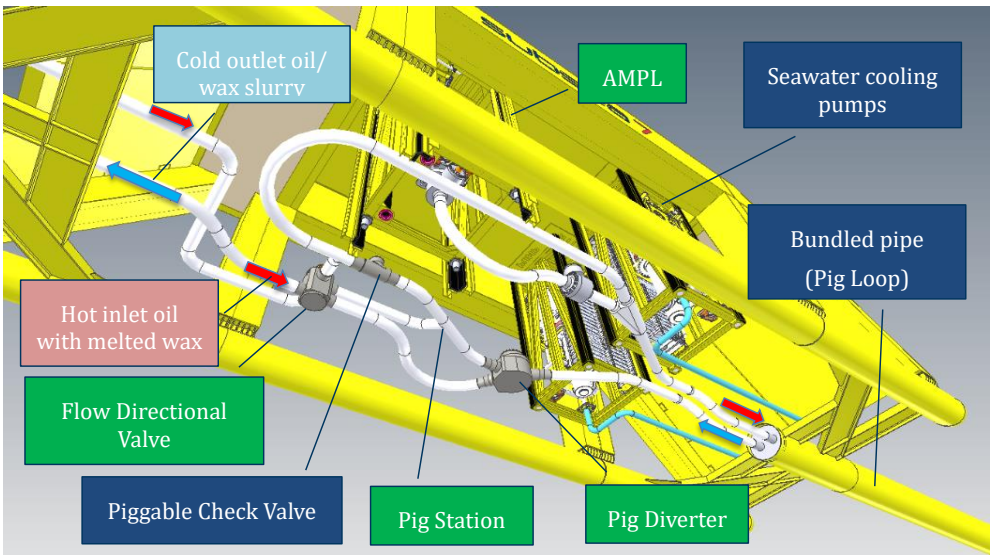

Figure 7 Main equipment Wax Control System- Green=Novel Equipment (part of qualification program), Blue=Already qualified Equipment

Wax Control System Qualification Rig

All the above-mentioned equipment has been designed and assembled into a qualification rig. The purposes of the Wax Control System-Qualification Rig are:

1. Replicate an actual WCS system as close as reasonable in a small scale
2. Qualify pigging principle in single phase
3. Confirm wax removal capability
4. Confirm literature claim of wax deposition condition that in case of no temperature difference between pipe wall temperature and oil bulk temperature there will be no wax deposition on the pipeline walls.

This rig was operated for approx. 15 months, and all required testing defined in before mention TQ-plan was conducted successfully.

Table 1 Main data WCS-Qualification Rig

Nominal pipe diameter:	6inch
Pipe length:	120 m
"Bundle" length:	~50m
Pressure differential between inlet and outlet	0-19 bar
Flow:	0-2200 l/min (flow velocity to be 0-2 m/sec)
Test liquid initial tests:	Fresh water
Test liquid main test period:	Single Phase oil with wax (hydraulic oil-paraffin wax)
Liquid volume:	4000l
Temperature oil:	Between ambient (~4°C) and 60°C
Wax content:	Up to 7,5%

The WCS qualification rig was installed at Dusavik Base in Stavanger, Norway.

Figure 8 Wax Control System Qualification Rig. Approx. 120 m 6" pipe. Picture show AMPL (right side), Pig loop, Pig Diverter, control container, Pig Station and Flow Directional Valve.

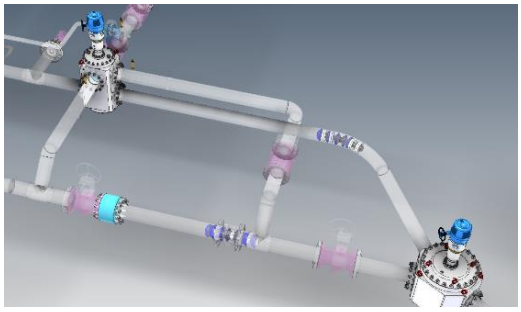

Figure 9 Flow and pig controlling equipment. Pig Diverter (right side), Pig Station and Flow Directional Valve (up left). Note that transparent pink valves are test equipment only and will not be a part of real life WCS.

Figure 10 Cleaning Pig. Articulated 3 section design.

Failure Modes, Effects and Criticality Analysis (FMECA)

Risk Assessment Workshop was conducted as a collaboration with DNV-GL. The main goal for the risk assessment was to reveal the important failure modes through general assessments and by using the FMECA method. Each of the main equipment objects mentioned below was systematically assessed, and all findings and threats for each object ID was quantified and evaluated.

Upon completion of the risk assessment, a Technology Qualification Plan was created. This document described the required equipment testing and gathering of evidence required to achieve TRL 4 on a system level. It is a systematic approach that list up each item and item ID from risk assessment, with test and evidence requirements.

A total of 105 failure modes have been evaluated and rated, through technology and threat assessments. A summary of the most critical failure modes is listed below, with a description on the results of the qualification tests.

Table 2 Examples of Failure modes/ Effect, results and mitigations

Equipment	Failure Mode/ Effect	Results from test	Mitigations
Flow Directional Valve	To high cross flow between closed branches. Will lead to temperature increase in fluid in export line	Test revealed too high leak from a practical point of view. Acceptable leak rate was set to 3%. Note that 'leaks' does not reach ambient water outside of the piping, only harmless through the diverter.	In order to reduce the leaks below limit, it is proposed to narrow fabrication tolerances to reduce the active leak exposure area.
Flow Directional Valve	Internal hub will not rotate due to jamming, or similar. Pigging principle not working	No sign of jamming, or change in operation torque during test period (>1500 operations)	N/A
Cleaning Pig	Structural failure or damage from wear on pig after long term use in Pig Loop. Pig will not scrape wax	Acceptable wear on seal rings. Lasted 3 times longer than expected and anticipated. Average 4.2% mass reduction on seal rings after 1457 rounds in pig loop.	N/A
Cleaning Pig	Wax build up in front of pig. Bypass flushing system not working. Pigging principle not working. Flow constricted.	No sign of wax build-up in front of pig, or in-between sections during entire test period.	N/A
Pig Diverter	Fail to divert due to wax or debris build up internally. Pigging principle not working. Not able to divert pig.	No sign of jamming during test period. Debris from broken pig (plastic parts) passed the Pig Diverter, or was flush out during normal operation	N/A

Equipment	Failure Mode/ Effect	Results from test	Mitigations
AMPL	Damage to Cleaning Pig seal rings from long time storage. Fail to launch Cleaning Pig	No sign of material degradation during test period. Cleaning Pig have been stored in AMPL magazine 4 months under various temperatures.	N/A
AMPL	Fail to hold the pigs due to mechanical overload. AMPL not able to launch Cleaning Pigs. Cleaning Pig damaged during launch	All launches successful. Impact load test performed. No sign of deformation or change in operation behavior after test. No damages to pigs.	N/A
Pig Loop	Wax deposition in Pig Loop is not accrding to specifications. Too large difference between simulated wax thickness values and actual measured values.	Wax built up after 3 hours was measured and compared to theoretical simulated values. Wax thickness difference was acceptable within a reasonable span of 20%.	N/A
Control System	Pig launch from Pig Station sequence started with no pig present. Pig potential to be pushed back into Pig Diverter	Test revealed that pig can be pushed back towards Pig Diverter if Pig Diverter and FDV is operated at same time, and Pig has not passed outlet T.	Blocking bars will be added in Pig Diverter internal hub in order to prevent pig from entering Pig Diverter internal voids.

The above table presents a selection of 105 different failure modes verified through the qualification program. The systematic response from the system on the test program demonstrates that a simple piggable routine inside a pigging loop works well and operates stably at a very high level.

Qualification activities, tests and results

Test procedures and test activities was established based on TQ-plan. The main tests comprised of the following types of tests:

1. Function and qualification test
2. Accelerated wear Test
3. Test of no wax deposit in export line
4. Control system test

Each of the main test included testing of several equipment units, e.g. the Function and Qualification test will include testing of pig looping principle, Pig Diverter, Cleaning Pig and Flow Directional Valve.

Function and qualification tests

This test includes testing of the WCS pigging principle, including the different main equipment under various conditions. The test demonstrates that the technology is functioning as planned, both as an assembly, and as standalone units. Further breakdown of test is described below.

Overall Test

Generally, the Overall Tests will be tests that spans over several equipment units.

These tests have shown that the pigging principle (circulation of pig) worked as planned. The system has been tested under various temperatures, wax % content, flow, sand loads, and similar. During test period wax have been added in step of 1%, 3%, 5% and finally 7,5%. This was done in order to verify that the pigging principle work under increasing wax content.

As a part of the overall tests a conservative amount of quarts sand was added at several stages during the test period, in order to simulate sand load.

The accidental case of several Cleaning Pig released from AMPL was tested, in order to verify that the system has the capability to handle “pig trains” without blocking main flow.

Function and Qualification test - Flow Directional Valve

The Flow Directional Valve’s main functions is to divert the hot inlet oil in such a way that the parked pig in Pig Station is launch for a new round. It also acts as a barrier between hot inlet oil and cold outlet oil.

The Flow Directional Valve have been subjected to several test during test period, in order to measure cross leak, actuation load, crash test of Cleaning Pig in FDV and sand/ debris build up. The FDV have been operated >1500 times back and forth, and it have generally worked as planned. Inspection and measure of wear will be covered under “Accelerated wear test” below.

The acceptable cross leak between inlet and outlet side have been set to less than 3%. This is to reduce the amount of hot inlet oil being bypassed directly in to cold outlet oil. This cross leak was measured to be higher than acceptable. As a mitigation to this the general tolerances between internal drum and housing will be narrowed down. Calculation have been done to verify that this is achievable within normal fabrication processes.

Function and Qualification tests - Cleaning Pig

The Cleaning Pig main function is to scrape wax from pipe sidewall while circulating in Pig Loop. It is an articulated 3 section design, with cup shaped seal/ scraper ring. It also comprises a bypass flushing system in order to prevent wax build up in front of pig.

It was generally found that Cleaning Pig work better than planned. The required delta pressure in order to move the pig through the Pig Loop was found to be far less than estimated, especially when moving in cold oil with high% wax particles. It is assumed that this is related to more resilient lubrication film for the high viscosity cold oil/wax slurry, compared to the low viscosity hot oil with melted wax.

The flushing system work as planned. No permanent wax built-up in front of pig, or in pig internal was discovered.

The Cleaning Pigs have been “crash-tested” by running in to, and through partly opened ball valve, finger grip (slips) and similar obstructions. None of these tests led to breakage of pig, or pig seal rings. Some imprint was observed on front bumper, without any sign of rupture.

The measured wear of pig is covered under “Accelerated wear test” below.

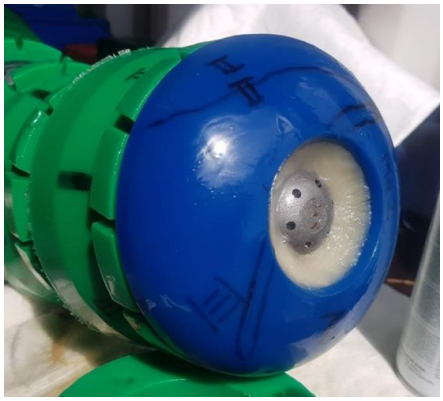

Figure 11 Front view Cleaning Pig. Note wax leftovers and 6x nozzle holes. This show that bypass flushing system work as planned

Figure 12 Front of Cleaning Pig with scratches and imprints (marked with black marker) from collision with partly opened valves.

Function and Qualification tests - Pig Diverter

The Pig Diverter have two main functions

- it diverts the Cleaning Pig into the Pig Station, or exit into export line
- it blocks the Pig Station inlet during launch of pig for new rounds.

The Pig Diverter is located at end (outlet) of pigging loop, hence it will only be subjected to cold oil with wax particles.

The Pig Diverter have been subjected to similar test as Flow Directional Valve, except for the cross-leak test. Cross-leak for the Pig Diverter is related to launch of pig from Pig Station, and not to barrier between inlet and outlet flow.

During a control system test it was revealed that a Cleaning Pig can travel backwards and slide into Pig Diverter internal void if the Pig Diverter is partly operated. This will be mitigated in the future by installing blocking bars in the hub that will prevent pig from entering internal void.

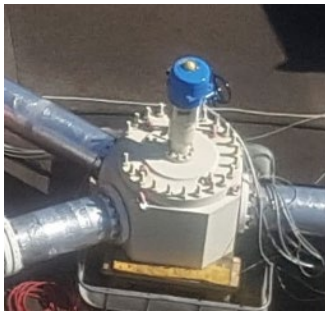

Figure 13 Pig Diverter in qualification rig

Figure 14 Inlet port Pig Diverter. Notice blocking bars (2 of) that prevent pig from entering in to void. Similar will be fitted on outlet port

Figure 15 Parts of broken seal ring and guide ring that was sent in the flow through the Pig Diverter.

Function and Qualification tests - Pig Loop

The main function of the Pig Loop is to cool oil in order to build wax deposit on pipewall for Cleaning Pig to remove/ scrape off.

The Pig Loop will be a bundled oil pipe, with sea water based cooling annulus. It is imperative that the internal surfaces are snag free and have a smooth finish. This to reduce wear and extend lifetime for Cleaning Pig.

The qualifications rig ability to produce realistic wax deposition was demonstrated. This demonstration was done by circulation of hot oil with fully melted wax, and then actively cooling in order to get a temperature gradient between oil and inner steel pipe surface. Test was repeated for each increasing wax% content from 0 to 7,5% wax, and thickness of wax layer was measured.

Figure 16 Wax layer after 3-hour cooling from 55°C to 15°C in rig. Wax was scraped from reference area inside pipe and weighed.

Figure 17 Oil/wax slurry in tank after cold night. Notice gel consistency. Also notice Cleaning Pig seal ring (green) that was stored in tank during test period

The design of the real life WCS Pig Loop is done in such a way that all wax build is either removed by pigging, or by cyclic flowing of hot oil during relaunch of pig from Pig Station. However, since the qualification rig was run for long periods in cold oil/wax only, some large wax build-up occurred at some section of the pipe. This was revealed after de-mounting Pig Loop at end of test period. As mentioned, this is not a problem since this part of the pipe will be regular flushed with hot oil. In fact, the wax builds up only proof that the Pig loop is suitable to build wax when required.

Figure 18 Large wax build up in part of Pig Loop that is not pigged or flushed with hot oil.

The wax layer thickness has been compared to software simulation of similar Pig Loop. This has been done in order to verify that wax layer in Pig Loop can be estimated based on software simulations.

Function and Qualification tests -Automated Multiple Pig Launcher (AMPL)

The AMPL main function is to launch Wax Cleaning Pig in to Pig Loop when required. The design comprises 2 main items; The Pig Launch Mechanism and the Pig Magazine. The Pig Launch Mechanism functionality launch one pig while holding back rest of pigs in magazine. Hence only one kick-line is required.

The entire AMPL will always be recovered during refill of pigs. This is a maintenance operation that will happened typically with 1-2.5-year intervals based on pig wear.

The AMPL have performed as planned during test period, with no errors detected. It has been used for 83 logged launches, 2 in water and rest in oil with increasing wax content and various temperatures. Debris in shape of gravel and metal bits have been added in to AMPL magazine and kick line inlet to verify robustness of mechanism. Cleaning Pigs have been launched through partly opened finger grip “pig slips”, and pig retainer wedge without damaging Cleaning Pig or Pig Launch Mechanism.

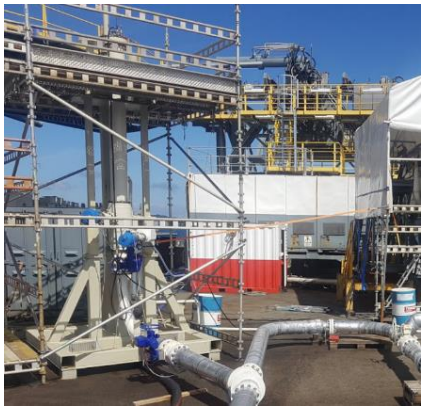

Figure 19 AMPL in qualification rig.

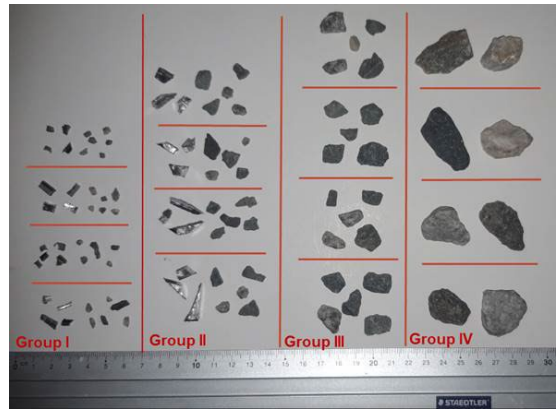

Figure 20 Gravel and metal debris inserted in to AMPL

Accelerated wear test

This test includes long term testing of the Flow Directional Valve, Cleaning Pig, Pig Diverter, Valve Stem and Pig Loop. This includes running same Cleaning Pig 1453 rounds in Pig Loop. Flow Directional Valve and Pig Diverter is operated once each round; hence more than 1500 activations have been done. After completion of test pig loop, Flow Directional Valve and Pig Diverter was dismounted and inspected.

Accelerated wear test – Flow Directional Valve

The Flow Directional Valve have been observed and checked during test period. Both Flow Directional Valve and Pig Diverter is operated by electric actuators. Power requirement for actuators have been logged, together with time to full stroke both ways. No significant changes in behaviour have been detected. Typical stroke time is 45-50 sec for flow velocities varying from 0-2 m/s.

Flow Directional Valve was dismantled and inspected after finished test period. Glider rings (plastic) thickness was measured without noticeable wear. No sign of erosion or abrasion from sand load was observed.

Figure 21 Metering of current during actuation. Internal hub in FDV lifted out for inspection. Notice glider rings (black) at top. Samples from oil/wax slurry was taken for later analyse.

Oil with wax sample was taken from internal voids. Inspection revealed no sign of sand/debris build up.

Accelerated wear test – Cleaning Pig

Since the life time of the Cleaning Pig is imperative for the WCS to be cost efficient, high focus have been on the tests of this unit. A service period for 100 days with 10 rounds in bundled Pig Loop each day will add up to 1000 rounds. Depending on bundle length the total travel distance could reach 10000km. However, since the internal surface of the bundled pipe will be smooth, and the pig will travel in waxy oil, the expected wear and tear on the Cleaning Pigs should be minimal.

During the test period one of the Cleaning Pigs have been run 1457 logged rounds in the qualification rig under various temperatures and conditions. After 1000 and 1457 rounds the Cleaning Pig was dismounted and inspected by weighing, dimensions and shore values. The results where compared to new, unused seal rings.

The average wear (mass reduction) for all seal ring on pig was 3,2% after 1000 rounds, and 4,2% after 1457 rounds. This indicates that most of the wear occurs at start of service time.

The diameter reduction for the seal rings indicates some creep. This is not considered a problem since the cup shape of the seal rings will give a "self-adjusting" function from back pressure.

The general experience was that the Cleaning Pig performance improved during test period, and its ability to remove wax was unchanged. The wear increase between 1st and 2nd measure show that the wear curve "flattens out" during service life.

In addition, one seal ring was placed inside oil tank for entire test period. This to verify that seal ring material does not deteriorate or change properties while stored in oil.

Accelerated wear test – Pig Diverter

This test is identical to Flow Directional Valve above. Also, the Pig Diverter was dismantled and inspected after finished test period. No sign of erosion or abrasion from sand load was observed.

Oil with wax sample was taken from internal voids. Inspection revealed no sign of sand/debris build up.

Figure 22 No erosion or abrasion around leak paths

Figure 23 Open and inspection of Pig Diverter. Oil/wax slurry sample from different internal voids was collected to look for sand deposits

Accelerated wear test – Multi Valve Stem

The multi valve stem is a generic designed seal system that is used on several equipment in the WCS. It will act as barrier between production flow and environment. It is used on the AMPL and on both Pig Diverter and Flow Directional Valve. These last two units will be permanent subsea equipment, with 25-year lifetime. This means that the valve stem will be operated up to 12 times each day for 25 year subsea.

The valve stem has been special designed for the WCS, with long life seal rings, environmental seals and scraper rings. It has been operated the same amount as the FDV and Pig Diverter, which is >1500 cycles.

In parallel, a technology search has been done in order to find already qualified valve stem, that can deal with similar conditions. This is done in order to avoid long term qualification testing.

Accelerated wear test – Pig Loop

The Pig Loop in the qualification rig is approximately 120m. This is significantly less that a real life WCS, where the Pig Loop could be up to 10km. However, it is assumed that most of the wear and tear on Cleaning Pig comes from moving over snag points, like flange splits, weld imperfections and bend. Hence the qualification rig Pig Loop consist of is flanged construction components it will be conservative

compared to a fully welded Pig Loop. The number of Cleaning Pig circulation in qualification rig is >1500, which represent more than 3 months operation time in a real life WCS.

After completion of test the Pig Loop was dismounted and visually inspected with special focus on 5D bend. No sign of wear and tear was revealed, but surface corrosion was found. This comes from fabrication and from initial test with water. This adds conservatism to the accelerated wear tests.

Figure 24 Part of Pig Loop with 5D bends

Figure 25 Inside 5D bend. Corroded surface from fabrication and initial testing with water

Test of no deposition in export line

The main goal for a cold flow plant is to prevent wax deposit in long export/ transport pipelines. The theory states that as long as there is a marginally small temperature gradient between bulk oil and pipewall, no deposition of wax will occur.

This was demonstrated with the specially designed “Test of no deposit in export line” test. In this test, cold oil with wax particles (oil/ wax slurry) was circulated in Pig Loop over several days, maintain same temperature in oil/wax slurry and steel pipe. This was done by running seawater cooling in Pig Loop annulus.

The test was run for 3 days a 7.5 hour, with the cooling water running all night and over the weekend. After this the Pig Loop was drained, split open and inspected for wax build up.

A shorter version of the test was done at a later stage, in order to check trend in wax build up. The test shows that when the temperature gradient is kept low, there will be very little wax deposit. The deposit was measured by scarping out wax from a reference area inside the pipe and weighing it. Weight of wax scrape out from 20cm section of pipe:

- Amount wax after short cold flow test: 6g
- Amount wax after long cold flow test: 11g

Amount wax after normal wax production from 55°C to 15°C: 165g

It was generally difficult to scrape out wax after cold flow test, due to low viscosity. It is assumed that most of the wax deposit was not actually deposited during regular flow, but rather as “leftover” when pipe was drained before splitting. Based on the findings it was concluded that the cold flow principle work well using the WCS test rig.

Figure 26 Amount of wax after cold flow test. Weight=11g

Figure 27 Amount of wax after normal wax production. Weight=165g

Control System Test

The control system for the WCS will be based on already qualified equipment, like temperature sensors, pressure sensors and pig detectors. A software with logical functions will run the pig bypass operations. This includes detection of pig in Pig Station, Operated Pig Diverter and FDV to launch, detection of pig entering Pig Loop and successive operate Pig Diverter and FDV back to default position.

Main functions for the control system will also be to monitor the pig positions, delta pressure in Pig Loop, temperatures in Pig Loop and wax thickness.

Test have been done on the control system in order to verify redundancy in case of faulty pig detectors. It has been shown that displayed pressure peak can be used to detect passing of pig.

Figure 28 Pressure peak when Cleaning Pig passes pressure sensor at start of Pig Loop

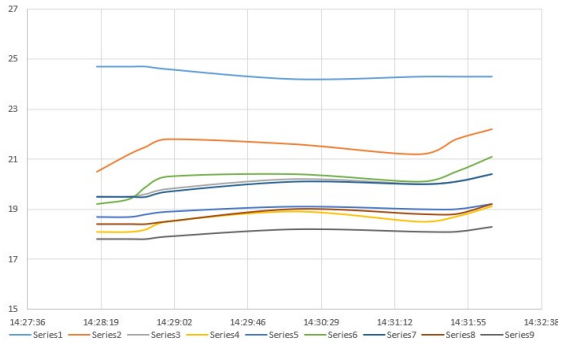

Figure 29 Temperature increase in step as Cleaning Pig removes wax on sensor tip in Pig Loop

It was proven that the temperature increase from removal of wax on sensor tip can be used to indicate wax thickness build-up in pipe. Thus, certain knowledge about the wax situation in the pigging loop will be available to the operation control room.

Conclusions

The WCS has been tested and qualified to TRL-4 according to DNV-RP-203. The test results from the TQ work proves that the Wax Control System is a simple, reliable and robust technology that allows for long distance transport of oil dominant flow at ambient temperatures. The qualified equipment is well suited for 20-year subsea operation, with little intervention requirement.

The developed software module provides comparable results to the test rig and can be applied for design of future WCS's.

Operation of the WCS allows for adjustments in e.g. pigging frequency if required to handle different fluid compositions.

The results from the technology qualification test period shows a superb performance and includes measurement of wear and tear for relevant equipment and logging of main parameters pressure, temperature and flow during testing.

More than 80 successful pig launches have been done using the AMPL technology under various wax conditions in water and in hot and cold oil.

The cleaning pigs and pig controlling equipment have been run for more than 1500 rounds under various condition. Wear and tear have been monitored during test period. Photos and videos have been used to document the successful results.

Long lasting cleaning pigs can be run up to 6 months before diverted out of loop, and novel design of pig controlling equipment ensure a simple, low cost, system with very low CO_2 footprint compared to topside solutions.

Future work

Long term testing of seal stem arrangement and Cleaning Pig seal ring material

As mentioned earlier, main purpose for the qualification work has been to verify that the pigging principle with continuously pigging in pipe loop functions as planned, and that the equipment used in the qualification rig is suitable for long term use subsea.

Even if the overall system has been qualified to TRL4 there are still some long-term testing required for the different equipment packages. Some of the equipment could be operated up to 12 times each day for 25 year. According to valve manufacturer this number of cycles is well within capabilities of existing seal solutions, however it has not been qualified. This applies for valve stem seal arrangement for permanent subsea installed equipment.

The polymer material used in the Cleaning Pig needs to withstand long term storage in crude oil, without compromise its ability to remove wax when in service. Long term tests in realistic conditions (crude oil, low temperature, deformed ("squeezed") seal rings) could be candidates for future work.

AMPL with large capacity pig magazine.

As an alternative to Wax Control System in bundled pipe loop, the export pipeline could in some cases be frequently pigged in order to prevent wax build up. This would require large capacity pig magazine in order to limit magazine replacement cycles and maintain economic feasibility.

The AMPL designed for use in Wax Control System today has a two-split design that allows for larger magazine to be fitted, typ. 50-100 pigs. Some concepts have been evaluated, like revolver magazine, or coiled pig magazine. Future work could include further qualification of such a system.

Acknowledgement

The authors would like to acknowledge Subsea 7 for permission to publish the results presented in the paper. The authors would like to thank Mr. Torstein Meling for his extensive design and testing efforts during the qualification work, as well as Mr. Ratnam Sathananthan in particular, for his long-term contribution through several decades within the subjects of *Flow Assurance* and *Cold Flow development*. The qualification project has received substantial public funding from the Norwegian Research Council.

References

1. Dr. Tin Win and Raj Amin, "Extended Tiebacks - The future of the Deepwater Offshore Developments", DOT 2000, Brown & Root Energy Services.

2. A.S. den Boer and E.J. Rooduyn, OTC 6430, 1990: "An Integrated Towed Flowline Bundle Production System for Subsea Developments", Rockwater Offshore Contactors.

3. Jim Brydon and Ratnam Sathananthan, OMAE01-4100, 2001: "Enhancing Subsea Production Using Pipeline Bundle Systems", Halliburton Subsea.

4. Sigbjørn Daasvatn, Rasmus Juhlin and Morten Sæterdal, OTC-29002-MS, 2018: "Modular Integration Platform – Submerged Production Unit for Large Subsea Plants", Subsea 7.

5. E.D. Burger; T.K. Perkins; J.H. Striegler, SPE-8788-PA, "Studies of Wax Deposition in the Trans Alaska Pipeline", J Pet Technol 33 (06): 1075–1086.

6. Sheng Zheng, Mohamed Saidoun, Thierry Palermo, Khalid Mateen, and H. Scott Fogler, “Wax Deposition Modeling with Considerations of Non-Newtonian Characteristics: Application on Field-Scale Pipeline”, Energy and Fuels 2017, 31, 5011-5023.

7. Singh, P., Venkatesan, R., Fogler, H. S., and Nagarajan, N. “Formation and aging of incipient thin film wax-oil gels”, AIChE Journal 46, 2000.

8. Singh, P., Venkatesan, R., Fogler, H. S., and Nagarajan, N. “Morphological evolution of thick wax deposits during aging”, AIChE Journal 47, 2001.

9. Zheng, S., Saidoun, M., Palermo, T., Mateen, K., and Fogler, H. S. “Wax deposition modeling with considerations of non-newtonian characteristics: Application on field-scale pipeline.”, Energy & Fuels 31 (5): 5011–5023, 2017. https://doi.org/10.1021/acs.energyfuels.7b00504.

10. Chilton, A. R. and Stainsby, R. 1998, “Pressure loss equations for laminar and turbulent non-newtonian pipe flow. Journal of Hydraulic Engineering-asce - J HYDRAUL ENG-ASCE 124: 522–529.

11. Darby, R. and Melson, J. 1981. “How to predict the friction factor for flow of bingham plastics.”, Chemical engineering 88 (26): 59–61.

12. Darby, R., Mun, R., and Boger, D. V. 1992. "Predict friction loss in slurry pipes.”, Chemical Engineering 99 (9):116–119.

13. Herschel, W. H. and Bulkley, R. 1926. "konsistenzmessungen von gummi-benzollösungen. Kolloid-Zeitschrift 39 (4): 291–300. Wikipedia: https://en.wikipedia.org/wiki/Herschel%E2%80%93Bulkley_fluid

14. Azevedo, L. F. A. and Teixeira, A. M. 2003. “A critical review of the modeling of wax deposition mechanisms”, Petroleum Science and Technology 21 (3): 393–408. https://doi.org/10.1081/LFT-120018528

15. Banki, R., Hoteit, H., and Firoozabadi, A. 2008. “Mathematical formulation and numerical modeling of wax deposition in pipelines from enthalpy–porosity approach and irreversible thermodynamics”, International Journal of Heat and Mass Transfer 51: 3387-3398.

16. Hoteit, H., Banki, R., and Firoozabadi, A. 2008. “Wax deposition and aging in flowlines from irreversible thermodynamics”, Energy & Fuels 22: 2693-2706

17. Bai, C. and Zhang, J. 2013. “Effect of carbon number distribution of wax on the yield stress of waxy oil gels”, Industrial and Engineering Research 52: 2732-2739

18. Lin, M., Li, C., Yang, F., and Ma, Y. 2011. “Isothermal structure development of qinghai waxy crude oil after static and dynamic cooling”, Journal of Petroleum Science and Engineering 77 (3): 351 – 358. https://doi.org/10.1016/j.petrol.2011.04.010

19. Venkatesan, R., Nagarajan, N., Paso, K., Yi, Y.-B., Sastry, A., and Fogler, H. S. 2005. “The strength of paraffin gels formed under static and flow conditions”, Chemical Engineering Science 60: 3587–3598. https://doi.org/10.1016/j.ces.2005.02.045

Chapter 6

Wax control system modeling

The purpose of the chapter is to present the main equations of the WCS model.

Nomenclature

Greek

α –	Volume fraction		
$\dot{\gamma}$ –	Shear rate, 1/s		
$\dot{\gamma}_0$ –	Limiting shear rate, 1/s		
ΔH_f –	Enthalpy of fusion, J/kg		
ϵ_D –	Turbulent mass diffusivity, m^2/s	A factor in turbulent term modelling	$-\overline{v_r' n'} = \epsilon_D \frac{\partial \overline{n}}{\partial r}$
ϵ_H –	Turbulent heat diffusivity, m^2/s	A factor in turbulent term modelling	$-\overline{v_r' T'} = \epsilon_H \frac{\partial \overline{T}}{\partial r}$
ϵ_m –	Turbulent momentum diffusivity, m^2/s	A factor in turbulent term modelling	$-\overline{v_r' v_z'} = \epsilon_m \frac{\partial \overline{v_z}}{\partial r}$
μ –	Dynamic viscosity, Pa·s		
μ_0 –	Limiting dynamic viscosity, Pa·s		
μ_{eff} –	Effective/apparent dynamic viscosity, Pa·s		
ρ –	Density, kg/m^3		
ρ_j –	Concentration of a component j, kg/m^3		
τ_0 –	Yield stress, Pa		
τ_{wall} –	Shear stress at the wall, Pa		

υ – Velocity, m/s

$\bar{\upsilon}$ – Average velocity, m/s

υ_r – Radial velocity component, m/s

υ_z – Axial velocity component, m/s

Latin

a, b, c – coefficients

C_1, C_2, C_3 – coefficients

C_{sup} – Max wax concentration at current temperature, kg/m^3

C_{par} – Solid wax particles concentration in oil bulk, kg/m^3 $= \frac{\alpha_{par}\rho_{par}}{\tilde{R}_w^2}$ for 1D formulation

C_{wb} – Dissolved wax concentration in oil fluid, kg/m^3 $= \frac{\alpha_{wb}\rho_{oil}}{\tilde{R}_w^2 - \alpha_{par}}$ for 1D formulation

C_{ws} – Max solubility of wax in oil at current temperature, kg/m^3

Cp – Heat capacity, J/kg/K $= \frac{\alpha_{wb}\rho_{oil}}{\tilde{R}_w^2 - \alpha_{par}}$ for 1D formulation

D – Diffusivity, m^2/s

D_e – Diffusivity of wax molecules inside wax gel, m^2/s

D_w – Diffusivity of dissolved wax in oil, m^2/s

$D_{w_{eff}}$ – Effective diffusivity of dissolved wax in oil, m^2/s

$D_{p_{eff}}$ – Effective diffusivity of solid wax particles in oil, m^2/s

E – Variable representing energy per length of pipe, J/m

F – A function

F_w – Wax concentration in gel layer

f – Darcy friction factor, -

f_{HB} – Fanning friction factor for Herschel-Bulkley fluid, -

h – Convective heat transfer coefficient, W/m^2/K

K – Consistency, parameter in viscosity correlation, Pa·s^n

k – Thermal conductivity, W/m/K

k_{eff} – Effective thermal conductivity, W/m/K

k_m – Mass transfer coefficient, m/s

k_p – Precipitation rate coefficient, 1/s

m – Mass, kg

n – Flow index parameter in viscosity correlation, -

n_1 – Parameter in viscosity correlation, -

N_s – Wax precipitation rate coefficient, 1/s

Nu – Nusselt number, -

n_j – Concentration of component j as mass fraction of total fluid $= \frac{\rho_j}{\rho}$

R – Radius, m

Re – Reynolds number, -

Res – Thermal resistance of pipe wall, m·K/W

$\tilde{R}$ – Normalized radius, m $= \dfrac{R}{R_i}$ for 1D formulation

Sc – Schmidt number, -

S_d – Wax deposition rate, kg/(m$^3 \cdot s$)

Sh – Sherwood number, -

S_p – Wax precipitation rate, kg/(m$^3 \cdot s$)

T – Temperature, K

$\vec{U}$ – Velocity vector, m/s

Subscripts

gel – Property related to oil/wax gel

i – Property related to the inner surface of a pipe, i.e. pipe/wax or pipe/oil interface

$inlet$ – Property at the inlet

int – Property at the interface

par – Particle, property related to a particle

$pipe$ – Property related to pipe

o – Property related to the outer surface of a pipe

oil – Oil, property related to oil

$outlet$ – Property at the outlet

w – Property related to wax or oil/wax layer interface

wb – Dissolved wax

6.1 Introduction

Nowadays, there is no practical way to tie back subsea oil fields in Arctic regions with distances to the shore of more than 50 km. A major problem is the formation of wax and hydrates in an oil pipeline. Waxes are heavy oil components that usually solidify at temperatures below 60 °C. Hydrates are crystalline structures that form from binding between light hydrocarbons and water molecules. The appearance of hydrates can be prevented by removing water from the multiphase mixture. The appearance of wax cannot be prevented in the same way because when waxes are in liquid form, it is hard to separate them from other oil components. The oil that comes from a well has a temperature above the appearance conditions in most cases, so all waxes are in liquid form. When oil is transported in a pipeline on a seabed, the oil temperature drops to the ambient conditions. The ambient temperature can be around -1 °C for areas near the Arctic or, for example, 10 °C in warmer regions. Eventually, conditions in a pipeline enable the appearance of wax. Wax starts to appear at pipeline walls as the walls have a lower temperature than the bulk. As wax sticks to the walls, it gradually reduces the pipeline diameter and can lead to pipe blockage.

Existing solutions for controlling wax are: maintaining temperature in a pipeline above the appearance conditions, regular pigging, or processing oil at a field on a platform/floating platform. Maintaining the higher temperature is achieved using insulation of a pipeline or/and with active heating. However, at distances above 50 km, the insulation and heating solution could demand an unreasonable amount of energy and become economically inefficient. Continuous scraping off the wax from pipeline walls with pigs as the primary flow assurance solution brings challenges for oils with high wax content and has not been implemented in the oil fields yet, but developments in this area are ongoing. For the floating/stationary process facilities at fields in the Arctic, the main problem comes from the inability to maintain such facilities for the whole year due to ice and icebergs. Production should be shut down in most cases until the danger of damaging the facility by ice or iceberg is removed, for example, by towing an iceberg away from the facility. "Cold flow" is another possible solution for tie back that has been considered in research projects for hydrate and wax control. "Cold flow" is a dewatered flow in a pipeline with a temperature equal to ambient. Without temperature gradient, there is no wax deposition on the pipe wall and, hence, no risk of blockage. Oil could be brought under the condition of "cold flow" by dewatering it and then cooling it in a heat exchanger. A heat exchanger model that can fulfill the task is presented in this work. This heat exchanger is a pipe-in-pipe with oil flowing in the inner pipe and water oppositely flowing in the annulus.

6.2 Flow simulator formulations

6.2.1 Non-Newtonian fluid

To describe the non-Newtonian behavior of the fluid the Herschel and Bulkley [1926] model is used:

$$\tau = \tau_0 + K\dot{\gamma}^n$$

$$\mu_{eff} = \begin{cases} \mu_0 = K|\dot{\gamma}_0|^{n-1} + \tau_0|\dot{\gamma}_0|^{-1} & ,|\dot{\gamma}| \leq \dot{\gamma}_0 \\ K|\dot{\gamma}|^{n-1} + \tau_0|\dot{\gamma}|^{-1} & ,|\dot{\gamma}| \geq \dot{\gamma}_0 \end{cases} \tag{6.1}$$

μ_0 is a limiting viscosity, and $\dot{\gamma}_0$ is the corresponding limiting shear rate; they are used to avoid infinite effective viscosity values at shear rates close to 0. The limiting viscosity should be chosen as large as practical to simulate solid-like behavior from one side and avoid numerical problems from the other.

6.2.2 One dimensional equations

Modeling is done by making a set of one-dimensional transient equations describing heat transfer, wax particle radial transport, wax layer build-up on the inner pipe wall, and selecting relevant correlations for friction factors and Nusselt numbers. The wax deposition model is taken from Singh et al. [2000]. The main assumptions of this model are:

- Wax layer has uniform wax content.
- There is no wax shear removal due to low shear rates of oil.
- There is no heat transfer due to the radial convection of wax particles.
- Densities of wax crystals and oil are the same and constant; this makes gel density constant over time, even if wax content in the gel layer changes.
- Heat capacities of wax crystals and oil are the same and constant.
- All properties of water like density, heat capacity, and thermal conductivity are constant.

Six coupled equations for six variables are used in the one-dimensional model. Variables are shown in Figure 6.1.

Energy

The heat exchanger modeling requires two energy equations: one for oil and one for coolant. During normal WCS operation, heat goes from hot oil to cold water through a wax layer and pipe wall, and heat generation occurs when wax changes phase from liquid to solid, see Figure 6.2.

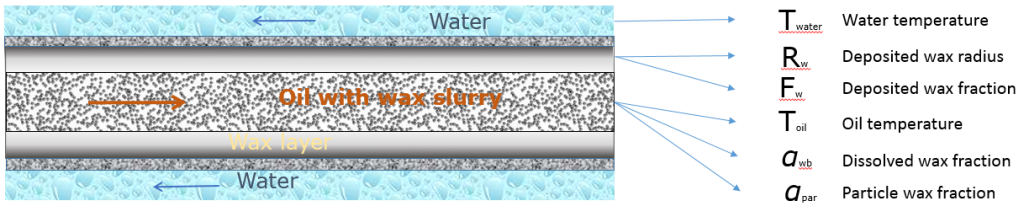

Fig. 6.1—*One dimensional model variables.*

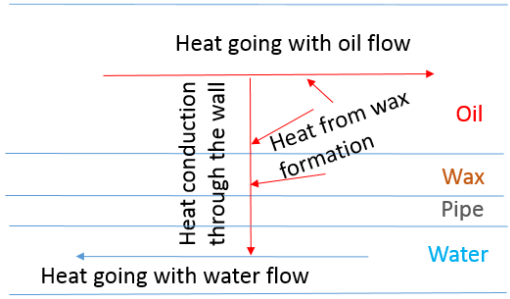

Fig. 6.2—*Heat path.*

Oil energy equation:

$$\begin{aligned} E &= R_w^2(Cp_{oil}\rho_{oil}\alpha_{oil}T_{oil} + Cp_{par}\rho_{par}\alpha_{parinoil}T_{par}) \\ \frac{\partial E}{\partial t} + \frac{\partial(E\upsilon)}{\partial x} &= -2R_w h_{oil}(T_{oil} - T_w) + R_w^2 N_s \Delta H_f C_c \\ \alpha_{oil} + \alpha_{parinoil} &= 1 \end{aligned} \tag{6.2}$$

Where α_{oil} and $\alpha_{parinoil}$ are volume fractions of oil and particles in oil. E is used as a variable representing energy per unit length, J/m, to shorten the differential equation expression. Note that π is not present on both right and left hand sides of the differential equation.

$$C_c = \begin{cases} C_{wb} - C_{sup}, & \text{if } C_{wb} > C_{sup} \\ C_{wb} - C_{sup}, & \text{if } C_{wb} < C_{sup} \& C_{par} > 0 \\ 0, & \text{otherwise} \end{cases} \tag{6.3}$$

Substituting R_w with non dimensional $\tilde{R}_w = \frac{R_w}{R_i}$, using the assumption that densities of oil and wax are equal and constant over time, and noting that $R_w^2\upsilon =$

constant, the following simplified equation is obtained:

$$\begin{aligned}\tilde{R}_w(\frac{\partial T_{oil}}{\partial t} + \upsilon_{oil}\frac{\partial T_{oil}}{\partial x}) + 2T_{oil}\frac{\partial R_w}{\partial t} = \\ \frac{-2h_{oil}}{Cp_{oil}\rho_{oil}R_i}(T_{oil} - T_w) + \frac{N_s\Delta H_f}{Cp_{oil}\rho_{oil}}\tilde{R}_w C_c\end{aligned} \tag{6.4}$$

Coolant energy equation in partial derivatives:

$$\begin{aligned}Cp_{water}\rho_{water}A_{water}(\frac{\partial T_{water}}{\partial t} + \upsilon_{water}\frac{\partial T_{water}}{\partial x}) = \\ \frac{T_i - T_{water}}{\frac{1}{2\pi h_{water}R_o} + \frac{ln\frac{R_o}{R_i}}{2\pi k_{pipe}}}\end{aligned} \tag{6.5}$$

The oil and water energy equations need a connection between the variables T_i, T_w and T_{water}. The pipe wall is assumed not to store heat, and the connection can be described using heat conduction equations through a pipe wall.

$$T_i = \frac{2k_w T_w Res + ln\frac{R_i}{R_w}T_{water}}{2k_w Res + ln\frac{R_i}{R_w}} \tag{6.6}$$

$$Res = \frac{1}{2h_{water}R_o} + \frac{ln\frac{R_o}{R_i}}{2k_{pipe}} \tag{6.7}$$

Wax Deposition

The wax deposition model consists of 3 equations: wax flux from bulk to wax gel/oil interface, wax flux from the interface into the gel layer, and heat equation describing the heat flow from bulk to the wall. In Figure 6.3 the light blue lines represent a wax layer and incoming dissolved wax from the bulk to the oil/wax interface; the red lines represent the diffusion inside the wax layer and growth of the layer.

Wax flux from bulk to the gel/oil interface:

$$\pi(R_i^2 - R_w^2)\frac{dF_w}{dt} - 2\pi R_w F_w \frac{dR_w}{dt} = \frac{2\pi R_w k_m}{\rho_{gel}}(C_{wb} - C_{ws}) \tag{6.8}$$

Wax flux from gel oil interface into the gel layer:

$$\begin{aligned}-2\pi R_w F_w \rho_{gel}\frac{dR_w}{dt} = 2\pi R_w k_m(C_{wb} - C_{ws}) \\ -2\pi R_w(-De\frac{dC_{ws}}{dT}\left.\frac{dT}{dr}\right|_{r=R_w})\end{aligned} \tag{6.9}$$

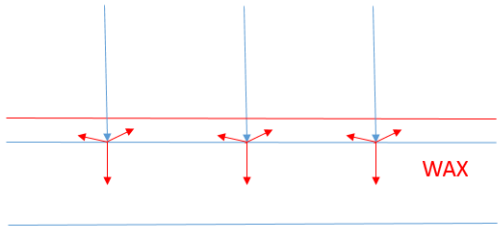

Fig. 6.3—*Wax layer growth.*

Subtracting Eq. 6.9 from Eq. 6.8 it is possible to obtain the evolution of wax content in gel layer equation. This equation was used in numerical integration instead of Eq. 6.8

$$\pi(R_i^2 - R_w^2)\rho_{gel}\frac{dF_w}{dt} = 2\pi R_w(-De\frac{dC_{ws}}{dT}\left.\frac{dT}{dr}\right|_{r=R_w}) \tag{6.10}$$

Then R_w is substituted with non dimensional variable $\tilde{R}_w = \frac{R_w}{R_i}$ So Eq. 6.10 becomes:

$$(1.0 - \tilde{R}_w^2)\frac{dF_w}{dt} = \frac{2\tilde{R}_w}{\rho_{gel}R_i}(-De\frac{dC_{ws}}{dT}\left.\frac{dT}{dr}\right|_{r=R_w}) \tag{6.11}$$

and Eq. 6.9 becomes:

$$-F_w R_i \rho_{gel}\frac{d\tilde{R}_w}{dt} = k_m(C_{wb} - C_{ws}) + De\frac{dC_{ws}}{dT}\left.\frac{dT}{dr}\right|_{r=R_w}) \tag{6.12}$$

As there is no convection in gel layer in axial direction, $\frac{d}{dt} = \frac{\partial}{\partial t}$ is set for these equations.

Heat flow equation: heat going through the wax layer towards the coolant is a sum of heat coming from oil bulk and heat generated due to wax solidification.

$$\begin{aligned} 2R_w h_{oil}(T_{oil} - T_w) = \\ \frac{2k_w(T_w - Ti)}{ln\frac{R_i}{R_w}} - 2R_w k_m(C_{wb} - C_{ws})\Delta H_f \end{aligned} \tag{6.13}$$

The most well-known formula for predicting wax deposition is based on the molecular diffusion mechanism with the assumption that the concentration gradient can be split into the solubility curve and the temperature gradient close to the wall.

$$\frac{dm}{dt} = Const\frac{dC}{dr} = Const\frac{dC}{dT}\frac{dT}{dr} \tag{6.14}$$

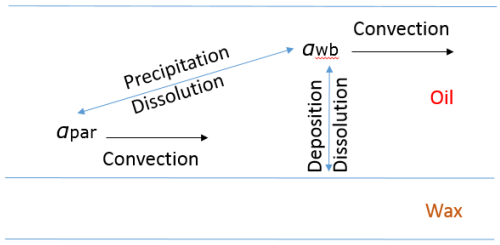

Fig. 6.4—*Concentration transport.*

This decomposition approach of $\frac{dC}{dr}$ assumes that concentration depends solely on temperature gradient and fixed solubility curve. It requires solving only for a temperature gradient to be able to predict deposition based on molecular diffusion. This mechanism could be described as wax molecules, dissolved in the oil bulk, moving towards the wall area because the concentration of wax molecules in the oil bulk is higher than that of wax molecules at the wall. The concentration of wax molecules at the wall is lower because, at the wall, the temperature is lower than at the bulk. Generally, oil supports a smaller amount of dissolved wax at lower temperatures. So wax driven by concentration gradient comes into the low-temperature region, where it cannot be maintained in dissolved form, and starts to precipitate. As the lowest temperature is at the wall, the main part of wax deposits at the wall, creating a concentration difference between the wall and the bulk.

This mechanism with the more precise formulation is seen as the primary mechanism driving wax deposition. For example, the concentration gradient can be coupled with the temperature gradient. Alternatively, the concentration of different wax-forming species could be used instead of using a concentration of "wax" molecules.

Mass

Overall mass conservation equation for the total fluid is simply $Sv = const$ for one dimension with constant density.

However, the heat exchanger could be relatively long, so some wax will precipitate in bulk as wax particles. Also, the concentration of dissolved wax particles in bulk will change along the length of the heat exchanger. Hence, a transport equation for the concentration variables should be established. The variables chosen to represent concentration transport are dissolved wax volume fraction and particle wax volume fraction: α_{wb} and α_{par} respectively. The illustration of mass transport is shown in Figure 6.4.

$$
\begin{aligned}
C_{wb} &= \alpha_{wb}\frac{R_i^2}{R_w^2}\rho_{oil} = \frac{\alpha_{wb}\rho_{oil}}{\tilde{R}_w^2} \\
C_{par} &= \alpha_{par}\frac{R_i^2}{R_w^2}\rho_{par} = \frac{\alpha_{par}\rho_{par}}{\tilde{R}_w^2} \\
\pi(2R_w\frac{dR_w}{dt}C_{par} + R_w^2\frac{dC_{par}}{dt}) &= \pi R_w^2 N_s C_c
\end{aligned}
\tag{6.15}
$$

Concentration of precipitated wax transport equation in volume fraction notation:

$$
\rho_{par}(\frac{\partial\alpha_{par}}{\partial t} + \frac{\partial v_{oil}\alpha_{par}}{\partial x}) = \tilde{R}_w^2 N_s C_c \tag{6.16}
$$

Dissolved wax concentration transport equation in volume fraction notation:

$$
\begin{aligned}
\rho_{oil}(\frac{\partial\alpha_{wb}}{\partial t} + \frac{\partial v_{oil}\alpha_{wb}}{\partial x}) = \\
-\frac{2\tilde{R}_w k_m}{R_i}(C_{wb} - C_{ws}) - \tilde{R}_w^2 N_s C_c
\end{aligned}
\tag{6.17}
$$

Notations are as follows: R - Radius in [m], T- Temperature in [K], w - wax or wax gel/oil interface, i - inner pipe inner wall, o - inner pipe outer wall, k_m - mass transfer coefficient wax in oil [m/s], De - diffusivity of wax molecules inside wax gel [m^2/s], ΔH_f - enthalpy of fusion [J/kg], oil - bulk oil property, water - bulk water property, k_{pipe} - thermal conductivity of pipe material [W/m/K], h - thermal convection coefficient [W/m^2/K], Res - sum of thermal resistance of pipe and convective thermal resistance of coolant, ρ - density [kg/m^3], C_{wb} and C_{ws} are wax concentrations [kg/m^3] in oil bulk and at gel/oil interface respectively, F_w- wax concentration in gel layer [-], N_s is precipitation speed coefficient [1/s], C_{sup} concentration of wax from solubility curve that solvent can support at current temperature [kg/m^3], C_c concentration difference as driving force for suspended wax particles formation [kg/m^3], C_{par} concentration of wax particles [kg/m^3] .

Momentum

Momentum equation for the given assumptions could be represented with Darcy-Weisbach equiation.

$$
-\frac{\partial p}{\partial x} = f\frac{\rho}{2}\frac{\bar{v}^2}{D} \tag{6.18}
$$

Parameters Estimation

The parameters correlations used are mainly the same as in Singh et al. [2000] with some additional considerations. Sherwood number for mass transfer coefficient of wax in oil was initially found as in Venkatesan and Fogler [2004]:

$$
Sh = \frac{dC}{dT}\Big|_{int}\frac{\Delta T}{\Delta C}Nu \tag{6.19}
$$

However, the mass flux does not depend on the concentration difference between bulk and interface anymore with this formulation.

$$\begin{aligned} Flux =& k_m(\Delta C) = \frac{ShD_w}{2R_w}(\Delta C) = \left.\frac{dC}{dT}\right|_{int} \frac{\Delta T}{\Delta C}\frac{NuD_w}{2R_w}(\Delta C) \\ =& \left.\frac{dC}{dT}\right|_{int} \frac{\Delta T NuD_w}{2R_w} \end{aligned} \tag{6.20}$$

So the mass flux is the same for 1 % bulk concentration and for 20 % by weight basis bulk concentration.

Due to this reason, Sherwood number was found according to:

$$Sh = 0.023 Re^{0.8} Sc^{\frac{1}{3}} \tag{6.21}$$

As waxy oil viscosity could be quite high, published correlations for Nusselt numbers are outside or on the edge of their area of applicability. The heat of fusion is found from the correlations by Won [1986], assuming the average molar mass of wax=400 g/mol:

$$T_f = 374.5 + 0.02617\mu_w - \frac{20172}{\mu_w} \tag{6.22}$$

$$\Delta H_f = 0.1426\mu_w T_f \tag{6.23}$$

T_f is the temperature of fusion in K, ΔH_f is the heat of fusion in cal/mol, note that the heat of fusion in the heat transfer equation is the specific heat of fusion in J/kg.

Pedersen correlation for wax suspension in oil is used if the wax precipitates in bulk, Pedersen and Roenningsen [2000].

$$\eta = \eta_{liq}\left(e^{D\phi_{wax}} + \frac{E\phi_{wax}}{\sqrt{\frac{dV_x}{dy}}} + \frac{F\phi_{wax}^4}{\frac{dv_x}{dy}}\right) \tag{6.24}$$

Where η is viscosity of suspension, η_{liq} is viscosity of liquid without precipitated wax, ϕ_{wax} is volume fraction of solid wax, $D = 37.82$, $E = 83.96$,$F = 8.559 * 10^6$. The Pedersen correlation could be adjusted to better fit the viscosity measurements of the fluid.

6.2.3 Two dimensional equations

Temperature and concentration profiles for each axial position are required to get a more realistic wax concentration gradient and wax flow toward the wall. Hence, the two-dimensional solution of the transport equations is required for a

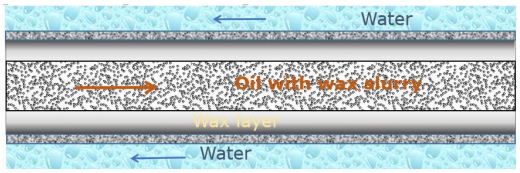

Fig. 6.5—*WCS model*

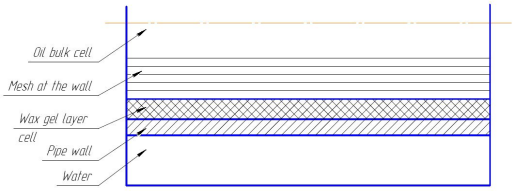

Fig. 6.6—*Two dimensional model mesh.*

single-phase mixture flow, where flow and heating conditions are assumed to be symmetrical around the axial axis. As the temperature of the oil along the WCS axial axis changes from around 50-60 °C to $\sim$ 4 °C, the wax will precipitate in the oil bulk and deposit on the pipe wall. The precipitated wax particle contributes to the viscosity of the oil wax mixture, making viscosity non-Newtonian. It is vital to capture the non-Newtonian behavior of the slurry oil as it affects the mass and heat transfer of both precipitated wax and still dissolved wax. The model selected for wax deposition description in WCS is based on the approach presented in Zheng et al. [2017].

Model

Figure 6.5 presents the WCS flow setup. A waxy oil slurry is inside the inner pipe, with cooling water flowing in the annulus between the inner and the outer pipes. The flow consists of oil α_{oil}, solid wax α_{par}, and dissolved wax particles α_{wb}. The temperatures and velocities of all particles in a control volume are assumed to be the same, so solving only one momentum and one energy equation

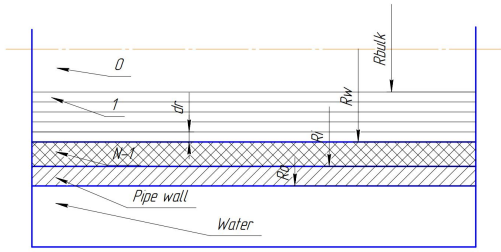

Fig. 6.7—*Two dimensional model radii definitions.*

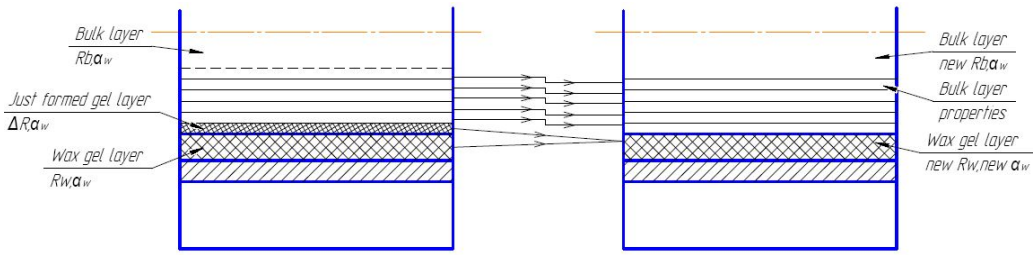

Fig. 6.8—***Two dimensional model deposition handling.***

for the control volume is required. Fick's law and turbulent mixing govern the particles' diffusion. The flow and heating conditions are taken to be axisymmetrical. The fluid's viscosity is the viscosity of a slurry; it is a non-Newtonian viscosity dependent on the temperature and the amount of solid wax particles. Figures 6.6 and 6.7 present model mesh at one axial cell position. The oil domain is a two-dimensional domain to get the temperature and concentration profiles. In contrast, the water domain is one-dimensional, as correlations for the Nusselt number are considered to be sufficient for representing the heat transfer in water. Knowing that the main change to parameters happens in the thin layer close to the wall, it is necessary to resolve this layer when doing the finite difference calculations. On the other hand, it is possible to represent the bulk of the fluid as one big cell to reduce the simulation time. Another suggestion to increase computation speed is to remove the gelled cells from the grid, accumulating the average gel layer thickness and wax content as another "big" grid cell. So the oil domain has a refined mesh close to the pipe wall, one "big" cell representing the bulk, and one "big" cell representing the wax layer at the wall. Doing so would make it possible to have a stationary grid with refinement only at a thin layer close to the pipe wall. The approach is considered valid to quantify the amount of deposited wax only when the gel layer thickness is much smaller than the pipe diameter and the wax layer thickness does not change rapidly along the pipe length.

The handling of deposition is done in the following way: when solid wax content in a cell is such that the yield stress of the mixture is higher than the shear stress provided by the flow, the control volume is considered to become gelled/stationary, i.e., velocity in the cell is set to zero. Each time a cell becomes stationary, its content is absorbed into the wax layer cell. All cells above it are shifted, so the grid is preserved. The mass balance is preserved by shrinking the "bulk" cell geometry and adjusting the bulk cell variables accordingly. Figure 6.8 illustrates the process. The "bulk" and "wax layer" cells have the same formulation as all other normal cells; furthermore, the "wax layer" cells have the fluid velocity set to zero.

For cells, where yield stress has become larger than fluid-imposed shear stress, the "absorption" based on volume will look like:

$$\Psi_{waxlayer}^{new} = \frac{\Psi_{waxlayer}(R_i^2 - R_w^2) + \Psi_{gelformed}(R_w^2 - (R_w - \delta R)^2)}{R_i^2 - (R_w - \delta R)^2} \qquad (6.25)$$
$$R_{waxlayer}^{new} = R_w - \delta R$$

Where Ψ is any variable, δR is the thickness of a cell with a newly formed gel. And subscripts $bulk$, $waxlayer$, and $gelformed$ correspond to the properties of bulk oil cell, wax layer cell at the pipe wall, and newly formed gel cell. The bulk flow keeps its parameters, except its thickness is reduced on δR. The system of differential equations includes:

- Two equations describing solid wax content and dissolved wax content transport and phase change.
- One energy equation for waxy oil slurry.
- One energy equation for water flow.

Mathematical description

The set of equations describing a model is presented in this section, and then each equation is discussed in the relevant subsection. Summary of the assumptions:

- Volumetric thermal expansion is small; hence enthalpy change due to thermal expansion is negligible compared to change due to temperature change. This is relevant for liquids where density has a very low dependency on temperature.
- Densities and heat capacities of all components in a mixture are equal. This assumption allows the elimination of enthalpy flux due to components diffusion.
- Heat capacities are constants.
- Turbulent enthalpy flux due of components $\overline{\upsilon_\phi' T'}$ and $\overline{\upsilon_z' T'}$ are negligible compared to component $\overline{\upsilon_r' T'}$.
- $\overline{\upsilon_r' T'}$ could be approximated with $-\epsilon_H \frac{\partial T}{\partial r}$.
- Turbulent and non-Newtonian effects on viscous dissipation are neglected.
- Fully developed flow, and no fluid coming or leaving through a pipe wall. $\upsilon_r = 0$.
- Axisymmetrical flow and heating. No dependency on ϕ coordinate.
- Boundary layer approximation. $\frac{\partial \upsilon_z}{\partial r} \gg \frac{\partial \upsilon_z}{\partial z}, \frac{\partial \upsilon_r}{\partial z}$.

The coupled system of equations to be solved:

$$\rho\frac{\partial\alpha_{wb}}{\partial t}+\rho\upsilon_z\frac{\partial\alpha_{wb}}{\partial z}-\frac{1}{r}\frac{\partial}{\partial r}\left(r\rho(D_w+\epsilon_D)\frac{\partial\alpha_{wb}}{\partial r}\right)=-k_pC_c \qquad \text{Transport Dissolved Wax}$$

$$\rho\frac{\partial\alpha_{par}}{\partial t}+\rho\upsilon_z\frac{\partial\alpha_{par}}{\partial z}-\frac{1}{r}\frac{\partial}{\partial r}\left(r\rho\epsilon_D\frac{\partial\alpha_{par}}{\partial r}\right)=k_pC_c \qquad \text{Transport Solid Wax} \tag{6.26}$$

$$\rho c_p\frac{\partial T}{\partial t}+\rho c_p\upsilon_z\frac{\partial T}{\partial z}-\frac{1}{r}\frac{\partial}{\partial r}\left(r(k+c_p\rho\epsilon_H)\frac{\partial T}{\partial r}\right)-\mu_{eff}\left(\frac{\partial\upsilon_z}{\partial r}\right)^2=k_pC_c\Delta H_f \qquad \text{Energy Oil Domain}$$

$$\rho_{water}c_{p_{water}}(R_{water}^2-R_o^2)(\frac{\partial T_{water}}{\partial t}+\upsilon_{water}\frac{\partial T_{water}}{\partial z})=\frac{T_i-T_{water}}{\frac{1}{2h_{water}R_o}+\frac{ln\frac{R_i}{R_w}}{2k_{wax}}+\frac{ln\frac{R_o}{R_i}}{2k_{pipe}}} \qquad \text{Energy Water}$$

As thermal and mass turbulent diffusivities are not constants, while density, molecular diffusivity, and heat conductivity are

considered constants, the equation takes the following form:

$$\frac{\partial \alpha_{wb}}{\partial t} + \upsilon_z \frac{\partial \alpha_{wb}}{\partial z} - \frac{D_w + \epsilon_D}{r}\left(\frac{\partial \alpha_{wb}}{\partial r} + r\frac{\partial^2 \alpha_{wb}}{\partial r^2}\right) - \frac{\partial \epsilon_D}{\partial r}\frac{\partial \alpha_{wb}}{\partial r} = -\frac{k_p C_c}{\rho} \quad \text{Transport Dissolved Wax}$$

(6.27)

$$\frac{\partial \alpha_{par}}{\partial t} + \upsilon_z \frac{\partial \alpha_{par}}{\partial z} - \frac{\epsilon_D}{r}\frac{\partial \alpha_{par}}{\partial r} - \frac{\partial \epsilon_D}{\partial r}\frac{\partial \alpha_{par}}{\partial r} - \epsilon_D \frac{\partial^2 \alpha_{par}}{\partial r^2} = \frac{k_p C_c}{\rho} \quad \text{Transport Solid Wax}$$

$$\frac{\partial T}{\partial t} + \upsilon_z \frac{\partial T}{\partial z} - \frac{\alpha + \epsilon_H}{r}\left(\frac{\partial T}{\partial r} + r\frac{\partial^2 T}{\partial r^2}\right) - \frac{\partial \epsilon_H}{\partial r}\frac{\partial T}{\partial r} - \frac{\mu_{eff}}{\rho C_p}\left(\frac{\partial \upsilon_z}{\partial r}\right)^2 = \frac{k_p C_c}{\rho C_p}\Delta H_f \quad \text{Energy Oil Domain}$$

$$\rho_{water} c_{p_{water}} (R_{water}^2 - R_o^2)\left(\frac{\partial T_{water}}{\partial t} + \upsilon_{water}\frac{\partial T_{water}}{\partial z}\right) = \frac{T_i - T_{water}}{\frac{1}{2h_{water}R_o} + \frac{ln\frac{R_i}{R_w}}{2k_{wax}} + \frac{ln\frac{R_o}{R_i}}{2k_{pipe}}} \quad \text{Energy Water}$$

The system 6.26 has specific boundary conditions for the oil layer that is adjacent to the wax layer. For example, the heat transferred to this layer still comes from flow, while heat taken goes through the stationary wax layer, pipe wall, and into the water. The temperature of the last two radial nodes M and $M-1$ represents water temperature, while the volume fractions of the nodes represent the wax layer volume fraction. The radial node $M-2$ is the last node of the flowing fluid.

The $M-2$ node's equations reflect the presence of the flow on one side and stationary wax on the other.

$$\frac{\partial \alpha_{wb}}{\partial t} + \upsilon_z \frac{\partial \alpha_{wb}}{\partial z} = \frac{-k_p C_c}{\rho} + \frac{1}{r_{M-2} dr}\left[(r_{M-2} - \frac{dr}{2})(D_w + \epsilon_D)\frac{\alpha_{wbM-3} - \alpha_{wbM-2}}{dr} - \frac{D_e(\alpha_{wbM-2} - \alpha_{wbM-1})}{ln(\frac{R_w+R_i}{2R_w})}\right] \tag{6.28}$$

$$\frac{\partial \alpha_{par}}{\partial t} + \upsilon_z \frac{\partial \alpha_{par}}{\partial z} - \frac{1}{r_{M-2} dr}\left[(r_{M-2} - \frac{dr}{2})\epsilon_D \frac{\alpha_{par\,M-3} - \alpha_{par\,M-2}}{dr}\right] = \frac{k_p C_c}{\rho}$$

$$\frac{\partial T}{\partial t} + \upsilon_z \frac{\partial T}{\partial z} - \frac{\mu_{eff}}{\rho C_p}\left(\frac{\partial \upsilon_z}{\partial r}\right)^2 = \frac{k_p C_c}{\rho C_p}\Delta H_f + \frac{1}{r_{M-2} dr}\left[(r_{M-2} - \frac{dr}{2})(\alpha + \epsilon_H)\frac{T_{M-3} - T_{M-2}}{dr} - \frac{1}{\rho C_p}\frac{T_{M-2} - T_{M-1}}{\frac{1}{h_{water} R_o} + \frac{ln\frac{R_i}{R_w}}{k_{wax}} + \frac{ln\frac{R_o}{R_i}}{k_{pipe}}}\right]$$

The momentum equation and relevant turbulent diffusivities are substituted with empirical approximations for the turbulent internal boundary layer. The substitution is based on the idea that diffusivities and velocity profile in non-Newtonian flow can be approximated with the well-known law of the wall function for Newtonian flow but with wall shear stress computed according to correlation for non-Newtonian flow. The idea is proposed by Zheng et al. [2017]. One of the additions to Zheng et al. [2017] in this work is that the parameters in the Herschel-Bulkley viscosity formulation are fitted to best match viscosities along the cross-section.

The system of equations with dimensionless variables:

$$\rho\frac{\partial\alpha_{wb}}{\partial t}+\frac{\rho\upsilon_{inlet}\tilde{\upsilon}_z}{Z}\frac{\partial\alpha_{wb}}{\partial\tilde{z}}-\frac{1}{R_w^2}\frac{1}{\tilde{r}}\frac{\partial}{\partial\tilde{r}}\left(r\rho(D_w+\epsilon_D)\frac{\partial\alpha_{wb}}{\partial r}\right)=-k_pC_c \qquad \text{Transport Dissolved Wax (6.29)}$$

$$\rho\frac{\partial\alpha_{par}}{\partial t}+\frac{\rho\tilde{\upsilon}_z\upsilon_{inlet}}{Z}\frac{\partial\alpha_{par}}{\partial\tilde{z}}-\frac{1}{R_w^2}\frac{1}{\tilde{r}}\frac{\partial}{\partial\tilde{r}}\left(r\rho\epsilon_D\frac{\partial\alpha_{par}}{\partial r}\right)=k_pC_c \qquad \text{Transport Solid Wax}$$

$$\rho c_pT_{inlet}\frac{\partial\tilde{T}}{\partial t}+\rho c_p\frac{T_{inlet}\upsilon_{inlet}}{Z}\tilde{\upsilon}_z\frac{\partial\tilde{T}}{\partial\tilde{z}}-\frac{T_{inlet}}{R_w^2}\frac{1}{\tilde{r}}\frac{\partial}{\partial\tilde{r}}\left(r(k+c_p\rho\epsilon_H)\frac{\partial T}{\partial r}\right)-$$

$$\mu_{eff}\frac{\upsilon_{inlet}^2}{R_w^2}\left(\frac{\partial\tilde{\upsilon}_z}{\partial\tilde{r}}\right)^2=k_pC_c\Delta H_f \qquad \text{Energy Oil Domain}$$

$$\rho_{water}c_{p_{water}}(R_{water}^2-R_o^2)(\frac{\partial\tilde{T}_{water}}{\partial t}+\frac{\upsilon_{inlet}\tilde{\upsilon}_{water}}{Z}\frac{\partial T_{water}}{\partial\tilde{z}})=\frac{\frac{T_i}{T_inlet}-\tilde{T}_{water}}{\frac{1}{2h_{water}R_o}+\frac{ln\frac{R_i}{R_w}}{2k_{wax}}+\frac{ln\frac{R_o}{R_i}}{2k_{pipe}}} \qquad \text{Energy Water}$$

$$\tilde{z}=\frac{z}{Z} \qquad Z \text{ is axial length scale}$$

$$\tilde{T}=\frac{T}{T_{inlet}} \qquad T_{inlet} \text{ is oil inlet temperature}$$

$$\tilde{r}=\frac{r}{R_w} \qquad R_w \text{ is wax radius}$$

$$\tilde{\upsilon}=\frac{\upsilon}{\upsilon_{inlet}} \qquad \upsilon_{inlet} \text{ is inlet oil velocity}$$

υ_z and $\frac{\partial\upsilon_z}{\partial r}$ are estimated based on Herschel-Bulkley fluid velocity profiles 6.46 and 6.47

Momentum

Instead of solving the momentum equation, to reduce the calculation power requirement Zheng et al. [2017] proposed to approximate the turbulent velocity profile with an empirical approximation based on the adjusted law of the wall. The suggested adjustment to the law is a modified calculation of the dimensionless distance $y+$ and calculation of the wall shear stress using the Chilton and Stainsby [1998] frictional pressure loss correlation for a non-Newtonian fluid described by the viscosity model of Herschel and Bulkley [1926]. Turbulent flow equations to solve for f_{HB}:

$$f_{HB} = 0.316\left[\frac{R_{HB}}{n^2(1-X)^4}\right]^{-0.25} \tag{6.30}$$

$$R_{HB} = \frac{\rho_{oil} \upsilon D}{\mu_{wall}\frac{3n+1}{4n}\frac{1}{1-aX-bX^2-cX^3}} \tag{6.31}$$

$$\mu_{wall} = \frac{\tau_{wall}}{\dot{\gamma}_w} = \tau_w^{(n-1)/n}\left(\frac{K}{1-X}\right)^{1/n} \tag{6.32}$$

$$\tau_{wall} = f_{HB}\rho\frac{\upsilon^2}{8} \tag{6.33}$$

$$X = \frac{\tau_0}{\tau_{wall}} = \frac{4L\tau_0}{D\Delta P} \tag{6.34}$$

$$\frac{\Delta P}{L} = \frac{\rho f_{HB}\upsilon^2}{2D} \tag{6.35}$$

$$a = \frac{1}{2n+1} \tag{6.36}$$

$$b = \frac{2n}{(n+1)(2n+1)} \tag{6.37}$$

$$c = \frac{2n^2}{(n+1)(2n+1)} \tag{6.38}$$

Laminar flow equations to solve for f_{HB}:

$$f_{HB} = \frac{8k}{\rho v^2}\left(\frac{8v}{D}\right)^n \left(\frac{3n+1}{4n}\right)^n \left(\frac{1}{1-X}\right)\left(\frac{1}{1-aX-bX^2-cX^3}\right)^n \tag{6.39}$$

$$X = \frac{\tau_0}{\tau_{wall}} = \frac{4L\tau_0}{D\Delta P} = \frac{8\tau_0}{\rho f_{HB} v^2} \tag{6.40}$$

$$\frac{\Delta P}{L} = \frac{\rho f_{HB} v^2}{2D} \tag{6.41}$$

$$a = \frac{1}{2n+1} \tag{6.42}$$

$$b = \frac{2n}{(n+1)(2n+1)} \tag{6.43}$$

$$c = \frac{2n^2}{(n+1)(2n+1)} \tag{6.44}$$

The correlations require an iterative process to solve for the friction factor. Instead of solving the equations, it is possible to use the approximate solution presented by Darby and Melson [1981] for n=1. It uses laminar friction factor from Swamee and Aggarwal [2011], and turbulent fraction factor from Darby et al. [1992].

$$f = (f_L^m + f_T^m)^{1/m} \tag{6.45}$$

$$m = 1.7 + \frac{40000}{Re}$$

$$Re = \frac{\rho v_{ave} D}{\mu_{\text{inf}}}$$

$$f_L = \frac{64}{Re} + \frac{64}{Re}\left(\frac{He}{6.2218Re}\right)^{0.958}$$

$$f_T = 4 \times 10^a Re^{-0.193}$$

$$a = -1.47[1 + 0.146e^{-2.9\times10^{-05}He}]$$

$$He = \frac{\rho D^2 \tau_0}{\mu_{\text{inf}}^2}$$

Velocity profile for laminar flow has the analytical solution for the Herschel-Bulkley fluid. In axisymmetrical cylindrical coordinates with boundary layer and fully

developed flow assumptions, the velocity is:

$$\tilde{v}_z = \begin{cases} \frac{\Pi_0 P_0 R \tilde{r}^2}{4\mu_0 v_{z_{ave}}} + C & , \tilde{r} \leq r_1 \\ \frac{2}{\Pi_0}\frac{n}{n+1}\left[\left(\frac{\Pi_0 \tilde{r}}{2} + \frac{\tau_0}{P_0}\right)^{\frac{n+1}{n}} - \left(\frac{\Pi_0}{2} + \frac{\tau_0}{P_0}\right)^{\frac{n+1}{n}}\right] & , \tilde{r} > r_1 \end{cases} \tag{6.46}$$

$$C = \frac{2}{\Pi_0}\frac{n}{n+1}\left[\left(\frac{\Pi_0 r_1}{2} + \frac{\tau_0}{P_0}\right)^{\frac{n+1}{n}} - \left(\frac{\Pi_0}{2} + \frac{\tau_0}{P_0}\right)^{\frac{n+1}{n}}\right] - \frac{\Pi_0 P_0 R r_1^2}{4\mu_0 v_{z_{ave}}}$$

$$\tilde{v}_z = \frac{v_z}{v_{z_{ave}}}$$

$$r_1 = -\frac{2\dot{\gamma}_0 \mu_0}{\Pi_0 P_0}$$

$$\tilde{r} = \frac{r}{r_s}$$

$$P_0 = k\left(\frac{v_{z_{ave}}}{r_s}\right)^n$$

$$\dot{\gamma}_0 \mu_o = k\dot{\gamma}_0^n + \tau_0$$

$$\Pi_0 = \frac{r_s}{P_0}\frac{\partial p}{\partial z}$$

Profile of averaged velocity for turbulent flow is formulated according to the law of the wall. Diffusivities are based on mixing length theory $\epsilon_m = l^2 \frac{\partial v}{\partial y}$ formulated

using van Driest exponential function for mixing length $l = \kappa y(1 - e^{-y^+/A})$.

$$
\begin{aligned}
v_z^+ &= \begin{cases} y^+ & y^+ \leq 5 \\ 5ln(y^+) - 3.05 & 5 < y^+ \leq 30 \\ 2.5ln(y^+) + 5.5 & y^+ \geq 30 \end{cases} \\
v_z^+ &= 1\frac{v_z}{\sqrt{\tau_{wall}/\rho}} \\
y^+ &= \frac{y}{\nu_{wall}}\sqrt{\frac{\tau_{wall}}{\rho}} \\
y &= r_s - r \\
\epsilon_D &= D\frac{Sc}{Sc_T}\frac{\epsilon_m}{\nu_{wall}} \\
\epsilon_H &= \frac{k}{\rho C_p}\frac{Pr}{Pr_T}\frac{\epsilon_m}{\nu_{wall}} \\
\frac{\epsilon_m}{\nu_{wall}} &= \begin{cases} (\kappa y^+)^2\left[1 - exp(-\frac{y^+}{A})\right]^2 & y^+ \leq 5 \\ (\kappa y^+)^2\left[1 - exp(-\frac{y^+}{A})\right]^2 \frac{5}{y^+} & 5 < y^+ \leq 30 \\ (\kappa y^+)^2\left[1 - exp(-\frac{y^+}{A})\right]^2 \frac{2.5}{y^+} & y^+ \geq 30 \end{cases} \\
\kappa &= 0.4 \\
A &= 26
\end{aligned}
\tag{6.47}
$$

Where r_s is the radius of the flow (could be the radius of the pipe wall or the radius of the wax layer), m; ϵ_m, ϵ_D, ϵ_H are respectively momentum, mass, and heat turbulent diffusivities, m/s^2; ν_{wall} kinematic viscosity at the wall, m/s^2; $A = 26$ gives the best fit for velocity profiles in tubes for Newtonian flows. It is also possible to use the empirical equation for A by Kays and Moffat [1975]:

$$
\begin{aligned}
A &= \frac{25}{a(v_s^+ + b(p^+/(1 + cv_s^+))) + 1} \\
a, b, c &= \begin{cases} 7.1, 4.25, 10 & p^+ \leq 0 \\ 7.1, 2.9, 0 & p^+ > 0 \end{cases}
\end{aligned}
\tag{6.48}
$$

Where v_s^+ is transpiration parameter, p^+ pressure gradient parameter in wall coordinates.

Note that the law of the wall $(2.5ln(y^+) + 5.5)$ provides a non-zero velocity gradient at the pipe center. It might be better to follow Reichardt [1951] and use the Newtonian flow empirical correlation for ϵ_m for the entire region outside the

sublayer ($y^+ \geq 30$) when solving the momentum equation and then make the same adjustment as to the law of the wall to account for non-Newtonian behavior. Then velocity and momentum diffusivity in the set of equations 6.47 are changed to:

$$v_z^+ = \begin{cases} y^+ & y^+ \leq 5 \\ 5ln(y^+) - 3.05 & 5 < y^+ \leq 30 \\ 2.5ln\left(y^+ \frac{1.5(1+r/r_s)}{1+2(r/r_s)^2}\right) + 5.5 & y^+ \geq 30 \end{cases} \tag{6.49}$$

$$\frac{\epsilon_m}{\nu_{wall}} = \frac{\kappa y^+}{6}\left[1 - exp(-\frac{y^+}{A})\right]\left(1 + \frac{r}{r_s}\right)\left[1 + 2\left(\frac{r}{r_s}\right)^2\right]$$

In the model proposed in this chapter, an additional modification is suggested to the Zheng et al. [2017] model. The temperature of the oil and concentration of the precipitated wax influence the viscosity along the radial axis, so the direct use of the Herschel-Bulkley model, where there is no oil temperature or solute concentration dependency of the coefficients, is not possible. The proposed solution is the adjustment of the Herschel-Bulkley viscosity model coefficients at each timestep to fit the radial viscosity profile of the previous timestep as best as possible. The viscosity could be based on values from the previous timestep because the viscosity change is slow compared to other variables change. The radial variation of temperature, concentration, and velocity are known for the previous time step. Hence, the viscosity radial profile based on slurry viscosity correlation 6.50 by Pedersen is also known.

$$\begin{aligned} \mu = \mu_{liq}\left[exp(C_1 F_w) + \frac{C_2 F_w}{\sqrt{\dot{\gamma}}} + \frac{C_3 F_w^4}{\dot{\gamma}}\right] \\ C_1 = 37.82 \\ C_2 = 83.96 \\ C_3 = 8.559E06, \end{aligned} \tag{6.50}$$

where μ_{liq} is the viscosity of a liquid without precipitated wax. The viscosity-temperature correlation comes from the oil composition. Coefficients in the Herschel-Bulkley model, equation 6.1 are adjusted to fit the viscosity radial profile.

Mass

The horizontal velocity profile is considered to be known. However, it is changing along the length because the fluid's properties and the pipe's inner diameter are changing. The adjacent longitudinal nodes can have different velocity profiles. As mass is conserved, there should be radial components of the velocities. The

vertical velocities distribution could be found explicitly from the known horizontal velocity profiles.

$$\rho(\frac{\partial(v)}{\partial z} + \frac{1}{r}\frac{\partial}{\partial r}(rv_r)) = 0 \tag{6.51}$$

Knowing the profile $v(z)$ and that the vertical velocity at the pipe center is 0, it is possible to find the vertical component of the velocity $v_r(r)$. These vertical components of the velocity add vertical convection fluxes to the equations 6.26.

6.3 Flow simulator solver

Nomenclature

$K -$	Number of equations/variables
$k -$	Equation index
$M -$	Number space nodes for the second coordinate
$m -$	Space node index for the second coordinate
$N -$	Number space nodes for the first coordinate
$n -$	Space node index for the first coordinate
$T -$	Maximum time node index
$t -$	Time node index, m
$\alpha -$	Set of variables at current timestep that should be found
$\alpha_{prev} -$	Set of variables at previous timestep
$\Phi -$	Variable
$\Phi_k@Node_{mn} -$	Variable k for the node with indexes n and m

The staring index is taken as 0, to make it consistent with the C++ code.

6.3.1 Forward explicit solver

Equations are discretized as first order for time step and as second order for space step:

$$\begin{aligned} \frac{\partial f}{\partial t} &= \frac{f_i^{t+1} - f_i^t}{\Delta t} \\ \frac{\partial f}{\partial x} &= \frac{f_{i+1}^t - f_{i-1}^t}{2\Delta x} \end{aligned} \tag{6.52}$$

It is a forward scheme, so the spatial difference is computed at timestep step t. So values at time step t+1 for a node are readily available:

$$f_i^{t+1} = f_i^t + g(f_i^t, t, i, \Delta x)\Delta t \tag{6.53}$$

This scheme is easy to code in any programming language. However, it is unstable for relatively large timesteps and space steps. For the case of wax deposition in the counter-current heat exchanger of 6 km with 20 m segmentation, it starts to produce instabilities even for timesteps as small as 0.1 s.

6.3.2 Backward Euler solver

Equations are discretized as first order for time step and as second order for space step:

$$\begin{aligned} \frac{\partial f}{\partial t} &= \frac{f_i^{t+1} - f_i^t}{\Delta t} \\ \frac{\partial f}{\partial x} &= \frac{f_{i+1}^{t+1} - f_{i-1}^{t+1}}{2\Delta x} \end{aligned} \tag{6.54}$$

It is backward discretization, so the spatial difference is computed at timestep step t+1. As values at t+1 are what we are looking for when iterating, it is required to solve for it, compared to explicit discretization where values at t+1 are available directly.

Solver logic presented in this section is for solving six equations presented in 6.2.2. However, the same logic could be used for any number of equations.

One dimensional

The whole length of the exchanger is split into space nodes:

$$\begin{bmatrix} 0 & 1 & \dots & n \dots & N \end{bmatrix}$$

For the case described in 6.2.2 there are six variables per space node per time. To find the evolution in time of all variables, they are assembled into a vector α so that the first six members of α correspond to the six variables in the first space node. Following six members in α correspond to six variables in the second space node. α essentially represents a state of the system at a timestep. Each space node is associated with six variables and six equations. Knowing the system's state at the previous timestep and guessing the state for the next one, it is possible to construct a vector of $g(\alpha, \alpha_{prev})$. If α is a correct state of the system then $g(\alpha, \alpha_{prev})$ will be equal to zero.

$$g(\alpha, \alpha_{prev}) = 0$$

where

$$g(\alpha, \alpha_{prev}) = \begin{bmatrix} eq_0(\alpha, \alpha_{prev})@node_1 \\ eq_1(\alpha, \alpha_{prev})@node_1 \\ \vdots \\ eq_5(\alpha, \alpha_{prev})@node_1 \\ eq_0(\alpha, \alpha_{prev})@node_2 \\ \vdots \\ eq_5(\alpha, \alpha_{prev})@node_N \end{bmatrix} = \begin{bmatrix} g_0 \\ g_1 \\ \vdots \\ g_5 \\ g_6 \\ \vdots \\ g_{6N} \end{bmatrix}$$

$$\alpha = \begin{bmatrix} \Phi_0@node_0 \\ \Phi_1@node_1 \\ \vdots \\ \Phi_5@node_0 \\ \Phi_0@node_1 \\ \vdots \\ \Phi_5@node_N \end{bmatrix} = \begin{bmatrix} g_0 \\ g_1 \\ \vdots \\ g_5 \\ g_6 \\ \vdots \\ g_{6N} \end{bmatrix}$$

The system is solved using the Newton-Rapson method:

$$\alpha_{new} = \alpha - \frac{g(\alpha, \alpha_{prev})}{Jacobian}$$

$$Jacobian_{i,j} = \frac{\partial g_i}{\partial \alpha_j}$$

This is the same as finding $\Delta\alpha$ and then updating α:

$$Jacobian\Delta\alpha = -g(\alpha, \alpha_{prev})$$

$$\alpha_{new} = \Delta\alpha + \alpha$$

Due to chosen discretization, each change in the element of α will influence values in g only in 3 nodes: same node, previous node, and next node. So Jacobian is a sparse matrix. If the corresponding spatial nodes of elements from g and from α are the same or adjacent, then change in the α element can affect change in the g element.

$$Jacobian_{i,j} = \begin{cases} 0, & \text{if } |\left\lfloor \frac{i}{6} \right\rfloor - \left\lfloor \frac{j}{6} \right\rfloor| > 1 \\ \frac{\partial g_i}{\partial \alpha_j}, & \text{otherwise} \end{cases} \tag{6.55}$$

where $\left\lfloor \frac{i}{6} \right\rfloor$ calculates the corresponding spacial node index for an equation g_i.

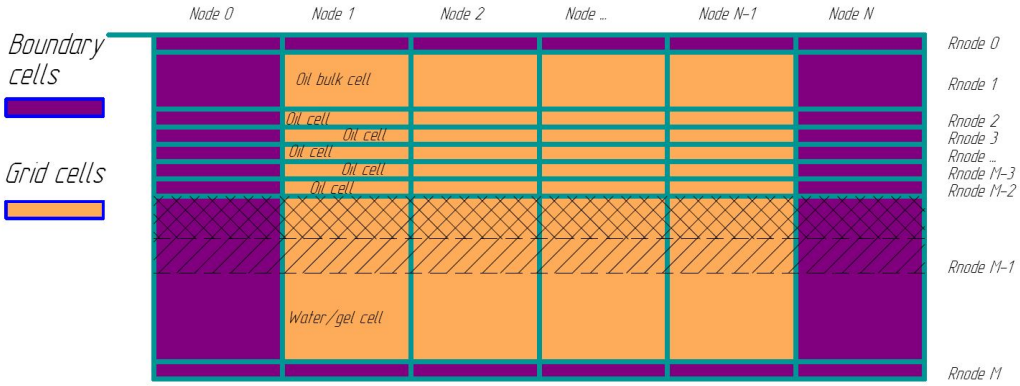

Fig. 6.9—*Two dimensional model grid.*

Sparse direct solver "SparseLU" from the C++ Eigen library is used.

Storage-wise, each variable is a matrix with rows representing time points and columns representing space nodes, and assuming that values are at the midpoints of the grid:

$$\Phi = \begin{bmatrix} Var_{00} & Var_{01} & \dots & Var_{0N} \\ Var_{10} & Var_{11} & \dots & Var_{1N} \\ \vdots & \vdots & \ddots & \vdots \\ Var_{T0} & Var_{T1} & \dots & Var_{TN} \end{bmatrix}$$

Two dimensional adjustment

System spacial nodes for two dimensions will look like

$$Node = \begin{bmatrix} 00 & 01 & \dots & 0n & \dots & 0N \\ 10 & 11 & \dots & 1n & \dots & 1N \\ \vdots & \vdots & \ddots & \vdots & & \vdots \\ m0 & m1 & \dots & mn & \dots & mN \\ \vdots & \vdots & & \vdots & \ddots & \vdots \\ M0 & M1 & \dots & Mn & \dots & MN \end{bmatrix}$$

For the case described with equations 6.26, using a thick oil bulk cell in the effort to reduce the time required for integration, and using the last radial node cells for representing cooling water, the grid structure can be visualized, see Figure 6.9. The vector α can be serialized to represent all 2D grid nodes as a 1D array to use the same integration engine as a one-dimensional problem. If the number of

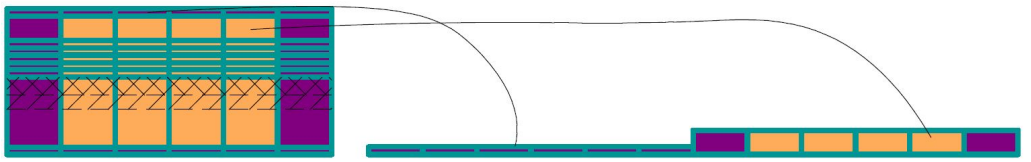

Fig. 6.10— *Two dimensional model grid serialization.*

variables and number of equations is K, then α for a certain timestep is constructed in the following way:

$$\alpha_i = \Phi_k @ Node_{mn} \tag{6.56}$$

$$i = mNK + nK + k \tag{6.57}$$

And to reinstate m,n,k from i:

$$\begin{aligned} m &= \left\lfloor \frac{i}{NK} \right\rfloor \\ n &= \left\lfloor \frac{(i - mNK)}{K} \right\rfloor \\ k &= (i - mNK - nK) \mod K \end{aligned} \tag{6.58}$$

Figure 6.10 illustrates the serialization process. Change of an element in α will now influence four adjacent nodes compared to only two adjacent for one-dimensional case.

$$Jacobian_{i,j} = \begin{cases} 0, & \text{if } |m(i) - m(j)| > 1 \& |n(i) - n(j)| > 1 \\ \frac{\partial g_i}{\partial \alpha_j}, & \text{otherwise} \end{cases} \tag{6.59}$$

where $m(i)$ and $n(i)$ are reinstated nodes coordinates from index i in α.

6.4 References

[1] Chilton, A. R. and Stainsby, R. 1998. Pressure loss equations for laminar and turbulent non-newtonian pipe flow. *Journal of Hydraulic Engineering-asce - J HYDRAUL ENG-ASCE* **124**: 522–529.

[2] Darby, R. and Melson, J. 1981. How to predict the friction factor for flow of bingham plastics. *Chemical engineering* **88** (26): 59–61.

[3] Darby, R., Mun, R., and Boger, D. V. 1992. "predict friction loss in slurry pipes. *Chemical Engineering* **99** (9): 116–119.

[4] Herschel, W. H. and Bulkley, R. 1926. "konsistenzmessungen von gummi-benzollösungen. *Kolloid-Zeitschrift* **39** (4): 291–300. https://doi.org/10.1007/BF01432034

[5] Kays, W. M. and Moffat, R. 1975. The behavior of transpired turbulent boundary layers. Technical report, Stanford University, Stanford, California. HMT20.

[6] Pedersen, K. S. and Roenningsen, H. P. 2000. Effect of precipitated wax on viscosities- a model for predicting non-newtonian viscosity of crude oils. *Energy & Fuels* **14**.

[7] Reichardt, H. 1951. Vollständige darstellung der turbulenten geschwindigkeitsverteilung in glatten leitungen. *Journal of applied mathematics and mechanics* **31** (7): 208–219.

[8] Singh, P., Venkatesan, R., Fogler, H. S., and Nagarajan, N. 2000. Formation and aging of incipient thin film wax-oil gels. *AIChE Journal* **46** (5): 1059–1074.

[9] Swamee, P. K. and Aggarwal, N. 2011. Explicit equations for laminar flow of bingham plastic fluids. *Journal of Petroleum Science and Engineering* **76** (3): 178–184. http://www.sciencedirect.com/science/article/pii/S092041051100026X

[10] Venkatesan, R. and Fogler, H. S. 2004. Formation and aging of incipient thin film wax-oil gels. *AIChE Journal* **50**.

[11] Won, K. W. 1986. Thermodynamics for solid solution-liquid-vapor equilibria wax phase formation from heavy hydrocarbon mixtures. *Fluid Phase Equilibria* **30**: 265–279.

[12] Zheng, S., Saidoun, M., Palermo, T., Mateen, K., and Fogler, H. S. 2017. Wax deposition modeling with considerations of non-newtonian characteristics: Application on field-scale pipeline. *Energy & Fuels* **31** (5): 5011–5023. https://doi.org/10.1021/acs.energyfuels.7b00504

Chapter 7

Qualification of wax control system: wax deposition simulation

This chapter presents the simulation of the experimental conditions described in Chapter 5 using model from Chapter 6 with intention to validate the model.

Nomenclature

a, b, c, C_1, C_2, C_3 –	Coefficients
F, F_1, F_2 –	Functions
ID –	Pipe inner diameter, m
K –	Consistency, parameter in viscosity correlation, Pa·s^n
m –	Mass, kg
n –	Flow index, parameter in viscosity correlation, -
OD –	Pipe outer diameter, m
T –	Temperature, K if not specified otherwise
WCS –	Wax control system
x –	Variable
x_a, x_b –	Variable values at points
$\dot{\gamma}$ –	Shear rate, 1/s
μ –	Dynamic viscosity, Pa·s
ϕ –	Wax content ratio, -
τ_0 –	Yield stress, Pa
τ_{wall} –	Shear stress at the wall, Pa
υ –	Velocity, m/s

7.1 Introduction

Wax deposition on a pipe wall is one of the problems of oil transport. The deposition leads to a reduction of the pipe diameter, a reduction in production, an increased requirement for pumping power, and issues with pigging. It is known (see e.g. Bidmus and Mehrotra [2009], Merino-Garcia and Correra [2008]) that in the absence of a temperature gradient at the pipe wall, wax does not deposit. Such a fact opens the possibility of having long-distance tie-backs using bare pipe without insulation or heating. Elimination of the temperature gradient could be done by transporting the oil at the temperatures of the ambient environment. These transport conditions are called "Cold flow." As the ambient temperature is usually lower than the oil temperature at the entrance to the export pipeline, the oil must be cooled down. The wax control system proposed by Subsea 7, see Stangeland et al. [2021], is a cooling pipe loop system with the possibility to scrape off wax in a controlled way. The design parameters of such a system depend on a cooling speed and wax deposition prediction inside the loop. The comparison of the experimental results obtained from the model test with results from simulation

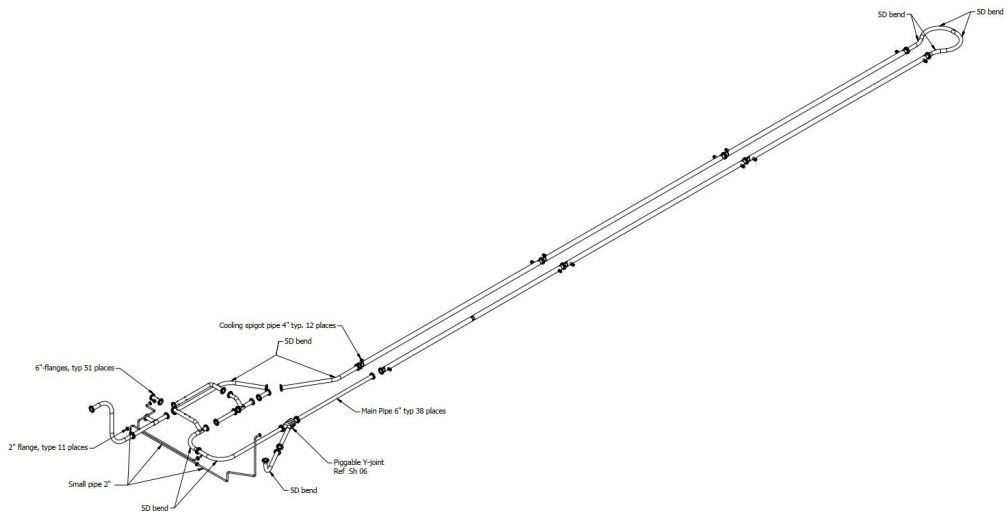

Fig. 7.1—***Flow loop isometrics.***

software is presented in this chapter. The simulation software was developed for the wax control system conditions.

7.2 Experimental stand

The complete experimental stand is described in Stangeland et al. [2021]. The stand was designed to observe and qualify the behavior of different components of the wax control system: a cooling loop with wax deposition, special design valves, a special design pig launcher, and a pig. The description here will only focus on the part of the stand related to the simulation of wax deposition inside the cooling loop. The loop, Figure 7.1, contains six 12 m pipe-in-pipe cooling sections. The sections' inner pipes are connected with boltable flanges. Outer pipes of the section are not interconnected directly. Flexible hoses are installed between sections to maintain the flow inside the annulus, Figure 7.2, (T2 and T7 in the Figure are temperature sensors). Construction with the boltable flanges and the hoses allows disconnection of the sections for inspection. All sections of the loop, the oil tank, and other items that are not meant to be cooled are insulated with glasswool coating. Temperature sensors locations are shown in Figure 7.3 and Figure 7.4. The sensors along the pipe are made such that their measuring tips are flush with the inner surface of the inner pipe. The sensor at the tank location has a measuring tip inside the tank. The tank has heating elements and a stirring device to mix the fluid.

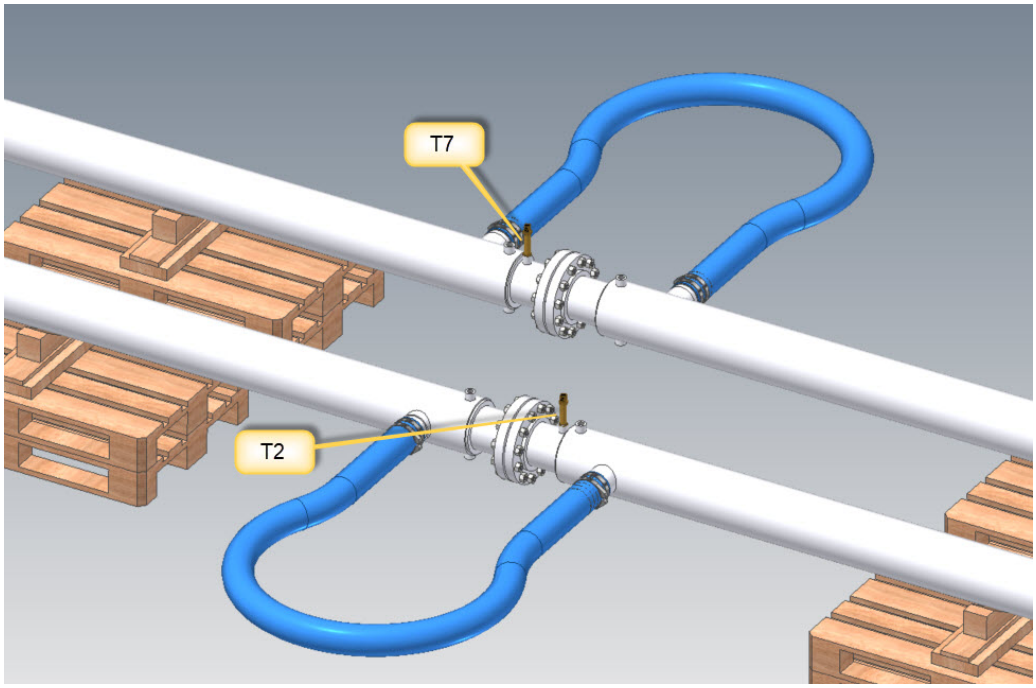

Fig. 7.2—***Connection with flex hoses.***

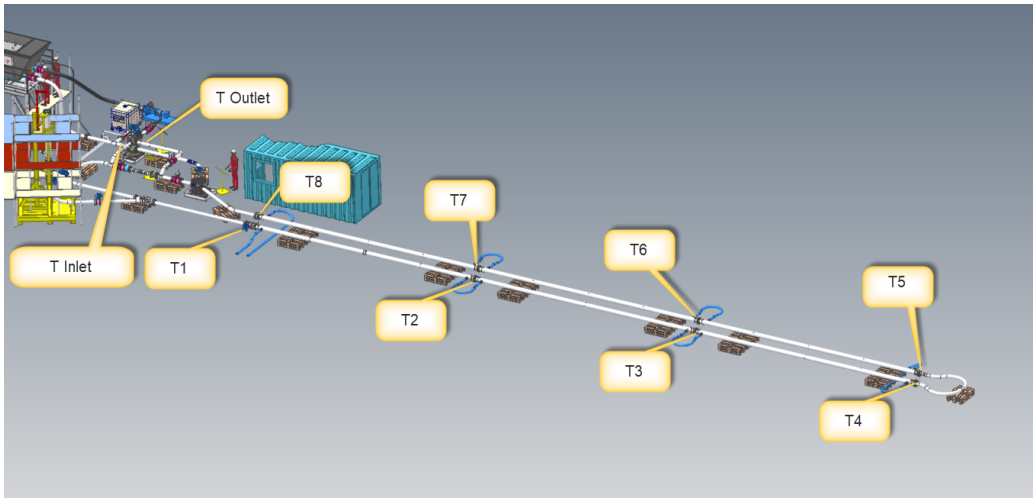

Fig. 7.3—***Temperature sensors locations overview.***

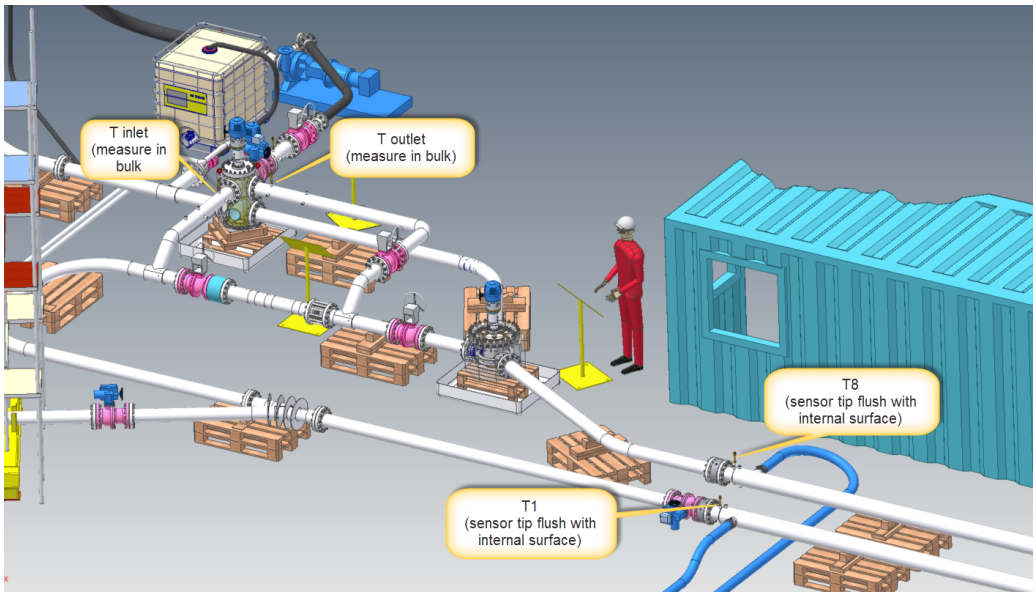

Fig. 7.4—*Temperature sensors locations.*

Table 7.1—*Flow loop parameters.*

Parameter	**Value**
Outer pipe ID, m	0.2064
Inner pipe OD, m	0.1683
Inner pipe wall thickness, mm	9.0
Total cooling sections length, m	62.0
Tank heating elements power, kW	10.0
Temperature sensors	K type thermocouple
Inner pipe fluid	Teboil hydraulic oil 15 + Sasol wax 5405
Annulus fluid	Water
Insulation type	Glasswool
Insulation thickness, mm	70
Thermal conductivity insulation, W/m/K	0.04

7.3 Experimental procedure

Several test runs were performed targeting various qualifications aspects of the system, Stangeland et al. [2021]. Three of them were covering wax deposition capability of the system. Wax deposition with 3 %, 5 %, and 7.5 % wax content in the supplied model oil was studied. Each wax deposition run was going through the procedure steps:

1. Heat the tank to 55 °C.
2. Switch off the heating for 7.5 % test; heating was ongoing throughout 3 % and 5 % tests.
3. Start oil circulation.
4. Start water flow.
5. Run the loop for 3 hours or until the oil temperature inside the tank stabilizes.
6. Drain the oil.
7. Inspect.

7.4 Simulation

Prediction of the deposition is sensitive to the correctness of the fluid viscosity and wax solubility representation. The simulation uses slurry flow viscosity correlation as per Eq. 7.2. The solubility curve was estimated with Eq. 7.1. The coefficients in the correlations were found by fitting to the measured viscosity of the studied model oil. The measurements were done with different wax content and under different shear stresses.

$$\phi_{sol} = a(T + b)^c \tag{7.1}$$

ϕ_{sol} is how much wax content can be dissolved, T is temperature in Celsius.

$$\mu_{slurry} = \mu(e^{C_1\phi} + \frac{C_2\phi^{0.1}}{\dot{\gamma}} + \frac{C_3\phi^4}{\dot{\gamma}}) \tag{7.2}$$

ϕ is solid wax content in the slurry, μ is the viscosity of the fluid without solid particles. When performing fitting of the coefficients in Eqs. 7.2 and 7.1, smoothing was required to avoid kinks in the functions. The smoothing was done around the

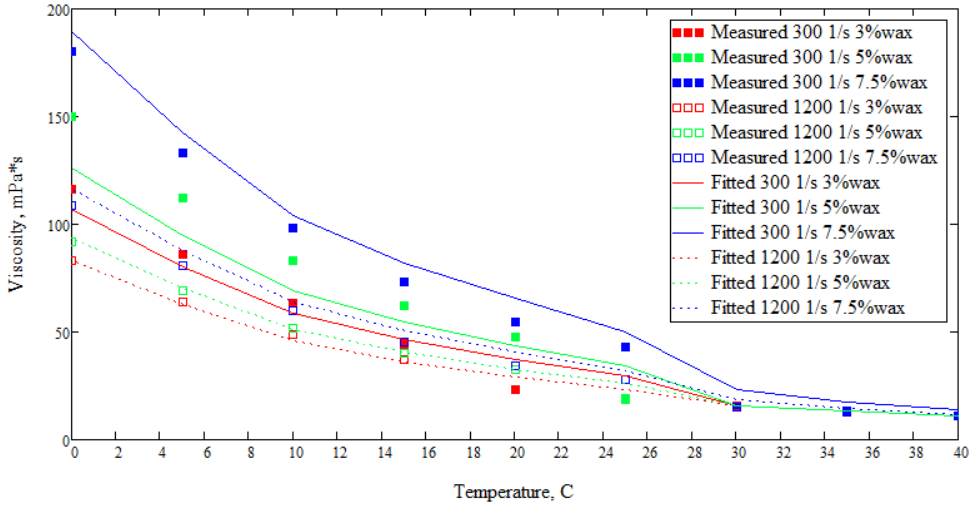

Fig. 7.5—*Model oil viscosity.*

Table 7.2—*Model oil solubility and viscosity coefficients.*

Coefficient	Value
a	4.31E-4
b	-9.937
c	1.783
C_1	4.334
C_2	159
C_3	9.5E6

kinks according to Eq. 7.3.

$$F(x) = \begin{cases} F_1(x), & x < x_a \\ F_2\left(\frac{tanh\frac{10(x-0.5(x_b+x_a))}{x_b-x_a}+1}{2}\right) + F_1\left(\frac{tanh\frac{10(x-0.5(x_b+x_a))}{x_a-x_b}+1}{2}\right), & x_a \le x \le x_b \\ F_2(x), & x > x_b \end{cases} \tag{7.3}$$

where x is a variable, x_a, x_b are variable values around a kink, F is smoothed function, F_1, F_2 are functions on the left and right sides of a kink. Initially, an attempt was made to use slurry viscosity correlation from Pedersen and Roenningsen [2000], but it did not match the measured data because the model oil is outside Pedersen's correlation applicability. Figure 7.5 illustrates the measured data and the fit, and Table 7.2 presents the coefficients. The obtained coefficients are presented in Table 7.2

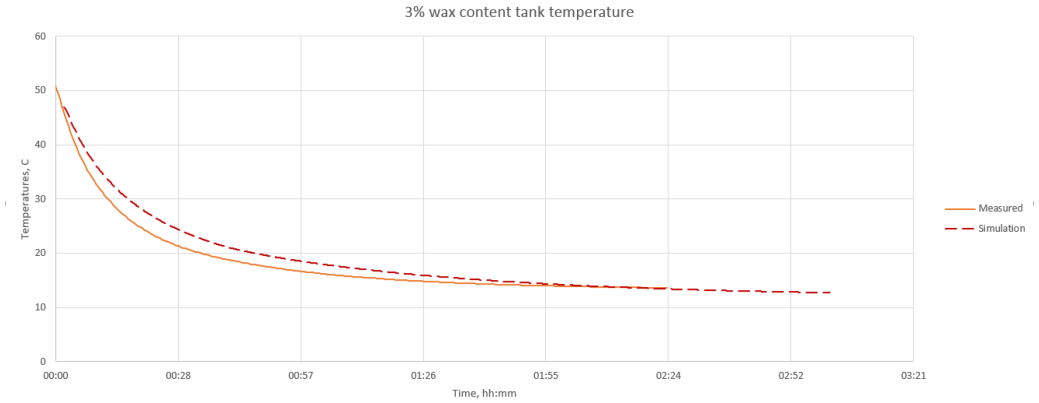

Fig. 7.6—*Tank temperatures for 3 % wax content. 2D simulation.*

7.5 Results and discussion

The results from the simulation that can be compared to the measurements from the experimental stand are:

- Temperature of the oil inside the tank.
- Thickness of wax layer. On the experimental stand, the thickness was obtained by opening a section of the flow loop.

Unfortunately, temperature readings from thermocouples mounted along the pipe loop could not be directly compared to the simulation because of their mounting position at the pipe sections connections, see Figure 7.2. The simulation model assumes the cooling annulus to be continuous and does not account for heat transfer in pipe walls on the longitudinal axis. So the experimental readings of the thermocouples are higher than simulation predictions because there is no cooling water at the exact position of the thermocouples, while the simulation model has cooling water along the whole length.
Wax thickness comparison for 30 m point is presented in Table 7.3. Comparison of the oil temperatures inside the tank for different wax content can be seen in Figures 7.6 to 7.8. The temperatures for 3 % and 5 % wax test did not approach water temperature because heating in the tank was switched on for those tests. Simulation prediction of the tank temperatures shows a good correlation with experimentally measured values. As a comparison to two-dimensional formulation with turbulent diffusivities as per Zheng et al. [2017] the one-dimensional formulation simulation based on Singh et al. [2000] and Singh et al. [2001] was run for the test with 7.5 % wax. For the conditions of the test loop, the results for one-dimensional and two-dimensional formulations look similar.
Wax thickness was measured after the full 180 minutes test duration, see Figure 7.9.

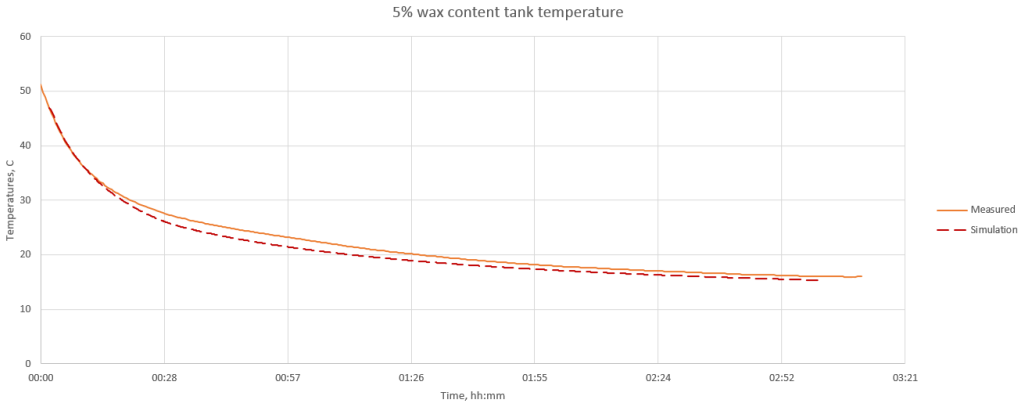

Fig. 7.7—*Tank temperatures for 5 % wax content. 2D simulation.*

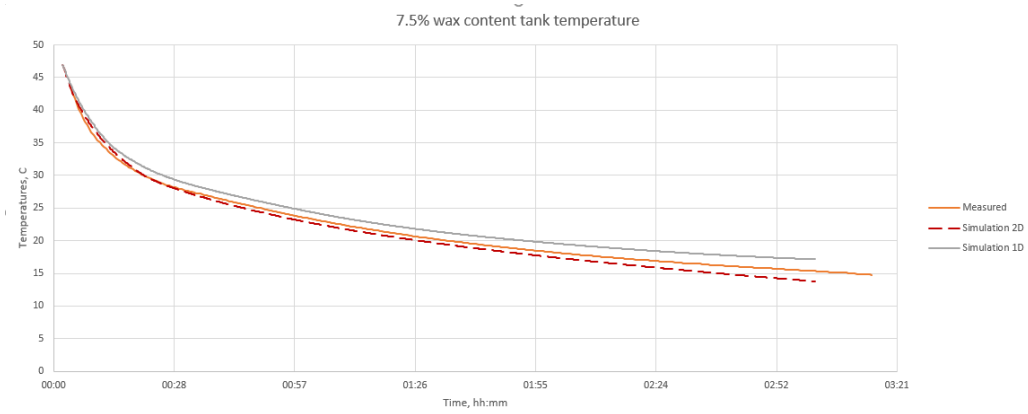

Fig. 7.8—*Tank temperatures for 7.5 % wax content. 1D and 2D simulations.*

Fig. 7.9—***Taking wax for measurements 7.5 % wax content.***

Table 7.3—*Wax thickness results.*

Wax content	Experiment	Simulation
0.03	0 mm	0.3
0.05	1 mm	0.9 mm
0.075	2 mm	1.8-2.0 mm

Both 1D and 2D simulations predict the development of a wax layer thickness, and temperature distribution along the pipe length. The 2D simulation also resolves the variables in the radial direction. The Figures 7.10 to 7.18 show the bulk results for 2D simulations. Figure 7.19 shows results for 1D simulation. The wax thickness and bulk temperature distribution are shown for three timestamps: 10 minutes, 90 minutes, and 180 minutes. Simulation results for 3 % wax content are shown in Figures 7.10 to 7.12, for 5 % wax content - in Figures 7.13 to 7.15, and for 7.5 % wax content in Figures 7.16 to 7.18.

The folder "CH7" in the attachment to the thesis contains the source videos of the Figures 7.10 to 7.19.

Figure 7.19 shows the resulting wax layer thickness.

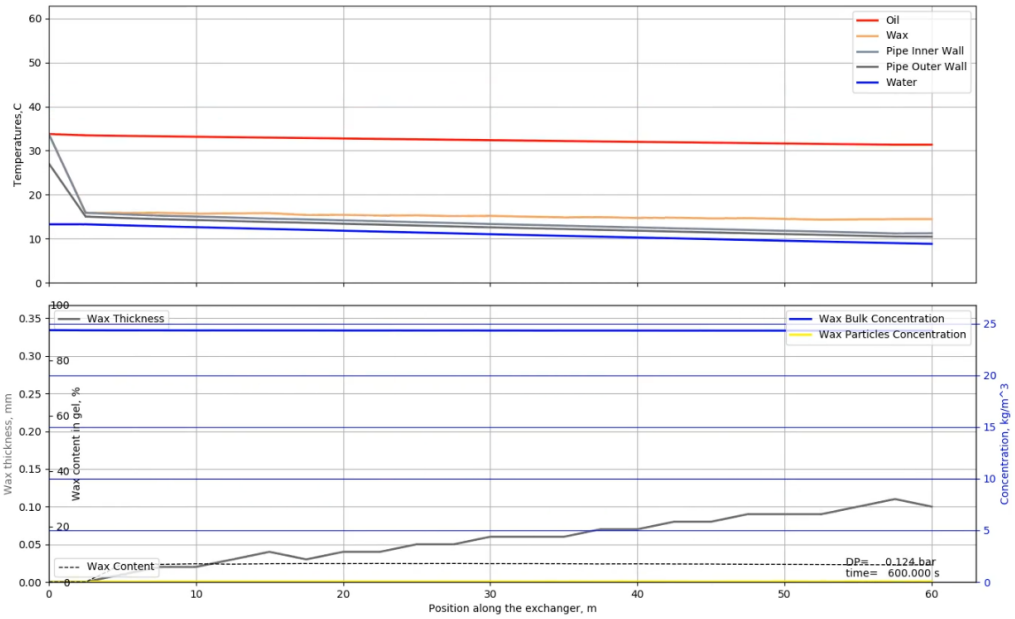

Fig. 7.10—
Simulated wax layer and temperatures along the length for 3 % wax content at 10 minutes 2D formulation.

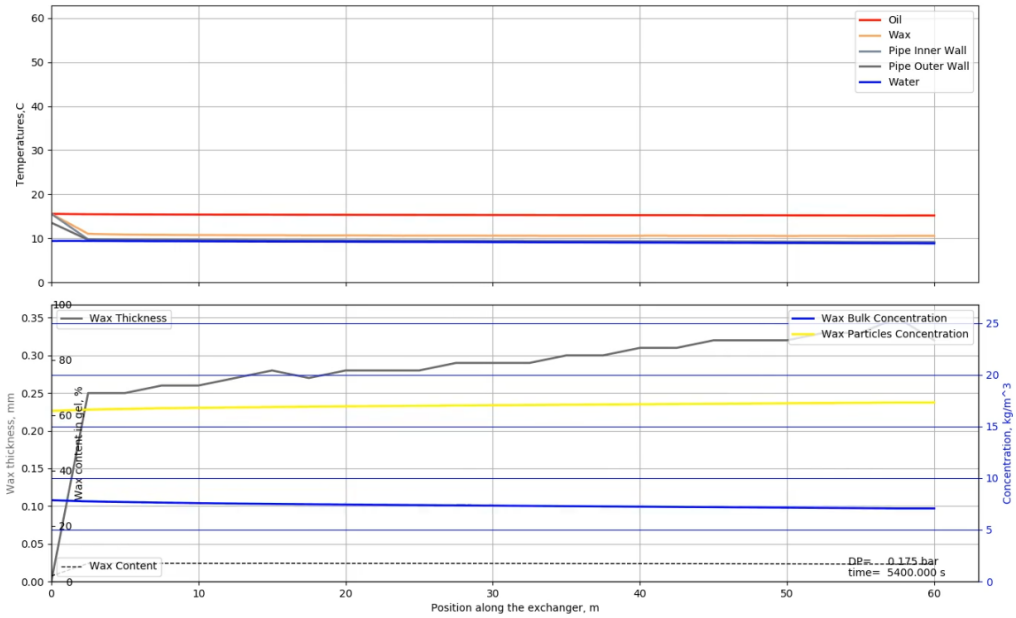

Fig. 7.11—
Simulated wax layer and temperatures along the length for 3 % wax content at 90 minutes 2D formulation.

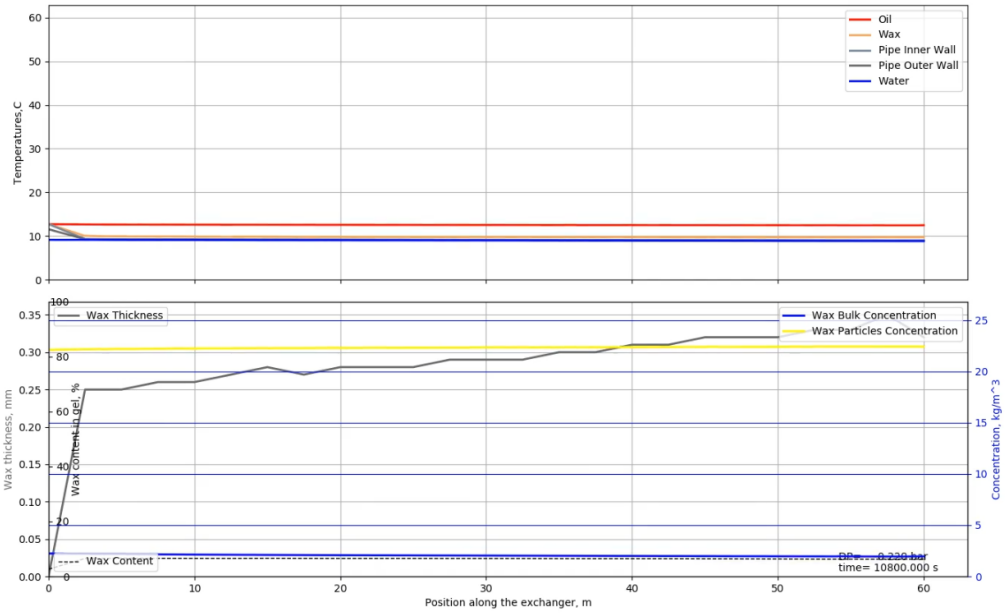

Fig. 7.12—
Simulated wax layer and temperatures along the length for 3 % wax content at 180 minutes 2D formulation.

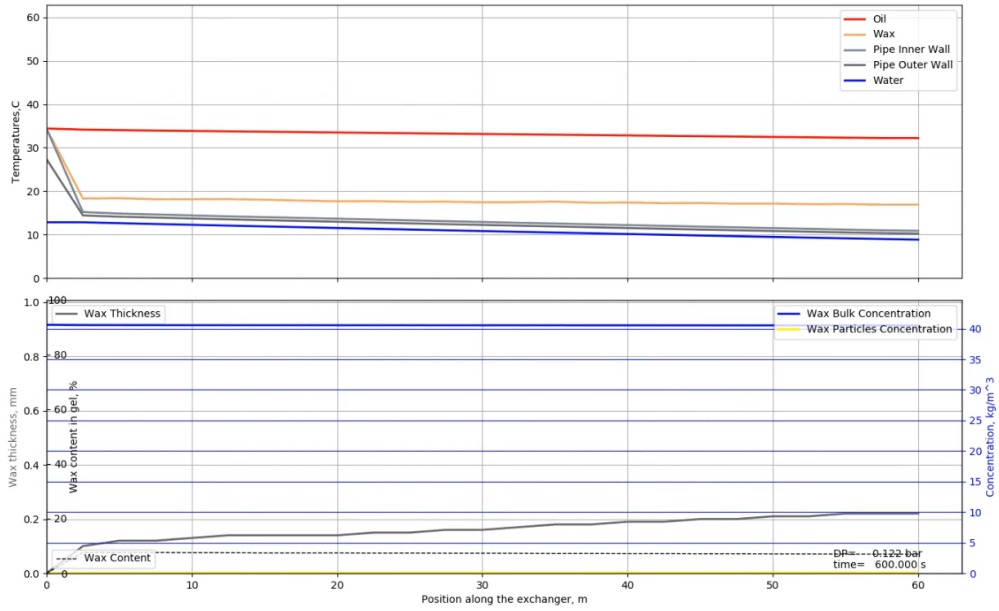

Fig. 7.13—
Simulated wax layer and temperatures along the length for 5 % wax content at 10 minutes 2D formulation.

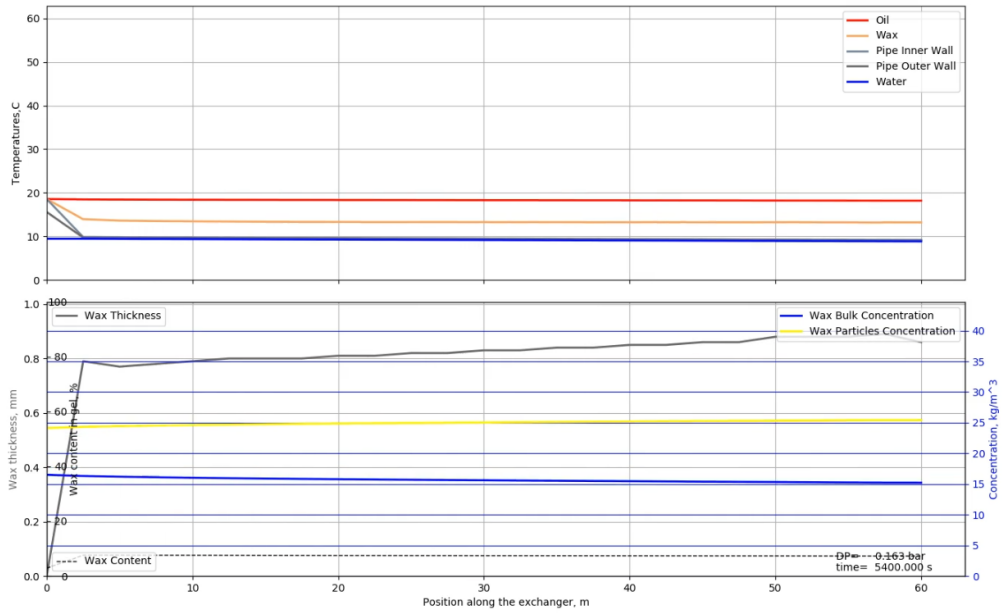

Fig. 7.14—
Simulated wax layer and temperatures along the length for 5 % wax content at 90 minutes 2D formulation.

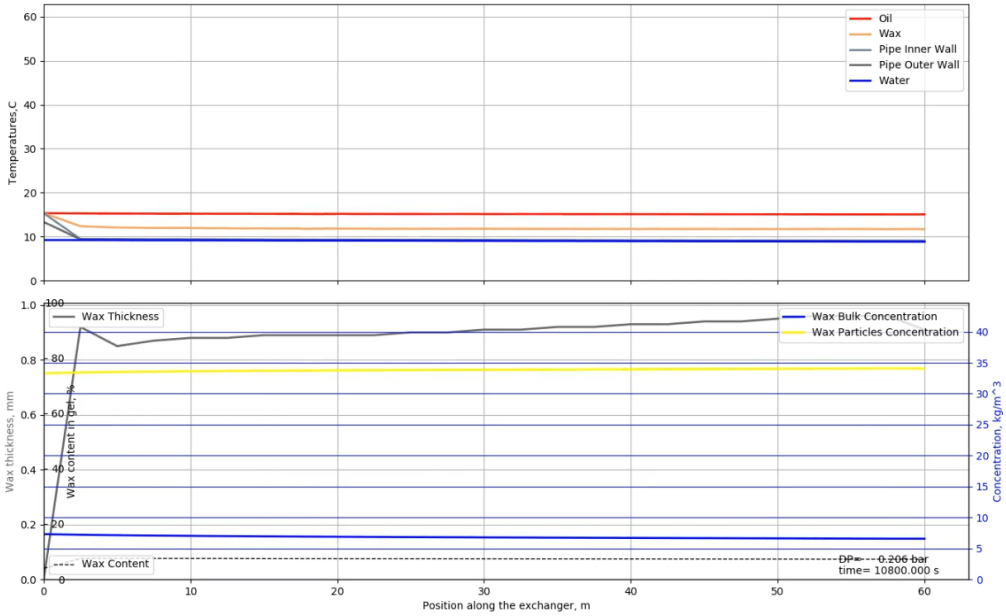

Fig. 7.15—
Simulated wax layer and temperatures along the length for 5 % wax content at 180 minutes 2D formulation.

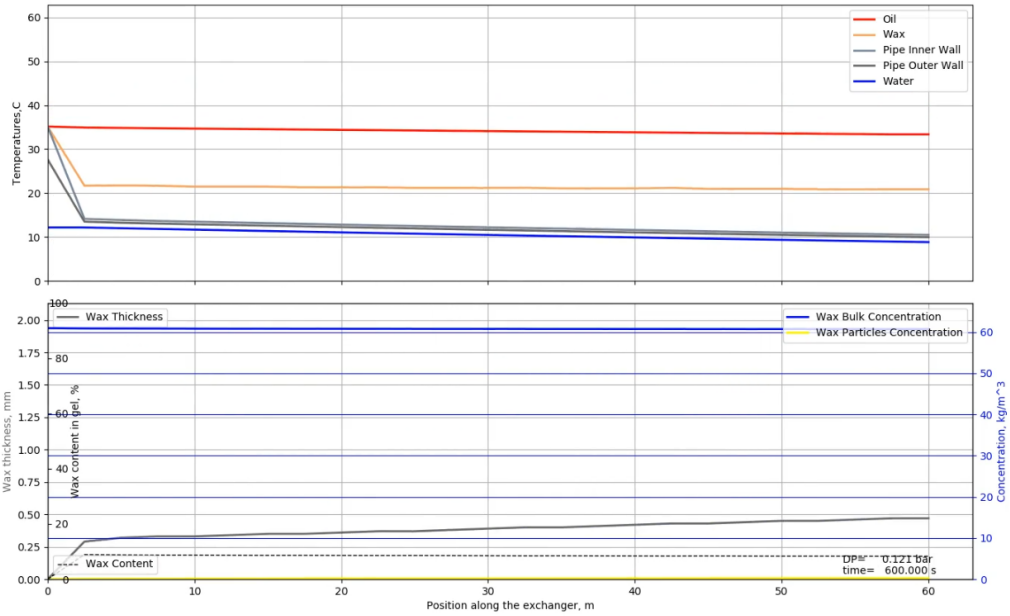

Fig. 7.16—*Simulated*
wax layer and temperatures along the length for 7.5 % wax content at 10 minutes 2D formulation.

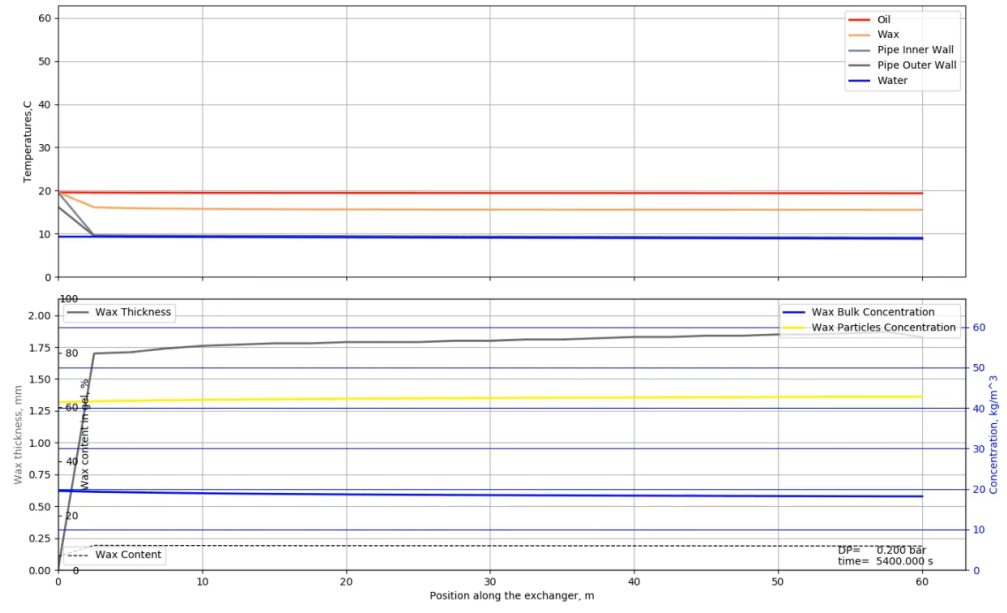

Fig. 7.17—*Simulated*
wax layer and temperatures along the length for 7.5 % wax content at 90 minutes 2D formulation.

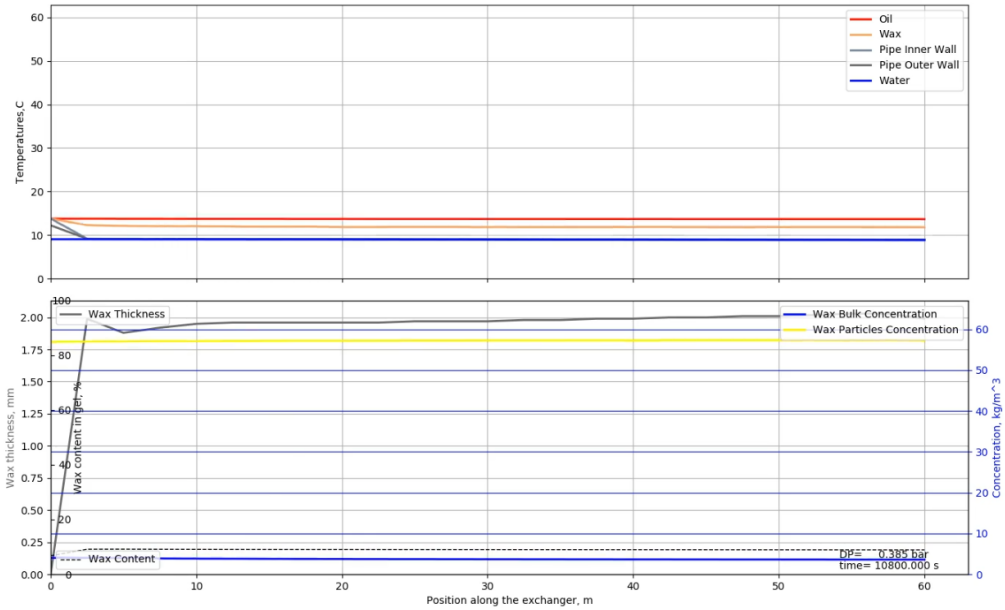

Fig. 7.18—*Simulated*
wax layer and temperatures along the length for 7.5 % wax content at 180 minutes 2D formulation.

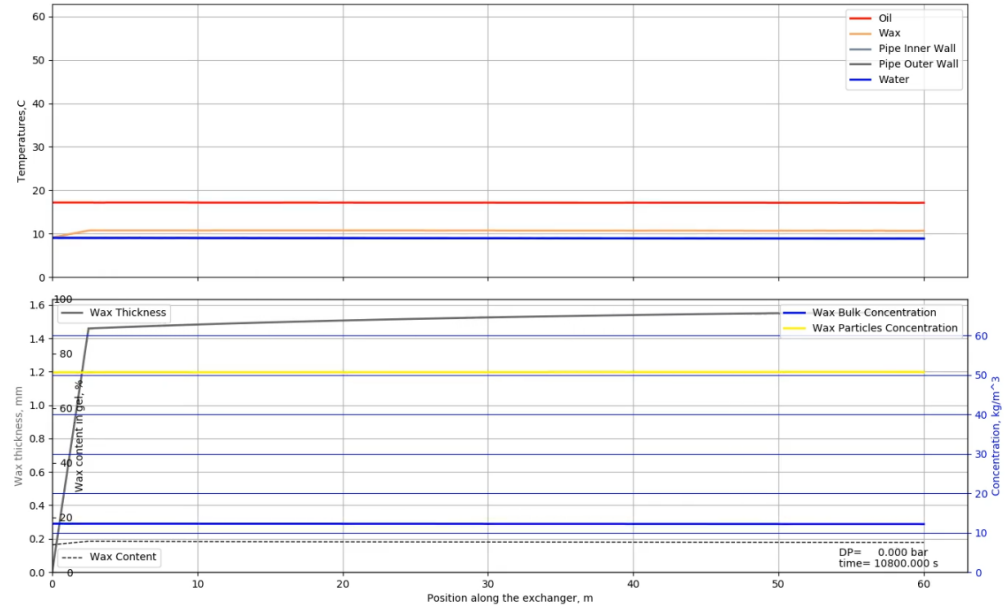

Fig. 7.19—*Simulated*
wax layer and temperatures along the length for 7.5 % wax content at 180 minutes 1D formulation.

7.6 Conclusion

Wax deposition in the wax control system qualification stand was simulated in the software developed for the WCS as described in chapter 6. The simulation predictions of bulk temperature and wax thickness for both one-dimensional and two-dimensional formulations agree with the experimental measurements obtained from the studied test stand. The input to the simulation requires either fitting of solubility curve and slurry viscosity to the measured viscosities of the oil or direct measurement of the wax solubility.

7.7 References

[1] Bidmus, H. O. and Mehrotra, A. K. 2009. Solids deposition during "cold flow" of wax-solvent mixtures in a flow-loop apparatus with heat transfer. *Energy & Fuels* **23** (6): 3184–3194. https://doi.org/10.1021/ef900224r

[2] Merino-Garcia, D. and Correra, S. 2008. Cold flow: A review of a technology to avoid wax deposition. *Petroleum Science and Technology* **26** (4): 446–459. https://doi.org/10.1080/10916460600809741

[3] Pedersen, K. S. and Roenningsen, H. P. 2000. Effect of precipitated wax on viscosities- a model for predicting non-newtonian viscosity of crude oils. *Energy & Fuels* **14**.

[4] Singh, P., Venkatesan, R., Fogler, H. S., and Nagarajan, N. 2000. Formation and aging of incipient thin film wax-oil gels. *AIChE Journal* **46** (5): 1059–1074.

[5] Singh, P., Venkatesan, R., Fogler, H. S., and Nagarajan, N. 2001. Morphological evolution of thick wax deposits during aging. *AIChE Journal* **47**.

[6] Stangeland, Ø., Sigbjørn, D., and Novoseltsev, Y. 2021. Qualification of wax control system. *Proc.,* Offshore Technology Conference, Houston, Texas, USA, 16-19 August.

[7] Zheng, S., Saidoun, M., Palermo, T., Mateen, K., and Fogler, H. S. 2017. Wax deposition modeling with considerations of non-newtonian characteristics: Application on field-scale pipeline. *Energy & Fuels* **31** (5): 5011–5023. https://doi.org/10.1021/acs.energyfuels.7b00504

Chapter 8

Concluding remarks and future work

8.1 Concluding remarks

One-dimensional and two-dimensional mathematical models for wax deposition in specific conditions of the wax control system (WCS) have been developed. The specific conditions include fast forced cooling, non-Newtonian behavior of the fluid, and rapid change of non-Newtonian parameters along the cooling loop. There was also a constraint to keep computation power requirements for solving model equations as low as possible. Chapter 6 presented the model, the solver, and meshing principles. The author carried out the development solely, and much effort was placed into making an efficient C++ computer code for the model.

During the WCS development process, three experiments were designed, executed, and post-processed by the author:

- Pilot experiment for checking the ability of a passive control system to keep a pig inside a loop. The information was shown in Section 2.2.
- Bypass pigging experiment in gas-liquid flow. The experiment was presented in Chapter 3.
- Two phase small scale wax deposition experiment. Chapter 4 described the experiment.

The author significantly contributed to the WCS qualification test presented in Chapter 5. The author was responsible for

- overall design of the loop,
- all items and sensors related to wax deposition,
- selection of the fluid,

- test procedure related to wax deposition,
- prediction and post-processing of wax deposition results.

The author also helped to design some other items that were qualified as integral parts of the WCS: pig and directional flow valve.

The work carried out by the author and presented in the thesis allowed WCS to pass qualification according to Norwegian regulations.

8.2 Future work

The developed WCS model is a starting point for making a validated design tool for the WCS system. The topics extending this research could be:

- Validation for a real oil.
- Implementation of a pigging model.
- Adding wax deposition module to a two-phase flow simulator.

Validation for real oil

In order to use the model and the software for the design of a real wax control system, it is necessary to run validation experiments on real oil in a model cooling loop and run simulations to compare with deposition in a full-scale loop. The full-scale WCS loop can be up to 14 km and will feature localized deposition at specific points along the pipeline. Such deposition cannot be reproduced in a 100 m loop with an 8-inch pipe.

Implementation of pigging

As pigging is intrinsic to WCS operation, it should be added to the simulation software. The pigging model should represent bypass pigging in a single-phase. Pigging may introduce local unsteady and highly turbulent effects resulting in additional heat and mass transfer that may complicate the wax deposition model.

Adding wax deposition module to a two-phase flow simulator

The WCS system was initially intended to operate with a two-phase gas/oil flow. However, during the development of the system, it was found that the practicality of this solution is doubtful due to issues with controlling pig motion in the loop and issues with predicting wax deposition. The more robust solution was to go for a single-phase WCS with either gas separation or pressure increase to a level when fluid is single-phase. However, the long-term goal is still to be able to design

a two-phase system. Then it is necessary to have a reliable prediction of wax deposition in two-phase flows and be able to simulate bypass pigging under those conditions. Several multiphase flow simulators can be used:

- OLGA
- LedaFlow
- Sluggit

OLGA and LedaFlow are closed-code commercial simulators used in the oil and gas industry; developing modules for them is not practicable. Sluggit is a multiphase flow simulator framework made by professor Ole Jørgen Nydal and developed further by his team such as Kjeldby [2013], Smith [2017]. It allows the implementation of additional code as modules making the software very flexible and easy to append.

Sluggit looks like a preferable software for future work on implementing pigging and wax deposition models relevant for WCS, if the multiphase flow is considered.

References

[1] Kjeldby, T. K. 2013. *Lagrangian Three-Phase Slug Tracking Methods*. PhD thesis, Norwegian University of Science and Technology.

[2] Smith, I. E. 2017. *A 7-field Lagrangian slug capturing and slug tracking model with higher order methods*. PhD thesis, Norwegian University of Science and Technology.

Appendices

Appendix A

Equations derivation

Nomenclature

Greek

α –	Volume fraction		
$\dot{\gamma}$ –	Shear rate, 1/s		
$\dot{\gamma}_0$ –	Limiting shear rate, 1/s		
ΔH_f –	Enthalpy of fusion, J/kg		
ϵ_D –	Turbulent mass diffusivity, m^2/s	A factor in turbulent term modelling	$-\overline{v_r' n'} = \epsilon_D \frac{\partial \overline{n}}{\partial r}$
ϵ_H –	Turbulent heat diffusivity, m^2/s	A factor in turbulent term modelling	$-\overline{v_r' T'} = \epsilon_H \frac{\partial \overline{T}}{\partial r}$
ϵ_m –	Turbulent momentum diffusivity, m^2/s	A factor in turbulent term modelling	$-\overline{v_r' v_z'} = \epsilon_m \frac{\partial \overline{v_z}}{\partial r}$
μ –	Dynamic viscosity, Pa·s		
μ_0 –	Limiting dynamic viscosity, Pa·s		
μ_{eff} –	Effective/apparent dynamic viscosity, Pa·s		
Π_0 –	Non dimensional pressure gradient, -	$= \frac{rs}{P_0} \frac{\partial p}{\partial z}$	
ρ –	Density, kg/m^3		
ρ_j –	Concentration of a component j, kg/m^3		
τ_0 –	Yield stress, Pa		
τ_{wall} –	Shear stress at the wall, Pa		
v –	Velocity, m/s		

v_r – Radial velocity component, m/s

v_z – Axial velocity component, m/s

$v_{za}ve$ – Average axial velocity, m/s

Latin

a, b, c – coefficients

C_1, C_2, C_3 – coefficients

C_{sup} – Max wax concentration at current temperature, kg/m^3

C_{par} – Solid wax particles concentration in oil bulk, kg/m^3 $= \frac{\alpha_{par}\rho_{par}}{\tilde{R}_w^2}$ for 1D formulation

C_{wb} – Dissolved wax concentration in oil fluid, kg/m^3 $= \frac{\alpha_{wb}\rho_{oil}}{\tilde{R}_w^2 - \alpha_{par}}$ for 1D formulation

C_{ws} – Max solubility of wax in oil at current temperature, kg/m^3

Cp – Heat capacity, J/kg/K $= \frac{\alpha_{wb}\rho_{oil}}{\tilde{R}_w^2 - \alpha_{par}}$ for 1D formulation

D – Diffusivity, m^2/s

D_e – Diffusivity of wax molecules inside wax gel, m^2/s

D_w – Diffusivity of dissolved wax in oil, m^2/s

$D_{w_{eff}}$ – Effective diffusivity of dissolved wax in oil, m^2/s

$D_{p_{eff}}$ – Effective diffusivity of solid wax particles in oil, m^2/s

F – A function

F_w – Wax concentration in gel layer

f – Darcy friction factor, -

f_{HB} – Fanning friction factor for Herschel-Bulkley fluid, -

h – Convective heat transfer coefficient, W/m^2/K

K – Consistency, parameter in viscosity correlation, Pa·s^n

k – Thermal conductivity, W/m/K

k_{eff} – Effective thermal conductivity, W/m/K

k_m – Mass transfer coefficient, m/s

k_p – Precipitation rate coefficient, 1/s

m – Mass, kg

n – Flow index parameter in viscosity correlation, -

n_1 – Parameter in viscosity correlation, -

N_s – Wax precipitation rate coefficient, 1/s

n_j – Concentration of component j as mass fraction of total fluid $= \frac{\rho_j}{\rho}$

P_0 – Non dimensional pressure scale for solving for Herschel-Bulkley fluid, - $= k\left(\frac{v_{za}ve}{r_s}\right)^2$

R – Radius, m

r_s – Radius of the flow/steel pipe inner radius, m

$\tilde{R}$ – Normalized radius, m $= \frac{R}{R_i}$ for 1D formulation

Sc – Schmidt number, -

S_d – Wax deposition rate, kg/(m$^3 \cdot s$)

S_p – Wax precipitation rate, kg/(m$^3 \cdot s$)

T – Temperature, K

$\vec{U}$ – Velocity vector, m/s

Subscripts

gel – Property related to oil/wax gel

i – Property related to the inner surface of a pipe, i.e. pipe/wax or pipe/oil interface

$inlet$ – Property at the inlet

int – Property at the interface

par – Particle, property related to a particle

$pipe$ – Property related to pipe

o – Property related to the outer surface of a pipe

oil – Oil, property related to oil

$outlet$ – Property at the outlet

w – Property related to wax or oil/wax layer interface

wb – Dissolved wax

A.1 Geometry

A.1.1 One dimensional

The geometry of the studied one-dimensional system is shown in Figure A.1

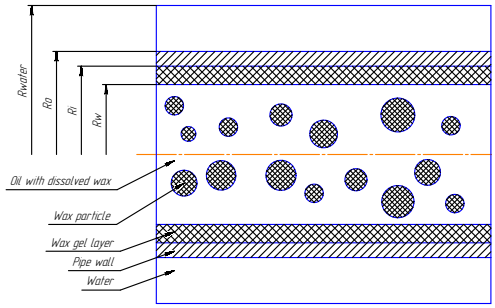

Fig. A.1—*Geometry.*

The total flow can be split into three fluids:

- Stationary wax gel layer at a pipe wall. α_{gel}
- Dissolved wax in the oil bulk. α_{wb}
- Precipitated/particle wax in the oil bulk. α_{par}

Basing the definition of volume fractions on an internal area of the pipe $A_i = \pi R_i^2$, volume fraction equations read:

$$\begin{aligned} \alpha_{gel} + \alpha_{oil} + \alpha_{par} + \alpha_{wb} &= 1 \\ \alpha_{oil} + \alpha_{par} + \alpha_{wb} &= \frac{R_w^2}{R_i^2} = \tilde{R}_w^2 \end{aligned} \tag{A.1}$$

where $\tilde{R}_w = \frac{R_w}{R_i}$ is a non dimensional radius of oil/wax interface.

A.1.2 Two dimensional

To resolve temperature and concentration gradients at the wall, it is convenient to introduce cylindrical coordinates with axial symmetry, essentially making the problem two-dimensional. The volume fractions have to be redefined with two dimensions as they are no longer tied to the inner pipe radius but to the volume of the current cell/control volume. Also, there is no entity "gel layer" inside a cell. A physical gel layer/ flow interaction is treated as a boundary condition to the most outer cell in the grid.

$$\alpha_{oil} + \alpha_{par} + \alpha_{wb} = 1 \tag{A.2}$$

A.2 Generic transport equation

Generic transport equation for a conserved property for constant density:

$$\frac{\partial(\rho\Psi)}{\partial t} + \nabla \cdot (\rho\vec{U}\Psi) - \nabla \cdot (\Gamma\nabla\Psi) = Sources \tag{A.3}$$

Where

Ψ-a conserved property, could be 1, enthalpy, mass concentration

$\frac{\partial\rho\Psi}{\partial t}$-change of the property in a control volume

$\nabla \cdot (\rho\vec{U}\Psi)$-convection of the property

$\nabla \cdot (\Gamma\nabla\Psi)$-diffusion

Γ-a corresponding diffusivity

This generic transport equation has only diffusion term based on the property; other terms like diffusion due to the temperature gradient and diffusion due to pressure gradient are neglected. In cylindrical coordinates, the equation takes the following form.

$$\begin{aligned}\frac{\partial(\rho\Psi)}{\partial t} + \frac{1}{r}\frac{\partial}{\partial r}(r\upsilon_r\rho\Psi) + \frac{1}{r}\frac{\partial}{\partial\phi}(\upsilon_\phi\rho\Psi) + \frac{\partial}{\partial z}(\upsilon_z\rho\Psi) + \frac{1}{r}\frac{\partial}{\partial r}\left(r\Gamma\frac{\partial\Psi}{\partial r}\right) + \\ + \frac{1}{r^2}\frac{\partial}{\partial\phi}\left(\Gamma\frac{\partial\Psi}{\partial\phi}\right) + \frac{\partial}{\partial z}\left(\Gamma\frac{\partial\Psi}{\partial z}\right) = Sources\end{aligned} \tag{A.4}$$

If there is symmetry around the z-axis, then the dependencies on ϕ drop out $\frac{\partial F}{\partial\phi} = 0$:

$$\frac{\partial(\rho\Psi)}{\partial t} + \frac{1}{r}\frac{\partial}{\partial r}(r\upsilon_r\rho\Psi) + \frac{\partial}{\partial z}(\upsilon_z\rho\Psi) + \frac{1}{r}\frac{\partial}{\partial r}\left(r\Gamma\frac{\partial\Psi}{\partial r}\right) + \frac{\partial}{\partial z}\left(\Gamma\frac{\partial\Psi}{\partial z}\right) = Sources \tag{A.5}$$

A.3 Mass transport

All equations in this section, if written in cylindrical coordinates, assume that the flow is axisymmetrical, i.e. symmetrical around the z-axis.

A.3.1 Continuity equation

$$\frac{\partial\rho}{\partial t} + \nabla \cdot (\rho\vec{U}) = Sources \tag{A.6}$$

Assuming quasi-steady flow where density very slowly depends on time, the dependency on time can be set to zero. $\frac{\partial \rho}{\partial t} = 0$. With this assumption, it is possible to simplify the continuity equation.

$$\nabla \cdot (\rho \vec{U}) = 0 \tag{A.7}$$

$$\frac{1}{r}\frac{\partial}{\partial r}(r\rho v_r) + \frac{\partial(\rho v_z)}{\partial z} = 0 \tag{A.8}$$

A.3.2 Components transport

There is an interdiffusion of components in the waxy oil with the wax slurry mixture, with components taken as dissolved wax particles, oil particles, and solid wax particles. Also, dissolved wax can precipitate, or solid wax can dissolve. Equation A.3 can be used with the mass concentration of the components. The mass concentration could be found from volume fractions. Taking the density of all components, including solid wax, to be the same, a mass concentration for a component, for example, dissolved wax, can be written as:

$$n_{wb} = \frac{\alpha_{wb}\rho_{wb}}{\alpha_{wb}\rho_{wb} + (1-\alpha_{wb})\rho_{oil}} = [\rho_{wb} = \rho_{oil}] = \alpha_{wb} \tag{A.9}$$

Expression for transport of a component:

$$\frac{\partial(\rho\alpha)}{\partial t} + \nabla \cdot (\rho\alpha\vec{U}) - \nabla \cdot (\rho D \nabla \alpha) = Sources \tag{A.10}$$

Using Reynolds decomposition for description of turbulent flow $\alpha = \overline{\alpha} + \alpha'$, $\rho = \overline{\rho}$, $\vec{U} = \overline{\vec{U}} + \vec{U}'$:

$$\frac{\partial(\rho\overline{\alpha})}{\partial t} + \nabla \cdot (\rho\overline{\alpha\vec{U}}) + \nabla \cdot (\rho\overline{\alpha'\vec{U}'}) - \nabla \cdot (\rho D \nabla \overline{\alpha}) = Sources \tag{A.11}$$

Assuming that the only significant component of $\overline{\alpha'\vec{U}'}$ in boundary layer is $\overline{\alpha' v_r'}$, and that it is proportional to $\frac{\partial \overline{\alpha}}{\partial r}$ with coefficient of proportionality $-\epsilon_D$ the equation A.11 can be written in cylindrical coordinates in the following way:

$$\begin{aligned}\frac{\partial(\rho\overline{\alpha})}{\partial t} + \frac{1}{r}\frac{\partial}{\partial r}(r\rho\overline{\alpha v_r}) + \frac{\partial}{\partial z}(\rho\overline{\alpha v_z}) - \frac{1}{r}\frac{\partial}{\partial r}\left(r\rho\epsilon_D\frac{\partial\overline{\alpha}}{\partial r}\right) - \\ \frac{1}{r}\frac{\partial}{\partial r}\left(r\rho D\frac{\partial\overline{\alpha}}{\partial r}\right) + \frac{\partial}{\partial z}\left(\rho D\frac{\partial\overline{\alpha}}{\partial z}\right) = Sources\end{aligned} \tag{A.12}$$

Invoking fully developed flow approximations $v_r = 0$; assuming that axial diffusion is negligible compared to radial, i.e. concentration gradients in axial directions are small compared to radial ones; and for simplicity, writing averaged properties without the upper bar, the components transport equation is further simplified:

$$\frac{\partial(\rho\alpha)}{\partial t} + \frac{\partial}{\partial z}(\rho\alpha v_z) - \frac{1}{r}\frac{\partial}{\partial r}\left(r\rho(\epsilon_D + D)\frac{\partial\alpha}{\partial r}\right) = Sources \tag{A.13}$$

Using the continuity equation A.6 with no external mass sources:

$$\rho\frac{\partial\alpha}{\partial t}+\rho\upsilon_z\frac{\partial\alpha}{\partial z}-\frac{1}{r}\frac{\partial}{\partial r}\left(r\rho(\epsilon_D+D)\frac{\partial\alpha}{\partial r}\right)=Sources \tag{A.14}$$

ϵ_D is called turbulent mass diffusivity. Transport equations for specific components with diffusion coefficients substituted with their effective counterparts look like this:

$$\begin{aligned}
&\rho\frac{\partial\alpha_{wb}}{\partial t}+\rho\upsilon_z\frac{\partial\alpha_{wb}}{\partial z}-\frac{1}{r}\frac{\partial}{\partial r}\left(r\rho D_{w_{eff}}\frac{\partial\alpha_{wb}}{\partial r}\right)=-S_p \\
&\rho\frac{\partial\alpha_{par}}{\partial t}+\rho\upsilon_z\frac{\partial\alpha_{par}}{\partial z}-\frac{1}{r}\frac{\partial}{\partial r}\left(r\rho D_{p_{eff}}\frac{\partial\alpha_{par}}{\partial r}\right)=S_p \\
&D_{w_{eff}}=D_w+\epsilon_D \\
&D_{p_{eff}}=D_p+\epsilon_D=\epsilon_D
\end{aligned} \tag{A.15}$$

Where ϵ_D is turbulent mass diffusivity, and S_p is a precipitation rate proportional to the difference between current dissolved wax concentration and wax concentration oil can support at current temperature with concentrations in kg/m^3. It is taken that wax does not precipitate immediately upon becoming colder than the equilibrium condition requires.

$$S_p=k_pC_c \tag{A.16}$$

$$C_c=\begin{cases}C_{wb}-C_{sup}, & \text{if } C_{wb}>C_{sup}\\ C_{wb}-C_{sup}, & \text{if } C_{wb}<C_{sup}\&C_{par}>0\\ 0, & \text{otherwise}\end{cases} \tag{A.17}$$

$C_{wb}=\rho\alpha_{wb}$ and C_{ws} are respectively dissolved wax concentration and maximum dissolved wax concentration the oil can support at specified conditions (temperature in most cases) based on EoS or wax solubility curve.

Summarizing assumptions and approximations used to develop equation A.14:

- Densities of solid wax, liquid wax, and oil are equal.
- Axisymmetrical flow, i.e. $\frac{\partial F}{\partial\phi}=0$.
- Diffusion in the axial direction is negligible compared to diffusion in the radial direction. $\frac{1}{r}\frac{\partial}{\partial r}\left(r\rho\frac{\partial\alpha_{wb}}{\partial r}\right)\gg\frac{\partial}{\partial z}\left(\rho\frac{\partial\alpha_{wb}}{\partial z}\right)$.
- Fully developed flow in a tube, so there are no average radial velocities present. υ_r=0.
- Boundary layer approximation. $\frac{\partial\upsilon_z}{\partial r}\gg\frac{\partial\upsilon_z}{\partial z},\frac{\partial\upsilon_r}{\partial z}$.
- In boundary layer the only significant component in turbulency based convection $\overline{\alpha'\vec{U}'}$ is $\overline{\alpha'\upsilon_r'}$ and it could be set that $\overline{\alpha'\upsilon_r'}=-\upsilon_D\frac{\partial\overline{\alpha}}{\partial r}$.

Discretization of mass transport equations

First let's look at the mass conservation equation, 6.51 that allows the finding of vertical components of the velocities. It is easier to discretize from the integral form: the sum of all fluxes is zero.

$$\upsilon_r^{m+1/2,n} S_r^{m+1/2,n} - \upsilon_r^{m-1/2,n} S_r^{m-1/2,n} = \upsilon_z^{m,n+1/2} S_z^{m,n+1/2} - \upsilon_z^{m,n-1/2} S_z^{m,n-1/2} \tag{A.18}$$

Dissolved wax transport and particle wax transport are discretized both in the same way. Using the dissolved wax transport as an example, and writing α_{wb} as just α for simplicity:

$$\rho \frac{\partial \alpha}{\partial t} + \rho \upsilon_z \frac{\partial \alpha}{\partial z} - \frac{1}{r} \frac{\partial}{\partial r} \left(r \rho D_{w_{eff}} \frac{\partial \alpha}{\partial r} \right) = -S_p \tag{A.19}$$

$$\frac{\alpha_{i,j}^t - \alpha_{i,j}^{t-1}}{\Delta t} + \upsilon_z \frac{\alpha_{i,j}^t - \alpha_{j,j-1}^t}{\Delta z} - \frac{(D_w + \epsilon_D)}{r} \frac{\partial \alpha}{\partial r} - \frac{\partial}{\partial r} \left((D_w + \epsilon_D) \frac{\partial \alpha}{\partial r} \right) = -\frac{S_p}{\rho} \tag{A.20}$$

Taking D_w to be constant, and ϵ_D to vary

$$\frac{\alpha_{i,j}^t - \alpha_{i,j}^{t-1}}{\Delta t} + \upsilon_z \frac{\alpha_{i,j}^t - \alpha_{i,j-1}^t}{\Delta z} - \frac{(D_w + \epsilon_D)}{r} \frac{\alpha_{i+1,j}^t - \alpha_{i-1,j}^t}{2\Delta r} - \frac{1}{\Delta r} \left[(D_w + \epsilon_{D_{i+1/2,j}^t}) \left(\frac{\partial \alpha}{\partial r} \right)_{i+1/2,j}^t - (D_w + \epsilon_{D_{i-1/2,j}^t}) \left(\frac{\partial \alpha}{\partial r} \right)_{i-1/2,j}^t \right] = -\frac{S_p}{\rho} \tag{A.21}$$

$$\begin{aligned} \frac{\alpha_{i,j}^t - \alpha_{i,j}^{t-1}}{\Delta t} + \upsilon_z \frac{\alpha_{i,j}^t - \alpha_{i,j-1}^t}{\Delta z} - \frac{(D_w + \epsilon_D)}{r} \frac{\alpha_{i+1,j}^t - \alpha_{i-1,j}^t}{2\Delta r} - \\ \frac{1}{\Delta r^2} [(D_w + 0.5(\epsilon_{D_{i+1,j}^t} + \epsilon_{D_{i,j}^t}))(\alpha_{i+1,j}^t - \alpha_{i,j}^t) - \\ (D_w + 0.5(\epsilon_{D_{i,j}^t} + \epsilon_{D_{i-1,j}^t}))(\alpha_{i,j}^t - \alpha_{i-1,j}^t)] = -\frac{S_p}{\rho} \end{aligned} \tag{A.22}$$

For the node adjacent to the wax layer there is a flow of dissolved wax from the oil and the flow of the dissolved wax into the wax layer. The diffusion coefficients for oil and solid wax are different. Dissolved wax transport equation for cell adjacent to wax layer become:

$$\begin{aligned} \frac{\alpha_{i,j}^t - \alpha_{i,j}^{t-1}}{\Delta t} + \upsilon_z \frac{\alpha_{i,j+1}^t - \alpha_{i,j}^t}{\Delta z} - \\ \frac{1}{r_i \Delta r^2} [(r_i - \frac{\Delta r}{2})(D_w + 0.5(\epsilon_{D_{i-1,j}^t} + \epsilon_{D_{i,j}^t}))(\alpha_{i,j}^t - \alpha_{i-1,j}^t) - \\ (r_i + \frac{\Delta r}{2}) D_e (\alpha_{i+1,j}^t - \alpha_{i,j}^t)] \end{aligned} \tag{A.23}$$

where De is dissolved wax diffusivity in the gel.

A.3.3 One dimensional adjustments

All dependencies on coordinate r in equation A.14 drop out. For one-dimensional formulation, the volume fractions are defined to be based on the inner radius of the pipe, ref. definitions A.1. It means that to find concentrations of dissolved wax or solid wax from corresponding volume fraction values one needs to know wax layer thickness, Figure A.1.

$$C_{wb} = \frac{\alpha_{wb}\pi R_i^2 \rho_{oil}}{\pi R_w^2 - \alpha_{par}\pi R_i^2} = \left[\tilde{R_w} = \frac{R_w}{R_i}\right] = \frac{\alpha_{wb}\rho_w}{\tilde{R}_w^2 - \alpha_{par}} \tag{A.24}$$
$$C_{par} = \frac{\alpha_{par}\pi R_i^2 \rho_{par}}{\pi R_w^2} = \frac{\alpha_{par}\rho_{par}}{\tilde{R}_w^2}$$

The concentration of dissolved wax is used to calculate wax molecules diffusion flux from oil bulk towards either deposition layer or particles, so this concentration should be concentration relative to liquid oil volume in the section, but not to the total section volume. In contrast, the concentration of the particles is relative to cell/section volume.

Volume fraction transport equation in general form neglecting axial diffusion:

$$\frac{\partial(\rho\alpha)}{\partial t} + \frac{\partial(\rho\alpha\upsilon)}{\partial x} = sources \qquad A_i = \pi R_i^2 \tag{A.25}$$

Oil "particles" and dissolved wax is essentially one continuous fluid, the density of dissolved wax is set to be oil density:

$$\begin{aligned} \frac{\partial(\rho_{oil}\alpha_{wb})}{\partial t} + \frac{\partial(\rho_{oil}\alpha_{wb}\upsilon)}{\partial x} &= -Sp - Sd \\ \frac{\partial(\rho_{par}\alpha_{par})}{\partial t} + \frac{\partial(\rho_{par}\alpha_{oil}\upsilon)}{\partial x} &= Sp \\ \frac{\partial(\rho_{oil}\alpha_{oil})}{\partial t} + \frac{\partial(\rho_{oil}\alpha_{oil}\upsilon)}{\partial x} &= F(Sd) \end{aligned} \tag{A.26}$$

Sp is a wax precipitation rate in the oil bulk (rate of appearance of solid wax particles inside the oil bulk), Sd is a wax molecules deposition rate, F(Sd) is a removal rate of oil "particles" from the oil bulk in form of trapped oil in the deposited wax gel.

$$Sd = \frac{2\pi R_w k_m (C_{wb} - C_{ws})}{A_i} = \frac{2R_w k_m (C_{wb} - C_{ws})}{R_i^2} = \frac{2\tilde{R}_w k_m (C_{wb} - C_{ws})}{R_i}$$
$$Sp = \frac{A_w}{A_i} N_s C_c = \frac{R_w^2}{R_i^2} N_s C_c = \tilde{R}_w^2 N_s C_c \tag{A.27}$$

$$C_c = \begin{cases} C_{wb} - C_{sup}, & \text{if } C_{wb} > C_{sup} \\ C_{wb} - C_{sup}, & \text{if } C_{wb} < C_{sup} \& C_{par} > 0 \\ 0, & \text{otherwise} \end{cases} \tag{A.28}$$

$$\rho_{oil}(\frac{\partial \alpha_{wb}}{\partial t} + \frac{\partial \upsilon_{oil}\alpha_{wb}}{\partial x}) = -\tilde{R}_w^2 N_s C_c - \frac{2\tilde{R}_w k_m}{R_i}(C_{wb} - C_{ws}) \tag{A.29}$$

A.4 Momentum transport

For momentum transport, the whole mixture is considered. It is assumed that all individual components have the same velocities and also have the same densities.

A.4.1 Momentum transport two dimensional

$$\frac{\partial(\rho\vec{U})}{\partial t} + \nabla \cdot (\rho\vec{U} \otimes \vec{U}) = -\nabla p + \nabla \cdot \tau + Sources \tag{A.30}$$

In cartesian tensor notations:

$$\frac{\partial(\rho\upsilon_i)}{\partial t}\vec{e}_i + \frac{\partial}{\partial x_j}(\rho\upsilon_j\upsilon_i)\vec{e}_i = \frac{\partial \sigma_{ji}}{\partial x_j}\vec{e}_i + Sources \tag{A.31}$$

Where σ is a stress tensor. Performing Reynolds decomposition ($\upsilon_i = \overline{\upsilon}_i + \upsilon_i'$, $\sigma_{ji} = \overline{\sigma}_{ji} + \sigma_{ji}'$) and averaging:

$$\frac{\partial(\rho\overline{\upsilon}_i)}{\partial t}\vec{e}_i + \frac{\partial}{\partial x_j}(\rho\overline{\upsilon}_j\overline{\upsilon}_i)\vec{e}_i + \frac{\partial}{\partial x_j}(\rho\overline{\upsilon_j'\upsilon_i'})\vec{e}_i = \frac{\partial \overline{\sigma}_{ji}}{\partial x_j}\vec{e}_i + Sources \tag{A.32}$$

Moving fluctuating velocities momentum term to the right and expanding stress term:

$$\frac{\partial(\rho\overline{\upsilon}_i)}{\partial t}\vec{e}_i + \frac{\partial}{\partial x_j}(\rho\overline{\upsilon}_j\overline{\upsilon}_i)\vec{e}_i = -\frac{\partial p}{\partial x_i}\vec{e}_i + \frac{\partial}{\partial x_j}\left(\overline{\tau}_{ji} - \rho\overline{\upsilon_j'\upsilon_i'}\right)\vec{e}_i + Sources \tag{A.33}$$

Projecting to $\vec{e}_1$ axis with notations $\upsilon_1 = u, \upsilon_2 = \upsilon, \upsilon_3 = \omega$, using continuity equation and writing averaged properties without overbar for simplicity:

$$\begin{aligned} \rho\frac{\partial u}{\partial t} + \rho(u\frac{\partial u}{\partial x} + \upsilon\frac{\partial u}{\partial y} + \omega\frac{\partial u}{\partial z}) = -\frac{\partial p}{\partial x} + \frac{\partial}{\partial x}\left(\tau_{xx} - \rho\overline{u'u'}\right) + \\ \frac{\partial}{\partial y}\left(\tau_{yx} - \rho\overline{\upsilon'u'}\right) + \frac{\partial}{\partial x}\left(\tau_{zx} - \rho\overline{\omega'u'}\right) + Sources \end{aligned} \tag{A.34}$$

For a boundary layer, it is generally taken that $\overline{\omega'u'}$ is zero due to experimental evidence. It is found that the gradient of $\overline{u'^2}$ can be neglected except near

boundary layer separation. Another simplification is that with boundary layer approximations, viscous stress tensor τ has only one component τ_{yx}. Using boundary layer and fully developed flow ($v = 0$) approximations equation A.34, and taking boundary layer to be two dimensional ($\omega = 0$) becomes:

$$\rho\frac{\partial u}{\partial t} + \rho u\frac{\partial u}{\partial x} = -\frac{\partial p}{\partial x} + \frac{\partial}{\partial y}\left(\tau_{yx} - \rho\overline{v'u'}\right) + Sources \tag{A.35}$$

In cylindrical coordinates:

$$\rho\frac{\partial v_z}{\partial t} + \rho v_z\frac{\partial v_z}{\partial z} = -\frac{\partial p}{\partial z} + \frac{1}{r}\frac{\partial}{\partial r}\left(r(\tau_{rz} - \rho\overline{v_r v_z'})\right) + Sources \tag{A.36}$$

A.4.2 Laminar velocity profile in a circular pipe for Herschel-Bulkley fluid

In laminar steady pipe flow without sources, the equation A.36 reduces to:

$$\frac{\partial p}{\partial z} = \frac{1}{r}\frac{\partial}{\partial r}\left(r\mu\frac{\partial v_z}{\partial r}\right) \tag{A.37}$$

And Herschel-Bulkley viscosity is given as:

$$\tau = \tau_0 + k\dot{\gamma}^n$$
$$\mu_{eff} = \begin{cases} \mu_0 = k|\dot{\gamma}_0|^{n-1} + \tau_0|\dot{\gamma}_0|^{-1} & ,|\dot{\gamma}| \leq \dot{\gamma}_0 \\ k|\dot{\gamma}|^{n-1} + \tau_0|\dot{\gamma}|^{-1} & ,|\dot{\gamma}| \geq \dot{\gamma}_0 \end{cases} \tag{A.38}$$

The limiting shear rate $\dot{\gamma}_0$ is used to prevent numerical errors at shear rates close to 0.

Nondimensionalization is performed with the following substitutions:

$$P_0 = k\left(\frac{v_{z_{ave}}}{r_s}\right)^n \tag{A.39}$$

$$\Pi_0 = \frac{r_s}{P_0}\frac{\partial p}{\partial z} \tag{A.40}$$

$$\tilde{r} = \frac{r}{r_s}$$

$$\tilde{v}_z = \frac{v}{v_{z_{ave}}}$$

Boundary conditions:

$$\left.\frac{\partial \tilde{v}_z}{\partial \tilde{r}}\right|_{\tilde{r}=0} = 0 \tag{A.41}$$

$$\tilde{v}_z|_{\tilde{r}=1} = 0 \tag{A.42}$$

$$\left|\frac{\partial \tilde{v}_z}{\partial \tilde{r}}\right|\Big|_{\tilde{r}=r_1} = \dot{\gamma}_0 \frac{r_s}{v_{z_{ave}}}$$

At a radius smaller than r_1 the shear rate is smaller than the limiting shear rate,$\dot{\gamma}_0$, so the flow inside r_1 will be considered Newtonian. Note that the corresponding viscosity μ_0 is relativity high in most cases, and can result in a "plug" at the pipe center.

For a pipe flow the gradient of axial velocity in radial direction is negative, $\frac{\partial \tilde{v}_z}{\partial \tilde{r}} \leq 0$, hence

$$\begin{aligned} \left|\frac{\partial \tilde{v}_z}{\partial \tilde{r}}\right| &= -\frac{\partial \tilde{v}_z}{\partial \tilde{r}} \\ \text{sign}\frac{\partial \tilde{v}_z}{\partial \tilde{r}} &= -1 \end{aligned} \tag{A.43}$$

Flow section $\tilde{r} \leq r_1$

Equation A.37 transforms to

$$\frac{\partial p}{\partial z} = \frac{\mu_0}{r}\frac{\partial}{\partial r}\left(r\frac{\partial v_z}{\partial r}\right) \tag{A.44}$$

The solution is a typical Newtonian parabolic profile in the circular pipe, using boundary conditions $\left.\frac{\partial \tilde{v}_z}{\partial \tilde{r}}\right|_{\tilde{r}=0} = 0$.

$$\frac{\partial \tilde{v}_z}{\partial \tilde{r}} = \frac{\Pi_0 P_0 r_s \tilde{r}}{2\mu_0 v_{z_{ave}}}, \tilde{r} \leq r_1 \tag{A.45}$$

$$\tilde{v}_z = \frac{\Pi_0 P_0 r_s \tilde{r}^2}{4\mu_0 v_{z_{ave}}} + C, \tilde{r} \leq r_1 \tag{A.46}$$

Using second boundary condition for a Newtonian part of the flow, $\left|\frac{\partial \tilde{v}_z}{\partial \tilde{r}}\right|\Big|_{\tilde{r}=r_1} = \dot{\gamma}_0 \frac{r_s}{v_{z_{ave}}}$, r_1 is found.

$$r_1 = -\frac{2\mu_0 \dot{\gamma}_0}{\Pi_0 P_0} \tag{A.47}$$

Flow section $\tilde{r} > r_1$

Then insert equation A.38 into A.37

$$\frac{\Pi_0 P_0}{r_s} = \frac{1}{\tilde{r} r_s} \frac{\partial}{r_s \partial \tilde{r}} \left(r_s \tilde{r} \left[k \left(\left| \frac{\partial \tilde{v}_z}{\partial \tilde{r}} \right| \frac{v_{z_{ave}}}{r_s} \right)^{n-1} + \tau_0 \left(\frac{v_{z_{ave}}}{r_s} \right)^{-1} \left| \frac{\partial \tilde{v}_z}{\partial \tilde{r}} \right|^{-1} \right] \frac{v_{z_{ave}}}{r_s} \frac{\partial \tilde{v}_z}{\partial \tilde{r}} \right) \tag{A.48}$$

Substituting $\frac{\partial \tilde{v}_z}{\partial \tilde{r}} = -\left| \frac{\partial \tilde{v}_z}{\partial \tilde{r}} \right|$ and pushing the gradient into the brackets:

$$\Pi_0 P_0 = \frac{1}{\tilde{r}} \frac{\partial}{\partial \tilde{r}} \left(\tilde{r} \left[P_0 \left| \frac{\partial \tilde{v}_z}{\partial \tilde{r}} \right|^n + \tau_0 \right] \right) (-1) \tag{A.49}$$

Integration gives:

$$-\frac{\Pi_0 P_0 \tilde{r}^2}{2} + C_1 = \tilde{r} \left[P_0 \left| \frac{\partial \tilde{v}_z}{\partial \tilde{r}} \right|^n + \tau_0 \right] \tag{A.50}$$

Using boundary condition $\left| \frac{\partial \tilde{v}_z}{\partial \tilde{r}} \right|\Big|_{\tilde{r}=r_1} = \dot{\gamma}_0 \frac{r_s}{v_{z_{ave}}}$

$$-\frac{\Pi_0 P_0 r_1^2}{2} + C_1 = r_1 \mu_0 \gamma_0 \tag{A.51}$$

Using A.47 the $C1$ is found to be zero. After second integration and bearing in mind A.43 the non-Newtonian part of the flow is:

$$\tilde{v}_z = \frac{n}{n+1} \frac{2}{\Pi_0} \left(\frac{\Pi_0}{2} \tilde{r} + \frac{\tau_0}{P_0} \right)^{\frac{n+1}{n}} + C2 \tag{A.52}$$

Using boundary condition $\tilde{v}_z|_{\tilde{r}=1} = 0$:

$$\tilde{v}_z = \frac{n}{n+1} \frac{2}{\Pi_0} \left[\left(\frac{\Pi_0}{2} \tilde{r} + \frac{\tau_0}{P_0} \right)^{\frac{n+1}{n}} - \left(\frac{\Pi_0}{2} + \frac{\tau_0}{P_0} \right)^{\frac{n+1}{n}} \right] \tag{A.53}$$

Solution summary

$$\tilde{v}_z = \frac{\Pi_0 P_0 r_s \tilde{r}^2}{4 \mu_0 v_{z_{ave}}} + C \qquad , \tilde{r} \leq r_1 \tag{A.54}$$

$$\tilde{v}_z = \frac{n}{n+1} \frac{2}{\Pi_0} \left[\left(\frac{\Pi_0}{2} \tilde{r} + \frac{\tau_0}{P_0} \right)^{\frac{n+1}{n}} - \left(\frac{\Pi_0}{2} + \frac{\tau_0}{P_0} \right)^{\frac{n+1}{n}} \right] \qquad , \tilde{r} > r_1$$

$$r_1 = -\frac{2 \mu_0 \dot{\gamma}_0}{\Pi_0 P_0}$$

$$C = \frac{2}{\Pi_0} \frac{n}{n+1} \left[-\left(\frac{\gamma_0 r_s}{v_{z_{ave}}} \right)^{n+1} - \left(\frac{\Pi_0}{2} + \frac{\tau_0}{P_0} \right)^{\frac{n+1}{n}} \right] - \frac{r_s \mu_0 \gamma_0^2}{v_{z_{ave}} \Pi_0 P_0}$$

C is selected such that Newtonian and non-Newtonian parts have the same velocity at r_1.

A.4.3 One dimensional adjustments

For one-dimensional steady pipe flow, momentum transport under conditions of constant density Darcy-Weisbach equation is used.

$$-\frac{\delta p}{dz} = f\frac{\rho}{2}\frac{\bar{v}^2}{D} \tag{A.55}$$

Where f is Darcy friction factor.

A.5 Energy transport

A.5.1 Energy transport two dimensional

General enthalpy transport equation:

$$\frac{\partial(\rho i)}{\partial t} + \nabla\cdot(\rho\vec{U}i) - \nabla\cdot(k\nabla T) - \nabla\cdot\left(\sum_j \rho D_j i_j \nabla(n_j)\right) - \mu\phi - \frac{dp}{dt} = Sources \tag{A.56}$$

Where ϕ is a dissipation function, j is an index of a component, $n_j = \frac{\rho_j}{\rho}$ is a concentration, i is a specific enthalpy J/K.

Applying continuity equation

$$\rho\frac{\partial i}{\partial t} + \rho\vec{U}\cdot\nabla i - \nabla\cdot(k\nabla T) - \nabla\cdot\left(\sum_j \rho_j D_j i_j \nabla(n_j)\right) - \mu\phi - \frac{dp}{dt} = Sources \tag{A.57}$$

Looking closer at pressure gradient and substituting enthalpy with its definition:

$$\begin{aligned}\rho\frac{\partial i}{\partial t} + \rho\vec{U}\cdot\nabla i - \frac{dp}{dt} = \rho\frac{di}{dt} - \frac{dp}{dt} = \left[di = C_p dT + \frac{1}{\rho}(1-\alpha_c T)dp\right] = \\ = \rho C_p\frac{dT}{dt} + (1-\alpha_c T)\frac{dp}{dt} - \frac{dp}{dt} = \rho C_p\frac{dT}{dt} - \alpha_c T\frac{dp}{dt},,\end{aligned} \tag{A.58}$$

where α_c is the volumetric thermal expansion coefficient. Assuming that the volumetric thermal expansion coefficient is small for liquid oil and the change of pressure is also small, the change of enthalpy due to pressure variation $\alpha_c T\frac{dp}{dt}$ could be considered negligible compared to the change of enthalpy due to temperature.

Enthalpy change due to diffusion of components could be simplified if it is assumed that densities and enthalpies of all components are the same. Then, because mass is conserved, the mass of components diffusing into the volume is equal to the mass of the components exiting the volume. So, the amount of energy brought into the volume with component diffusion should be equal to the energy removed with the counter diffusion. Hence, the sum of energy flux due to diffusion should

be zero. Looking at an example of a mixture with two components with diffusion coefficients D_{12} and D_{21}.

$$\nabla \cdot \left(\sum_j \rho_j D_j i_j \nabla(n_j) \right) = \nabla \cdot (\rho_1 D_{12} i_1 \nabla(n_1) + \rho_2 D_{21} i_1 \nabla(n_2)) = \\ = \begin{bmatrix} D_{12} = D_{21} \\ i_1 = i_2 \\ \rho_1 = \rho_2 \\ n_2 = 1 - n_1 \end{bmatrix} = \\ \nabla \cdot (\rho_1 D_{12} i_1 \nabla(n_1) + \rho_1 D_{12} i_1 \nabla(1 - n_1)) = \nabla \cdot (\rho_1 D_{12} i_1 \nabla(1)) = 0 \tag{A.59}$$

So, after applying the following assumptions:

- Densities of all components are equal. Even if solidified wax can have up to 10 % volume difference compared to solid wax, the percentage of wax content in the oil is generally less than 20 %, and 10 % volume change due to solidification(slow process) considered to influence transport in a weak way, the assumption of equal densities considered to be valid.
- Heat capacities of all components are equal.
- Volumetric thermal expansion contributions to the enthalpy of all components are negligible compared to temperature change contributions. As all components are either liquid or solid, it is considered to be a valid assumption.
- Heat capacities of all components are taken constants as the change of heat capacities during cooling from 60° C to 4 ° C is less than 10 %.

The equation A.56 becomes:

$$\rho c_p \frac{\partial T}{\partial t} + \rho c_p \vec{U} \cdot \nabla T - \nabla \cdot (k \nabla T) - \mu \phi = Sources \tag{A.60}$$

or using continuity equation:

$$c_p \frac{\partial (\rho T)}{\partial t} + c_p \nabla \cdot (\rho \vec{U} T) - \nabla \cdot (k \nabla T) - \mu \phi = Sources \tag{A.61}$$

After performing Reynolds decomposition $T = \overline{T} + T'$, $\rho = \overline{\rho}$, $\vec{U} = \overline{\vec{U}} + \vec{U}'$ to describe the turbulent flow and disregarding turbulent dissipation:

$$c_p \frac{\partial (\rho \overline{T})}{\partial t} + c_p \nabla \cdot (\rho \overline{\vec{U}} \overline{T}) + \nabla \cdot (c_p \rho \overline{\vec{U}' T'}) - \nabla \cdot (k \nabla \overline{T}) - \mu \overline{\phi} = Sources \tag{A.62}$$

When applying boundary layer approximation in cylindrical coordinates, it is generally assumed that components of turbulent enthalpy flux $\overline{\vec{U}' T'}$ are negligible

except the component $\overline{v_r'T'}$ Using cylindrical coordinates with axial symmetry around the z-axis and applying approximations for boundary layer and fully developed flow, with averaged property written without a bar $\overline{T} = T$ for simplicity:

$$\rho c_p \frac{\partial T}{\partial t} + \rho c_p v_r \frac{\partial T}{\partial r} + \rho c_p v_z \frac{\partial T}{\partial z} - \frac{1}{r}\frac{\partial}{\partial r}\left(rk\frac{\partial T}{\partial r}\right) - \frac{\partial}{\partial z}\left(k\frac{\partial T}{\partial z}\right) + \frac{1}{r}\frac{\partial}{\partial r}\left(rc_p\rho\overline{v_r'T'}\right) - \mu\phi = Sources \tag{A.63}$$

Then, using fully developed flow for a pipe($v_r = 0$) and assuming that axial temperature diffusion is negligible compared to the radial one ($\frac{1}{r}\frac{\partial}{\partial r}\left(rk\frac{\partial T}{\partial r}\right) \gg \frac{\partial}{\partial z}\left(k\frac{\partial T}{\partial z}\right)$) the equation can be simplified further:

$$\rho c_p \frac{\partial T}{\partial t} + \rho c_p v_z \frac{\partial T}{\partial z} - \frac{1}{r}\frac{\partial}{\partial r}\left(rk\frac{\partial T}{\partial r} - rc_p\rho\overline{v_r'T'}\right) - \mu\phi = Sources \tag{A.64}$$

Assuming that average of fluctuation $-\overline{v_r'T'}$ is proportional to $\frac{\partial T}{\partial r}$, it is possible to set a coefficient of proportionality ϵ_H and name it turbulent diffusivity of heat.

$$-\overline{v_r'T'} = \epsilon_H \frac{\partial T}{\partial r} \tag{A.65}$$

Applying boundary layer and fully developed flow approximations to the dissipation function ϕ the heat generated due to viscous dissipation becomes:

$$\mu\phi = \mu\left(\frac{\partial v_z}{\partial r}\right)^2 \tag{A.66}$$

Note that this dissipation function assumes that turbulent dissipation can be neglected. μ is a non-Newtonian viscosity based on any non-Newtonian model.

Plugging A.65 and A.66 into A.64:

$$\rho c_p \frac{\partial T}{\partial t} + \rho c_p v_z \frac{\partial T}{\partial z} - \frac{1}{r}\frac{\partial}{\partial r}\left(r(k + c_p\rho\epsilon_H)\frac{\partial T}{\partial r}\right) - \mu\left(\frac{\partial v_z}{\partial r}\right)^2 = Sources \tag{A.67}$$

The heat source is heat generated from the phase change of wax components.

$$Sources = S_p \Delta H_f \tag{A.68}$$

Where ΔH_f is the latent heat of solidification, S_p is the amount of wax molecules having a phase change, defined as in equation A.16.

Summary of the approximations and assumptions:

- Volumetric thermal expansion is small; hence enthalpy change due to thermal expansion is negligible compared to change due to temperature change. This assumption is relevant for liquids where density has a low dependency on temperature.
- Densities and heat capacities of all components in a mixture are equal. This assumption allows the elimination of enthalpy flux due to components diffusion.
- Heat capacities are constants.
- Turbulent enthalpy flux due of components $\overline{v'_\phi T'}$ and $\overline{v'_z T'}$ are negligible compared to component $\overline{v'_r T'}$.
- $\overline{v'_r T'}$ could be approximated with $-\epsilon_H \frac{\partial T}{\partial r}$.
- Turbulent and non-Newtonian effects on viscous dissipation are neglected.
- Fully developed flow, and no fluid coming or leaving through a pipe wall. $v_r = 0$.
- Axisymmetrical flow and heating. No dependency on ϕ coordinate.
- Boundary layer approximation. $\frac{\partial v_z}{\partial r} \gg \frac{\partial v_z}{\partial z}, \frac{\partial v_r}{\partial z}$.

Discretization of energy equation

Discretization of equation A.67 can be complicated, especially when talking about the boundary node at the oil/pipe interface. Note that $\rho\epsilon_H$ is not constant.

$$\frac{\partial T}{\partial t} + v_z \frac{\partial T}{\partial z} - \frac{1}{r}\frac{\partial}{\partial r}\left(r(\alpha + \epsilon_H)\frac{\partial T}{\partial r}\right) - \frac{\mu}{\rho c_p}\left(\frac{\partial v_z}{\partial r}\right)^2 = \frac{Sources}{\rho c_p} \tag{A.69}$$

The most interesting term is radial diffusion. Taking heat diffusivity α constant:

$$\begin{aligned}\frac{1}{r}\frac{\partial}{\partial r}\left(r(\alpha + \epsilon_H)\frac{\partial T}{\partial r}\right) = \frac{1}{r}\left((\alpha + \epsilon_H)\frac{\partial T}{\partial r}\right) + \frac{\partial}{\partial r}\left((\alpha + \epsilon_H)\frac{\partial T}{\partial r}\right) = \\ \frac{\alpha + \epsilon_H}{r}\frac{\partial T}{\partial r} + \frac{\partial}{\partial r}\left(\epsilon_H \frac{\partial T}{\partial r}\right) + \alpha\frac{\partial^2 T}{\partial r^2}\end{aligned} \tag{A.70}$$

For radial node i discretization of the radial diffusion term, A.70 is:

$$\begin{aligned}
\frac{\alpha+\epsilon_H}{r_i}\frac{T_{i+1}-T_{i-1}}{2\Delta r}+\frac{\epsilon_{Hi+1/2}(\frac{\partial T}{\partial r})_{i+1/2}-\epsilon_{Hi-1/2}(\frac{\partial T}{\partial r})_{i-1/2}}{\Delta r}+\\
\alpha\frac{T_{i+1}-T_i-T_i+T_{i-1}}{\Delta r^2}=\\
\frac{\alpha+\epsilon_H}{r_i}\frac{T_{i+1}-T_{i-1}}{2\Delta r}+\frac{\frac{\epsilon_{Hi+1}+\epsilon_{Hi}}{2}(\frac{T_{i+1}-T_i}{\Delta r})-\frac{\epsilon_{Hi}+\epsilon_{Hi-1}}{2}(\frac{T_i-T_{i-1}}{\Delta r})}{\Delta r}+\\
\alpha\frac{T_{i+1}-T_i-T_i+T_{i-1}}{\Delta r^2}=\\
\frac{\alpha+\epsilon_H}{r_i}\frac{T_{i+1}-T_{i-1}}{2\Delta r}+\\
\frac{1}{2\Delta r^2}\left(\epsilon_{Hi+1}(T_{i+1}-T_i)-\epsilon_{Hi}(T_{i+1}-2T_i+T_{i-1})+\epsilon_{Hi-1}(T_{i-1}-T_i)\right)+\\
\alpha\frac{T_{i+1}-2T_i+T_{i-1}}{\Delta r^2}
\end{aligned} \tag{A.71}$$

For the cell adjacent to oil/pipe or oil/wax interface formulation is easier to illustrate from a cell energy balance.

$$\begin{aligned}
2\pi R\delta r\delta x\rho C_p\frac{\partial T}{\partial t}+2\pi R\delta r\rho C_p\upsilon_z\delta(T_x)=\\
2\pi(R-\frac{\delta r}{2})\delta x(k+\rho C_p\frac{\epsilon_{Hi}+\epsilon_{Hi-1}}{2})\frac{T_{i-1}-T_i}{\delta r}-2\pi R_o\delta x\frac{T_i-T_{water}}{Res}
\end{aligned} \tag{A.72}$$

where R is the radius of the cell center, Res is a combined thermal resistance of water, pipe wall, and wax layer with the outer pipe radius, R_o, as a reference radius. Division by $2\pi R\delta r\delta x\rho C_p$ leads to

$$\frac{\partial T}{\partial t}+\upsilon_z\frac{\delta(T_x)}{\delta x}=\frac{(R-\frac{\delta r}{2})}{R}(\alpha+\frac{\epsilon_{Hi}+\epsilon_{Hi-1}}{2})\frac{T_{i-1}-T_i}{\delta r^2}-\frac{1}{\rho C_p}\frac{R_o}{R\delta r}\frac{T_i-T_{water}}{Res} \tag{A.73}$$

In case heat diffusivity α is not constant, then A.70 discretization changes to:

$$\begin{aligned}
\frac{1}{r}\frac{\partial}{\partial r}\left(r(\alpha+\epsilon_H)\frac{\partial T}{\partial r}\right)=\\
\frac{\alpha+\epsilon_H}{r_i}\frac{T_{i+1}-T_{i-1}}{2\Delta r}+\\
\frac{(\alpha_{i+1/2}+\epsilon_{Hi+1/2})(\frac{\partial T}{\partial r})_{i+1/2}-(\alpha_{i-1/2}+\epsilon_{Hi-1/2})(\frac{\partial T}{\partial r})_{i-1/2}}{\Delta r}=\\
\frac{\alpha+\epsilon_H}{r_i}\frac{T_{i+1}-T_{i-1}}{2\Delta r}+\\
\frac{(\alpha_{i+1}+\alpha_i+\epsilon_{Hi+1}+\epsilon_{Hi})(T_{i+1}-T_i)-(\alpha_i+\alpha_{i-1}+\epsilon_{Hi}+\epsilon_{Hi-1})(T_i-T_{i-1})}{2\Delta r^2}
\end{aligned} \tag{A.74}$$

A.5.2 One dimensional adjustments

In one dimension there is no dependency on r coordinate, so equation A.67 reduces to:

$$\rho c_p \frac{\partial T}{\partial t} + \rho c_p \upsilon_z \frac{\partial T}{\partial z} = Sources \tag{A.75}$$

Note that viscous dissipation is entirely disregarded.

Sources are heat generated due to wax precipitation in bulk and heat generated from wax molecules leaving the domain due to deposition on the wall. So compared to the two-dimensional case, there is an additional source due to deposition.

$$Sources = S_p \Delta H_f + S_d \Delta H_f \tag{A.76}$$

Where S_p and S_d are defined as in equation A.27, that is definition for the relevant one-dimensional mass transport equation.

A.6 Wax deposition model Singh

The wax deposition model proposed by [2] assumes the density of solid wax to be equal to the density of liquid wax; hence the density of oil wax gel does not change with wax content. [1] The model consists of 3 equations: wax flux equation from bulk to wax gel/oil interface, wax flux equation from the interface into the gel layer, and heat equation describing the heat flow from bulk to the wall.

Wax flux from bulk to the gel/oil interface:

$$\pi(R_i^2 - R_w^2)\frac{dF_w}{dt} - 2\pi R_w F_w \frac{dR_w}{dt} = \frac{2\pi R_w k_m}{\rho_{gel}}(C_{wb} - C_{ws}) \tag{A.77}$$

Wax flux from gel oil interface into the gel layer:

$$-2\pi R_w F_w \rho_{gel} \frac{dR_w}{dt} = 2\pi R_w k_m (C_{wb} - C_{ws}) - 2\pi R_w (-De \frac{dC_{ws}}{dT} \left.\frac{dT}{dr}\right|_{r=R_w}) \tag{A.78}$$

Subtracting Eq. A.78 from Eq. A.77 it is possible to get evolution of wax content in gel layer equation.

$$\pi(R_i^2 - R_w^2)\rho_{gel}\frac{dF_w}{dt} = 2\pi R_w (-De \frac{dC_{ws}}{dT} \left.\frac{dT}{dr}\right|_{r=R_w}) \tag{A.79}$$

Then to make in non dimensional against diameters and radii R_w is substituted with non dimensional variable $\tilde{R}_w = \frac{R_w}{R_i}$ Hence, Eq. A.79 becomes:

$$(1.0 - \tilde{R}_w^2)\frac{dF_w}{dt} = \frac{2\tilde{R}_w}{\rho_{gel} R_i}(-De \frac{dC_{ws}}{dT} \left.\frac{dT}{dr}\right|_{r=R_w}) \tag{A.80}$$

and Eq. A.78 becomes:

$$-F_w R_i \rho_{gel} \frac{d\tilde{R}_w}{dt} = k_m(C_{wb} - C_{ws}) + De \frac{dC_{ws}}{dT} \left. \frac{dT}{dr} \right|_{r=R_w} \tag{A.81}$$

As there is no convection in gel layer in axial direction $\frac{d}{dt} = \frac{\partial}{\partial t}$ is set for these equations.

Heat flow equation: heat going through the wax layer towards the coolant is a sum of heat coming from oil bulk and heat generated due to the solidification of wax.

$$2R_w h_{oil}(T_{oil} - T_w) = \frac{2k_w(T_w - Ti)}{ln\frac{R_i}{R_w}} - 2R_w k_m(C_{wb} - C_{ws})\Delta H_f \tag{A.82}$$

C_{wb} is dissolved wax concentration in waxy oil in kg/m^3. When the wax is dissolved, its density is taken as the wax/oil solution density. Note that this is concentration in liquid solution without volume occupied by solid wax particles. Liquid solute volume is the volume of "pure oil fluid" and dissolved wax volume.

$$C_{wb} = \frac{\rho_{oil} V_{wb}}{V_{solution}} = \rho_{oil} \frac{\alpha_{wb}}{\alpha_{oil} + \alpha_{wb}} = \rho_{oil} \frac{\alpha_{wb}}{\tilde{R}_w^2 - \alpha_{par}} \tag{A.83}$$

A.7 References

[1] O'Donoghue, A. F. 1996. *On the steady state motion of conventional pipeline pigs using incompressible drive.* PhD thesis, Durham University.

[2] Singh, P., Venkatesan, R., Fogler, H. S., and Nagarajan, N. 2000. Formation and aging of incipient thin film wax-oil gels. *AIChE Journal* **46** (5): 1059–1074.

Appendix B

Reference formulas

B.1 Gradient

B.1.1 Scalar

$$\begin{aligned}\nabla a = & \\ &= \frac{\partial a}{\partial x}\vec{x_e} + \frac{\partial a}{\partial y}\vec{y_e} + \frac{\partial a}{\partial z}\vec{z_e} \\ &= \frac{\partial a}{\partial \rho}\vec{\rho_e} + \frac{1}{\rho}\frac{\partial a}{\partial \phi}\vec{\phi_e} + \frac{\partial a}{\partial z}\vec{z_e}\end{aligned} \tag{B.1}$$

B.1.2 Vector

$$\begin{aligned}\nabla \cdot \vec{a} = div\vec{a} = & \\ &= \frac{\partial a_x}{\partial x} + \frac{\partial a_y}{\partial y} + \frac{\partial a_z}{\partial z} \\ &= \frac{\partial a_\rho}{\partial \rho} + \frac{1}{\rho}\frac{\partial a_\phi}{\partial \phi} + \frac{\partial a_z}{\partial z} + \frac{a_\rho}{\rho} \\ &= \frac{1}{\rho}\frac{\partial (\rho a_\rho)}{\partial \rho} + \frac{1}{\rho}\frac{\partial a_\phi}{\partial \phi} + \frac{\partial a_z}{\partial z}\end{aligned} \tag{B.2}$$

B.2 Laplacian

B.2.1 Scalar

$$\begin{aligned}\nabla^2 a = \triangle a = & \\ &= \frac{\partial^2 a}{\partial x^2} + \frac{\partial^2 a}{\partial y^2} + \frac{\partial^2 a}{\partial z^2} \\ &= \frac{1}{\rho}\frac{\partial}{\partial \rho}\left(\rho \frac{\partial a}{\partial \rho}\right) + \frac{1}{\rho^2}\frac{\partial^2 a}{\partial \phi^2} + \frac{\partial^2 a}{\partial z^2}\end{aligned} \tag{B.3}$$

B.3 Diffusion type formulation

$$\begin{aligned}\nabla \cdot (k \nabla a) = div(k \nabla a) = & \\ &= \frac{\partial}{\partial x}\left(k \frac{\partial a}{\partial x}\right) + \frac{\partial}{\partial y}\left(k \frac{\partial a}{\partial y}\right) + \frac{\partial}{\partial z}\left(k \frac{\partial a}{\partial z}\right) \\ &= \frac{1}{\rho}\frac{\partial}{\partial \rho}\left(\rho k \frac{\partial a}{\partial \rho}\right) + \frac{1}{\rho^2}\frac{\partial}{\partial \phi}\left(k \frac{\partial a}{\partial \phi}\right) + \frac{\partial}{\partial z}\left(k \frac{\partial a}{\partial z}\right)\end{aligned} \tag{B.4}$$

B.4 Viscous dissipation function

The viscous dissipation $= \mu\Phi$ defined here is for Newtonian type fluid.

B.4.1 Cartesian

$$\begin{aligned}\Phi = 2\left[\left(\frac{\partial \upsilon_x}{\partial x}\right)^2 + \left(\frac{\partial \upsilon_y}{\partial y}\right)^2 + \left(\frac{\partial \upsilon_z}{\partial z}\right)^2\right] + \left(\frac{\partial \upsilon_x}{\partial y} + \frac{\partial \upsilon_y}{\partial x}\right)^2 + \\ \left(\frac{\partial \upsilon_y}{\partial z} + \frac{\partial \upsilon_z}{\partial y}\right)^2 + \left(\frac{\partial \upsilon_z}{\partial x} + \frac{\partial \upsilon_x}{\partial z}\right)^2 - \\ \frac{2}{3}\left(\frac{\partial \upsilon_x}{\partial x} + \frac{\partial \upsilon_y}{\partial y} + \frac{\partial \upsilon_z}{\partial z}\right)^2\end{aligned} \tag{B.5}$$

B.4.2 Cylindrical

$$\begin{aligned}\Phi = 2\left[\left(\frac{\partial \upsilon_r}{\partial r}\right)^2 + \left(\frac{1}{r}\frac{\partial \upsilon_\phi}{\partial \phi} + \frac{\upsilon_r}{r}\right)^2 + \left(\frac{\partial \upsilon_z}{\partial z}\right)^2\right] + \left[r\frac{\partial}{\partial r}\left(\frac{\upsilon_\phi}{r}\right) + \frac{1}{r}\frac{\partial \upsilon_r}{\partial \phi}\right]^2 + \\ \left[\frac{1}{r}\frac{\partial \upsilon_z}{\partial \phi} + \frac{\partial \upsilon_\phi}{\partial z}\right]^2 + \left[\frac{\partial \upsilon_r}{\partial z} + \frac{\partial \upsilon_z}{\partial r}\right]^2 - \frac{2}{3}(\nabla \cdot \vec{U})^2\end{aligned} \tag{B.6}$$

B.5 Diada

B.5.1 Cartesian

Diadic multiplication of two vectors is a tensor.

$$\vec{U} \otimes \vec{V} = U_i V_j \tag{B.7}$$

B.6 Discretization

$$\frac{\partial}{\partial r}\left(r\frac{\partial \alpha}{\partial r}\right) = \frac{\partial \alpha}{\partial r} + r\frac{\partial^2 \alpha}{(\partial r)^2} = \frac{\alpha_{m+1} - \alpha_{m-1}}{2\Delta r} + r_n \frac{\alpha_{m+1} - 2\alpha_m + \alpha_{m-1}}{(\Delta r)^2} \tag{B.8}$$

$$\frac{\partial}{\partial r}\left(\frac{\partial \alpha}{\partial r}\right) = \frac{\alpha_{m+1} - 2\alpha_m + \alpha_{m-1}}{(\Delta r)^2} \tag{B.9}$$